

GROWTH AND CHARACTERISATION OF TIN DICHALCOGENIDE CRYSTALS

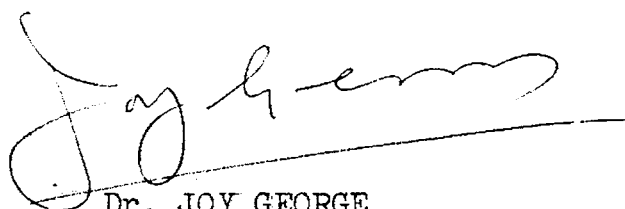
THESIS SUBMITTED BY
C. K. VALSALA KUMARI
*IN PARTIAL FULFILMENT OF THE
REQUIREMENTS FOR THE DEGREE OF
DOCTOR OF PHILOSOPHY*

SOLID STATE PHYSICS LABORATORY
DEPARTMENT OF PHYSICS
UNIVERSITY OF COCHIN
1984

CERTIFICATE

Certified that this thesis is based on the work done by Miss C.K. Valsala Kumari under my guidance in the Department of Physics, University of Cochin and no part of this has been presented by her for any other degree.

Cochin - 22,
20th September 1984,

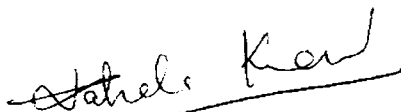


Dr. JOY GEORGE
(Supervising Teacher)
PROFESSOR IN INDUSTRIAL PHYSICS
DEPARTMENT OF PHYSICS
UNIVERSITY OF COCHIN.

DECLARATION

Certified that the work presented in this thesis is based on the original work done by me under the guidance of Professor Joy George in the Department of Physics, University of Cochin, and has not been included in any other thesis submitted previously for the award of any degree.

Cochin-22,
20th September 1984.



C.K. VALSALA KUMARI.

SYNOPSIS

GROWTH AND CHARACTERISATION OF TIN DICHALCOGENIDE CRYSTALS

During the past few decades, a wide spread interest in the structural, optical, electrical and other physical properties of the transition metal dichalcogenide layer compounds has evolved. The members of this family of compounds can be regarded as strongly bonded two dimensional chalcogen-metal-chalcogen layers which are loosely coupled to one another by the weak van der Waal's forces. Because of this type of bonding, the crystals are easily cleavable along the basal plane and show highly anisotropic properties.

This thesis contains the growth and the study of the physical properties of certain tin dichalcogenide crystals (SnS_2 and SnSe_2). Tin disulphide and tin diselenide crystallize in the hexagonal CdI_2 type crystal structure. This structure consists of layers of tin atoms sandwiched between two layers of chalcogen atoms. A tin atom is surrounded by six chalcogen atoms octahedrally. In the layers the atoms are held together by covalent bonding and in between the layers there is van der Waal's bonding.

These crystals are normally grown by chemical transport method with iodine as the transporting agent, the growth time being about 8 to 24 hours. But crystals grown using transporting agent are usually contaminated by the transporting agent and this has a pronounced effect on the physical properties. Therefore physical vapour transport method was used for the growth of crystals in the present investigations. Eventhough a relatively larger period of growth time is necessary for the physical vapour transport method (40-150 hrs), the crystals obtained from this method have a much less impurity concentration than that obtained from chemical vapour transport method.

Since the growth temperatures of tin disulphide and tin diselenide are comparatively high, fused quartz tubes were used for the growth. Stoichiometric proportion of the starting materials were filled in precleaned quartz ampoules and evacuated to a pressure of 10^{-5} Torr and sealed. For the growth process a horizontal two zone linear gradient furnace and temperature controllers with accuracy better than $\pm 1^{\circ}\text{C}$ were used. A source temperature of 700°C and a growth temperature of 630°C was used for the growth of tin disulphide crystals. After a growth period of 40 - 150 hours, golden yellow platelet like crystals of approximately 1.5 cm^2 in area and

10 - 60 μm thickness were obtained. For the growth of tin diselenide crystals, a source temperature of 640° C and a growth temperature of 475° C was used. Usually thin platelets of metallic coloured crystals having a thickness of $\leq 100 \mu\text{m}$ were obtained.

Crystals with good plane surfaces were selected for morphological studies. Beautiful circular and hexagonal spirals were observed on the as grown faces of tin disulphide and tin diselenide crystals. These observations reveal that these crystals grow from the vapour phase by the screw dislocation mechanism. Spirals with hollow core and change of curvature were observed on tin disulphide crystals. The change of curvature of the spiral step depends on the stress field around the dislocation. Eccentric spirals originating from single screw dislocation were also observed. The eccentricity of the spirals depends on the supersaturation gradient of the growing crystal. Eccentric spirals and spirals showing change of curvature were observed on tin diselenide crystals also. One of the most striking features observed on SnSe_2 crystals was the interlaced spirals. Interlaced spirals result from the dependence of growth rates on crystallographic direction.

Optical studies provide a wealth of information on the band structure of the semiconductor and also about the impurity levels in the band gap. Optical properties of the crystals were studied by transmission measurements. Refractive index of the crystals was determined from the interference fringes obtained in the transmission spectra of thin crystals. Absorption coefficient was also calculated from the transmission spectra of the crystals.

In tin disulphide crystals, it was found that there is a shoulder in the absorption just before the onset of band to band transitions. This shoulder is caused by transitions from valence band to donor levels (due to doubly ionizable sulphur vacancy) situated 0.17 eV below the conduction band. From absorption edge measurements it was also found that, in tin disulphide the valence band is split into three due to spin-orbit interaction and crystal field splitting.

The fundamental absorption data was analyzed in terms of the theory of Bardeen et al /1/ and from this analysis, an indirect forbidden band gap of 2.07 eV and a direct forbidden band gap of 2.40 eV have been detected in tin disulphide crystals. In the case of tin diselenide crystals, the indirect band gap

obtained is 1.03 eV. From the functional dependence of absorption coefficient on photon energy it was found that the transition is forbidden.

Conductivity type of the crystals was determined by the hot probe method. All the tin disulphide and tin diselenide crystals grown were n-type.

From the electrical measurements, activation energy required for conduction, mobility, carrier concentration etc. were determined. Resistivity of tin diselenide crystals was measured at different temperatures and from the temperature dependence of resistivity, activation energy for conduction parallel to c-axis was, obtained (0.072 eV). Resistivity and Hall effect perpendicular to c-axis were measured by van der Pauw's technique /2/. From these values, mobility and carrier concentration of tin diselenide crystals were calculated. From the results it was found that crystals grown by physical vapour transport (carrier concentration $\sim 10^{16}$) are less contaminated than that grown from chemical transport (carrier concentration $\sim 10^{18}$) method.

Electrical conduction mechanism in tin disulphide crystals was studied using Al-SnS₂-Al (MIM) structures. The current voltage characteristics obtained

show four discrete regions. At low voltages, the current is proportional to the voltage (ohmic law region) followed by a square law region at high fields. This region is the shallow trap square law region. The square law region is followed by another region where current increases sharply with voltage ($I \propto V^n$; $n \geq 3$) and this is due to the filling up of the traps. This region is followed by the trap free square law region. These observations indicate a charge injection into the semiconductor. The log I versus log d plot in the shallow trap square law region shows a d^3 dependence establishing that the conduction mechanism is space charge limited. From the threshold voltage, where the ohmic current cross over to space charge limited current in the absence of traps, the density of thermally generated free carriers was determined ($2.3 \times 10^{11} \text{ cm}^{-3}$). Mobility of the charge carriers was calculated using the equation for SCL conduction ($6 \text{ cm}^2/\text{V. sec.}$). From this mobility, conductivity of the specimen was calculated ($2.2 \times 10^{-7} \Omega^{-1} \text{ cm}^{-1}$) and the calculated value agrees very well with the experimental value obtained from the ohmic law region. Due to the filling of the traps in the semiconductor, current increases sharply after the shallow trap square law region. The trap filled limit voltage measures the fraction of the total concentration of traps that is empty in thermal equilibrium

and from the trap filled limit voltage, the trap concentration was calculated ($2.3 \times 10^{13} \text{ cm}^{-3}$). Trap depth, Fermi level, effective density of states in the conduction band etc. have also been determined from the measurements. Dependence of the current on temperature in the ohmic law region gave an activation energy of 0.40 eV.

References

1. J. Bardeen, F.J. Blatt and L.H. Hall, Proceedings of Photoconductivity Conference, Atlantic City (New York : Wiley 1956) p-146.
2. L.J. van der Pauw, Philips Res. Repts. 13 (1958) 1.

CONTENTS

	page
INTRODUCTION	1
Chapter - I RELEVANT SEMICONDUCTOR PHYSICS	8
1.1 Optical properties of crystalline semiconductors	15
1.2 Current injection in solids	27
1.3 Hall effect	36
References	41
Chapter - II THEORIES OF CRYSTAL GROWTH	42
2.1 Atomic theory of the growth of a perfect crystal	43
2.2 Growth of real crystals	49
References	55
Chapter - III GROWTH OF CRYSTALS FROM VAPOUR	57
3.1 Diffusion	59
3.2 Stefans flow	62
3.3 Viscous flow of gas	68
3.4 Convection	70
3.5 Growth by physical vapour transport (PVT)	72
References	75

Chapter - IV	EXPERIMENTAL TECHNIQUES	76
4.1	Fabrication of the furnace	76
4.2	Temperature controller	77
4.3	Ampoules and pre-treatment	81
4.4	Optical microscopy	85
4.5	Determination of optical constants	86
4.6	Determination of conductivity type	89
4.7	Measurement of Hall voltage	90
4.8	Measurement of electrical properties using MIM structures	91
	References	95
Chapter - V	GROWTH AND MORPHOLOGY OF TIN DISULPHIDE CRYSTALS	96
5.1	Crystal growth	97
5.2	Results and discussion	99
	References	112
Chapter - VI	OPTICAL PROPERTIES OF TIN DISULPHIDE CRYSTALS	114
6.1	Experimental	116
6.2	Results and discussion	116
	References	131

Chapter - VII	ELECTRICAL PROPERTIES OF TIN DISULPHIDE CRYSTALS	134
7.1	Experimental	136
7.2	Results and discussion	136
	References	150
Chapter - VIII	GROWTH AND MORPHOLOGY OF TIN DISELENIDE CRYSTALS	151
8.1	Experimental	151
8.2	Results and discussion	153
	References	164
Chapter - IX	OPTICAL AND ELECTRICAL PROPERTIES OF TIN DISELENIDE CRYSTALS	166
9.1	Experimental	168
9.2	Results and discussion	169
9.3	Electrical properties	174
	References	180

INTRODUCTION

Modern solid state electronics is based on crystal growth revolution and the advancement of semiconductor research and technology depend largely on the basic and applied studies on crystal growth of semiconductors and other electronic materials. Certain members of the IV-VI compounds, especially the Pb salts, have been grown and studied for many years, as they form an interesting series of semiconductors having in most cases the NaCl structure, and because they have provided sensitive photoconductive detectors operating in the IR region. The study of IV-VI semiconductors received fresh impetus in the mid 1960's with the discovery at Lincoln laboratories that PbTe and SnTe, and also PbSe and SnSe form solid solutions in which the energy gap varies continuously through zero, so that it is possible, by selecting the appropriate composition, to get any required small band gap. Sulphides and selenides of tin are much different from the lead chalcogenides; they have large band gaps (~ 2 eV) and low charge carrier mobility (≤ 30 cm² / Volt. sec.) and hence are not suitable as infrared detectors. But they are interesting at present from the point of view of basic research, as they have a layered crystal structure which exhibits polytypism like the well known SiC crystals.

Tin disulphide and tin diselenide crystallize in a lattice having the cadmium iodide structure. They have the general form MX_2 where M is an element of the IVth group of the periodic table and X is a chalcogen. The atomic arrangement of these crystals is shown in figure 1. The cadmium iodide lattice has an almost perfect hexagonal close packing of anions (chalcogen) with the smaller cations (metal) nestled in octahedral interstices between alternate layers of the anions. In this structure, only half of the octahedral interstices are filled. The resulting strongly covalently bonded X-M-X sandwiches almost fully satisfy the primary valencies of the constituent ions, and adjacent sandwiches are held together by weak van der Waal's forces. Covalent bonding of the atoms in the layers and the van der Waal's bonding in between the layers make the atomic lattice highly anisotropic, with easy cleavage and extended growth perpendicular to the c-axis. Since the structure is formed of close-packed hexagonal nets of anions, the unit cell is referred to hexagonal axis.

Most of the layered compounds exhibit polytypism; they crystallize into more than one crystallographic modifications with the same chemical composition, but with different number and manner of stacking layers in the unit cell. A polytypic substance usually

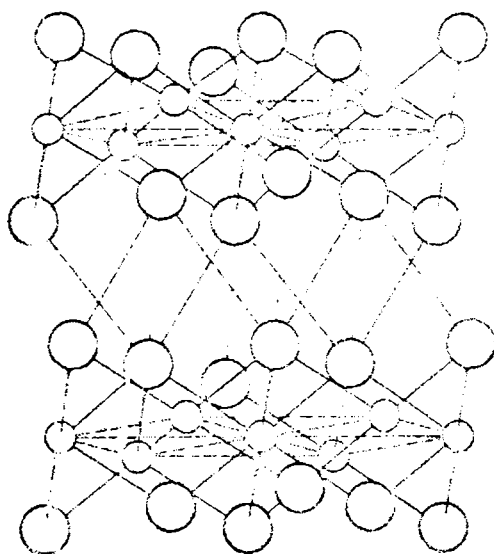


Fig. 1. The layer structure of
sandwiches are and
bonds. All are
larger and

mini
H₂O
and

crystallize into a basic structure which is referred to as its most common polytype. Only occasionally it crystallizes into other polytypes which have higher periodicities than the common polytype. Tin dichalcogenides usually crystallize in the basic 2H polytype.

One of the most striking features of crystals with layered structures is the existence of screw dislocations with Burgers vector perpendicular to the plane of the layers giving rise to growth spirals. The greatest experimental support for the dislocation theory of polytypism has come from the observation of, and measurements on, growth spirals on the crystal surfaces of polytypic substances. Frank /1/ has interpreted the various polytypes as originating by growth around screw dislocations in certain basic structures. Franks theory received direct experimental support from the observation of growth spirals on the (0001) face of SiC crystals and the measurement of their step heights /2,3/.

While vapour growth methods were used at different times for the preparation of many of the simple inorganic compounds, it has been also possible to grow most of them from the melt by the Bridgmann-Stockbarger method and the liquid encapsulated Czochralski pulling method. In the case of the solid

solutions, however, melt growth methods inevitably lead to problems with constitutional supercooling, and if this is avoided, samples will still in general have a composition gradient along their direction of growth. Vapour growth methods thus become the only practicable way of producing good homogeneous bulk crystals.

Chemical vapour transport method is usually used for the growth of dichalcogenide crystals. In this method, the material is transported from one end of the ampoule to the other end by means of some transporting agent. Crystals obtained from this method are generally contaminated due to the incorporation of the transporting agent. In physical vapour transport (PVT) method no transporting agent is used. The technique is, less susceptible to contamination and has thus been more extensively developed for the growth of pure semiconductors. Because of this, PVT method has been used for the growth of crystals in this work.

Semiconductor crystals can be characterised optically, electrically and morphologically. Optical characterisation of the crystals by spectrophotometric method yields a wealth of information about the band structure of the material. From the transmission data

obtained, refractive index, absorption coefficient and band gap of the material can be calculated.

Electrical characterisation can be done by measuring the current against voltage. Using metal-insulator-metal (MIM) structures, the conduction mechanism in the crystals can be found. From the current voltage characteristics at different temperatures, activation energy for conduction is obtained. Trap depth, trap concentration, Fermi level etc. can be calculated from these electrical studies.

Optical microscopy is another tool for the study of the surface topographic features of the as grown faces of crystals to assess the perfection and growth mechanism of these crystals.

This thesis contains the growth of tin disulphide and tin diselenide crystals by physical vapour transport method and their optical, electrical and morphological properties.

Part of the work reported in this thesis is published in the form of the following papers:

- 1) "Temperature controller adaptor for a microvoltmeter"
Int. J. Electronics 52 (1982) 299.

- 2) "Absorption edge of tin disulphide single crystals"
J. Appl. Phys. 54 (1983) 5347.
- 3) "Growth and characterisation of tin disulphide crystals grown by physical vapour transport method"
J. Crystal Growth 63 (1983) 233.
- 4) "Electrical characterisation of tin disulphide crystals"
Solid State Commun. 49 (1984) 103.
- 5) "Optical and electrical properties of SnSe_2 crystals grown by physical vapour transport method"
Solid State Commun. (communicated).

CHAPTER - I

RELEVANT SEMICONDUCTOR PHYSICS

Consider an isolated atom, the building unit of a solid. The atom is composed of a concentrated nucleus with neutrons and protons; surrounded by an electron cloud. According to Pauli's exclusion principle, every electron must have a different set of quantum numbers, since they are fermions, each energy level in the atom can have a maximum of two electrons. When a large number of these atoms are brought together to form a solid, the overlap of wave-functions in the entire crystal causes all of the atoms in the crystal to collectively obey the Pauli's exclusion principle. Thus the discrete levels of the separated atoms are changed into bands of levels in the solid. Figure 1 shows the energy levels of the outer shells of the single atom on the left side and the right side shows what happens when N atoms are brought together to form a solid. Each of the single atom levels splits up into a band which contains energy levels for $2N$ electrons. Between the adjacent bands, there is a region of unfilled energy levels called forbidden energy levels. Solids are so designed that the minimum amount of energy is used and at absolute zero all energy levels below the highest filled level are filled, all levels above that level are empty. That level is the Fermi level and it occurs at the so called Fermi energy.

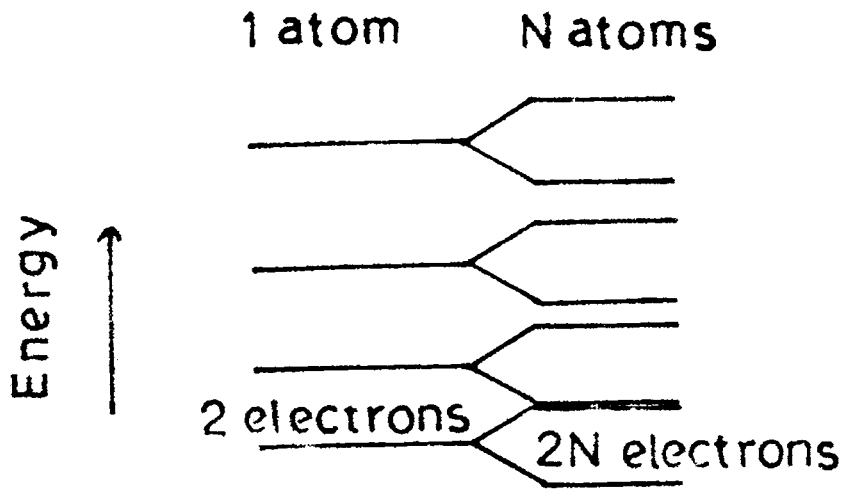


Fig.1. Left: energy levels for the electrons in the outer shells of a free atom. Right: energy bands for the electrons in a solid made up of N of these atoms.

Depending on the valence of the single atoms in the solid, there are several possibilities for the resulting band structure. Figure 2 shows the band structure of an insulator, metal and an intrinsic semiconductor. Because each energy level in the single atom contain two electrons, an insulator forms when the valence is an even number, otherwise there is a possibility of overlap as in the bottom levels of figure 1. In the second figure energy is plotted increasing vertically and the zero level of energy is at the top. The bands shown in the diagram are the bands at the top most energy band structure for that element, lower bands are so far down that it is impossible to excite their electrons and therefore they are not used in electrical conduction. There is a large energy gap between the filled valence band and the empty conduction band in the case of an insulator. So an amount of energy equal to the energy gap would have to be given to an electron to get excited from the valence band to conduction band. Since this value is very much larger than the thermal energy of electrons at room temperature, this is an insulator (Figure 2a). Band structure of a metal is shown in figure 2b. A metal commonly results, when a solid is made up of atoms whose valence is an odd number because this results in a partially filled band at the top of the band structure. Because the band is only partially filled, there are empty electron states just above the Fermi level.

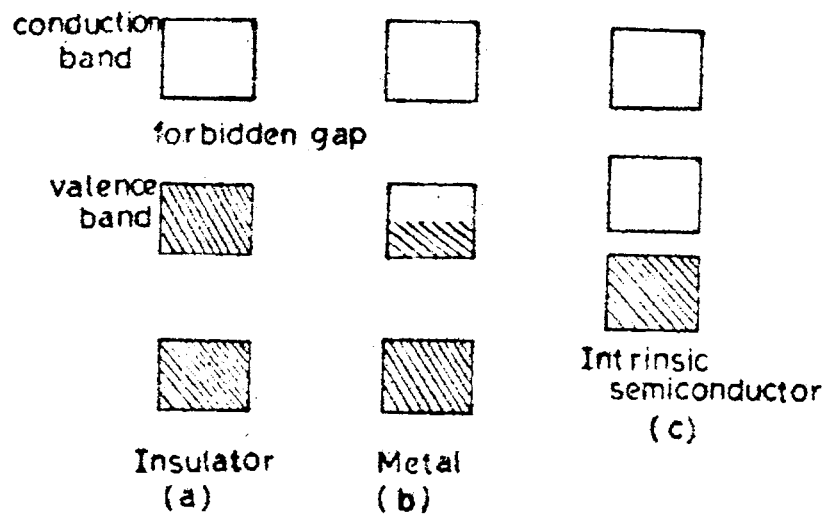


Fig.2. Energy bands for an insulator, a metal, and an intrinsic semiconductor.

Figure 2c shows the band structure of an intrinsic semiconductor. Here the valence band is completely filled and the conduction band is completely empty at absolute zero, but the energy gap between these two bands is quite small. Thus the distinction between insulators and intrinsic semiconductors is only a quantitative one. The main feature used to distinguish semiconductors from metals and insulators was their negative temperature coefficient of resistance (TCR). The semiconducting properties are brought up by thermal excitation, impurities, lattice defects or non-stoichiometry. At room temperature the resistivity of a semiconductor lies in the range of 10^{-2} to $10^9 \Omega \text{ cm}$ intermediate between good conductors ($10^{-6} \Omega \text{ cm}$) and insulators (10^4 to $10^{22} \Omega \text{ cm}$).

A highly purified semiconductor exhibits intrinsic conductivity. The temperature range at which intrinsic conductivity is exhibited, the electrical properties of the crystal are not modified by impurities. In semiconductors, as the temperature is increased from absolute zero, electrons are thermally excited from the valence band to the conduction band. In this excitation process the vacant sites left behind in the valence band are called 'holes'. Both electrons in the conduction band and holes in the valence band contribute to electrical conductivity. The conductivity σ in the presence of electrons and holes is given by $\sigma = (n e \mu_e + p e \mu_h)$, where n and μ_e are the carrier concentration and mobility

of electrons respectively and p and N_h are that of holes. In an intrinsic semiconductor the number of electrons is equal to the number of holes. The expression for the carrier concentration is given by

$$\left. \begin{aligned} n_i &= N_c \exp (E_F/k_B T) \\ \text{and } p_i &= N_v \exp \left[-(E_F+E_g)/k_B T \right] \end{aligned} \right\} \quad (1.1)$$

where N_c and N_v are the density of states in the conduction band and valence band respectively, E_g is the forbidden energy gap, k_B is the Boltzmann constant and T is the absolute temperature. N_c and N_v are given by

$$N_c = 2(2\pi m_e^* k_B T/h^2)^{3/2} \quad (1.2)$$

$$N_v = 2(2\pi m_h^* k_B T/h^2)^{3/2} \quad (1.3)$$

where m_e^* and m_h^* are the effective mass of electrons and holes respectively. Since $n_i = p_i$

$$\begin{aligned} n_i = p_i &= 2(2\pi k_B T/h^2)^{3/2} (m_e^* m_h^*)^{3/4} \exp (-E_g/2k_B T) \\ &= A \exp (-E_g/2k_B T) \end{aligned} \quad (1.4)$$

where A is a constant. If we assume that the variation of mobility of electrons and holes in an electric field with temperature is small, then the conductivity σ , which is proportional to the number of carriers has a variation of the form

$$\sigma = \sigma_0 \exp (-E_g/2k_B T) \quad (1.5)$$

where σ_0 is a constant. Such an exponential variation of conductivity had long been known for semiconductors at high temperatures.

At temperatures below the intrinsic range, the electrical properties are controlled by the impurity and this is the extrinsic case. Addition of impurities to a semiconductor is called doping. Impurity atoms that can give up an electron are called donors and atoms which can accept electrons from the valence band, leaving mobile holes in the band are acceptors. In a material if donor atoms are dominant, the thermal ionization of donors will cause electrons to be set free in the conduction band. In this case, the conductivity of the specimen will be controlled by electrons, and the material is said to be n-type. If acceptors are dominant, holes will be set free in the valence band and the conductivity will be controlled by positively charged holes. Such materials are p-type. The density of free electrons in the conduction band due to a donor with activation energy E_d is given by

$$n_c = (2n_d)^{1/2} (2\pi m_e^* k_B T/h^2)^{3/4} \exp(-E_d/2k_B T) \quad (1.6)$$

where n_d is the donor density. It is to be noted that n_c is proportional to the square root of donor concentration. A similar expression holds for the case of acceptors also.

1.1 OPTICAL PROPERTIES OF CRYSTALLINE SEMICONDUCTORS

The most direct method for probing the band structure of semiconductors is the optical absorption studies. From the frequency dependence of the absorption coefficient, we can determine the energy gap of the material as well as whether the valence band and conduction band extrema occur at the same or at different points in the K-space.

The absorption and dispersion of a plane electromagnetic wave is described by the complex refractive index $N = n + ik$, where n is the real refractive index and k the extinction coefficient. The plane wave can be represented by

$$E = E_0 \exp [i (K \cdot r - \omega t)] \quad (1.1.1)$$

$$H = H_0 \exp [i (K \cdot r - \omega t)] \quad (1.1.2)$$

where K is the propagation wave vector, $K = K_1 + iK_2$. Equations (1.1.1) and (1.1.2) form a solution of Maxwell's equations for the electromagnetic field in a medium of magnetic permeability unity if

$$K \cdot K = \omega^2 \epsilon / c^2 \quad (1.1.3)$$

The complex dielectric constant ϵ which includes the effects of the conduction and displacement currents is

defined as

$$\epsilon = \epsilon_1 + i \epsilon_2 = \epsilon_1 + i \frac{\sigma}{\omega \epsilon_0} \quad (1.1.4)$$

The complex refractive index N is also defined by

$\epsilon = N^2$ giving

$$\epsilon_1 = n^2 - k^2$$

$$\epsilon_2 = \frac{\sigma}{\omega \epsilon_0} = 2nk$$

In the case of homogenous plane waves

$$K_1 = \frac{n\omega}{c}, \quad K_2 = \frac{k\omega}{c}$$

Substituting in equation (1.1.1) we obtain

$$E_x = E_{0x} \exp \left[i\omega \left(\frac{nx}{c} - t \right) \right] \exp (-\omega kx/c) \quad (1.1.5)$$

This equation represents a wave with a velocity c/n which is attenuated by $\exp (-\omega kx/c)$ travelling in x -direction.

The absorption coefficient \mathcal{C} , defined by the relative decrease of the intensity per unit distance in the direction of propagation is

$$\mathcal{C} = \frac{2k\omega}{c} = \frac{4\pi k}{\lambda} \quad (1.1.6)$$

The reflection R is referred as the ratio of the time averaged energy flow reflected from the surface to the incident flow. For normal incidence, R is given by

$$R = \frac{(n-1)^2 + k^2}{(n+1)^2 + k^2} \quad (1.1.7)$$

when $k = 0$, i.e., in the transparent range

$$R = (n-1)^2 / (n+1)^2$$

Different types of absorption processes.

Fundamental absorption, free carrier absorption, excitonic absorption, impurity absorption etc. are the mechanisms which are responsible for absorption of electromagnetic radiation in semiconductors. In fundamental absorption, electrons can be excited from the valence band to the conduction band with the absorption of a photon of energy equal to the band gap of the material. The absorption coefficient in this case is $\approx 10^5$ to 10^6 cm^{-1} . One of the characteristic features of semiconductor is that, on the low energy side of the absorption band, the absorption coefficient drops rapidly and the material becomes fairly transparent. This marked drop in absorption is called the absorption edge.

Excitation of an electron from the valence band to the conduction band leads to a free electron and hole capable of moving independently under the influence of an applied field. The system of electron and hole mutually bound by their coulomb attraction is known as exciton. The binding energy of exciton is small, about 0.01 eV and hence the excitation level falls slightly below the

edge of the conduction band. The ground state ($n=1$) excitonic level will be observed as absorption peak on the long wavelength side of the direct absorption edge. The exciton absorption is more pronounced in insulators than in semiconductors and can lead to strong narrow line absorption as in atomic spectra.

As the wavelength is increased beyond the absorption edge, slowly the absorption coefficient also increases. This rise in absorption is due to the electronic transitions within the conduction band or valence band. This process is referred to as free carrier absorption. The free carrier absorption takes place even when the energy of the incident photon is less than the forbidden gap of the material and frequently this absorption dominates the spectrum below the fundamental edge.

The transition between a neutral donor and the conduction band or between the valence band and the neutral acceptor can occur by the absorption of a low energy photon. For this absorption process the energy of the photon must be at least equal to the ionization energy of the impurity. For donor levels lying deeper, the impurity absorption will be well separated from the fundamental absorption. For shallow impurities, the absorption spectrum will take the form of a series of

lines in approximately the same position as would be expected for the exciton spectrum.

The fundamental absorption.

When the energy of the incident photon exceeds E_g , the band gap of the material, an electron can be excited from the valence band into the conduction band. There are two types of transitions; direct and indirect. Transition involving photons is called direct transition and the transition involving photons and phonons is called indirect transition.

Direct transitions.

In the case of direct transition, the valence band maximum and the conduction band minimum appear at the same point in the Brillouin zone at $K = 0$. Figure 3 shows a direct vertical optical transition near the fundamental absorption edge in a semiconductor.

The momentum of a photon h/λ is very small compared to the crystal momentum h/a , where λ is the wavelength of light and a is the lattice constant. Because of this, the photon absorption process should conserve the momentum of the electron. The absorption coefficient $\alpha(h\nu)$ for a given photon energy $h\nu$ is proportional to the probability P_{if} for the transition from the initial

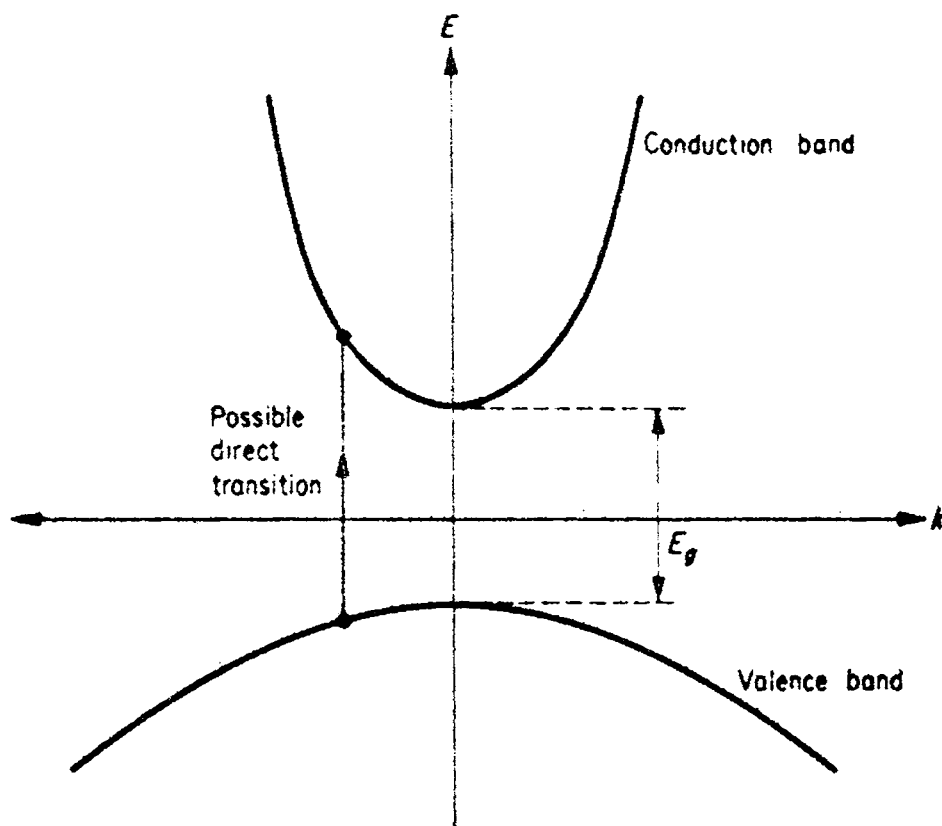


Fig.3. Direct transitions from the valence band to the conduction band.

state to the final state and to the density of electrons in the initial state n_i and to the density of available final states n_f . This process must be summed for all possible transitions between states separated by an energy difference equal to the photon energy $h\nu$.

$$\mathcal{L}(h\nu) = A \sum_{if} P_{if} n_i n_f \quad (1.1.8)$$

In the case of absorption transitions between two direct valleys where all the momentum-conserving transitions are allowed, the transition probability P_{if} is independent of photon energy. Every initial state at E_i is associated with a final state at E_f such that

$$E_f = h\nu - |E_i| \quad (1.1.9)$$

But in the case of parabolic bands

$$E_f - E_g = \frac{\hbar^2 K^2}{2m_e^*} \quad (1.1.10)$$

and $E_i = \frac{\hbar^2 K^2}{2m_h^*}$

Therefore,

$$h\nu - E_g = \frac{\hbar^2 K^2}{2} \left(\frac{1}{m_e^*} + \frac{1}{m_h^*} \right) \quad (1.1.11)$$

The density of states can be given by

$$N(h\nu) d(h\nu) = \frac{8\pi K^2}{(2\pi)^3} dK = \frac{(2m_r)^{3/2}}{2\pi^2 \hbar^3} (h\nu - E_g)^{1/2} d(h\nu) \quad (1.1.12)$$

where m_r is the reduced mass given by

$$\frac{1}{m_r} = \frac{1}{m_e^*} + \frac{1}{m_h^*}$$

The absorption coefficient is given by

$$\mathcal{L}(h\nu) = A(h\nu - E_g)^{1/2} \quad (1.1.13)$$

where A is a constant.

In some materials, quantum selection rules forbid direct transitions at $K = 0$, but allow them at $K \neq 0$, the transition probability increases proportionately to $h\nu - E_g$. Since the density of states linked in direct transitions is proportional to $(h\nu - E_g)^{1/2}$, the absorption coefficient for the forbidden transition has the spectral dependence

$$\mathcal{L}(h\nu) = B(h\nu - E_g)^{3/2} \quad (1.1.14)$$

where B is a constant.

Indirect transitions.

When a transition requires a change in both energy and momentum, a double transition process is required because the photon cannot provide a change in momentum. This situation can be overcome with the emission or absorption of phonons. Momentum is conserved via

a phonon interaction, and is illustrated in figure 4.

Phonons, the quantum of lattice vibration has a characteristic energy E_p . The minimum frequency for a phonon assisted transition is given by

$$h\nu = E_f - E_i + E_p \quad (1.1.15)$$

for emission of a phonon, and

$$h\nu = E_f - E_i - E_p \quad (1.1.16)$$

for absorption of a phonon. In indirect transitions, all the occupied states of the valence band are connected to all the empty states of the conduction band. The density of initial states at an energy E_i is

$$N(E_i) = \frac{1}{2\pi^2} \frac{1}{\hbar^3} (2m_h^*)^{3/2} |E_i|^{1/2} \quad (1.1.17)$$

The density of states at E_f is

$$N(E_f) = \frac{1}{2\pi^2} \frac{1}{\hbar^3} (2m_e^*)^{3/2} (E_f - E_g)^{1/2}$$

using equation (1.1.15)

$$N(E_f) = \frac{1}{2\pi^2} \frac{1}{\hbar^3} (2m_e^*)^{3/2} (h\nu - E_g + E_p + E_i)^{1/2} \quad (1.1.18)$$

The absorption coefficient is proportional to the product of the densities of initial states and final states integrated over all possible combinations of

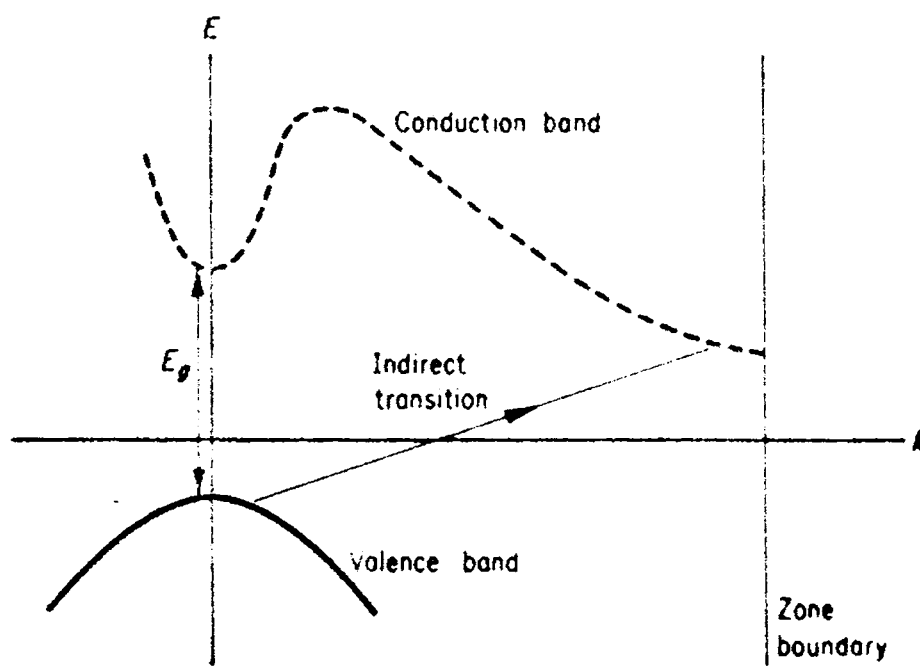


Fig.4. Indirect transitions from the valence band to the conduction band.

states separated by $h\nu \mp E_p$; \mathcal{C} is also proportional to the probability of interacting with phonons, which is a function $f(N_p)$ of the number N_p of phonon of energy E_p . The number of phonons is given by the Bose-Einstein statistics

$$N_p = 1 / [\exp(E_p/k_B T) - 1] \quad (1.1.19)$$

$$(h\nu) = A f(N_p) \int_0^{-(h\nu - E_g + E_p)} |E_i|^{1/2} (h\nu - E_g \mp E_p + E_i)^{1/2} dE_i \quad (1.1.20)$$

After simplification, absorption coefficient for a transition with phonon absorption is obtained as

$$\mathcal{C}_a = \frac{A (h\nu - E_g + E_p)^2}{\exp(E_p/k_B T) - 1} \quad \text{for } h\nu > E_g - E_p \quad (1.1.21)$$

The probability of phonon emission is proportional to $N_p + 1$. The contribution \mathcal{C}_e to the absorption coefficient is given by

$$\mathcal{C}_e = \frac{A (h\nu - E_g - E_p)^2}{1 - \exp(-E_p/k_B T)} \quad \text{for } h\nu > E_g + E_p \quad (1.1.22)$$

where A is a slowly varying function of ν . Since both phonon absorption and phonon emission are possible when $h\nu > E_g + E_p$, the absorption coefficient \mathcal{C}_i is given by

$$\mathcal{C}_i = \mathcal{C}_e + \mathcal{C}_a$$

$$\alpha_i = \frac{A (h\nu - E_g + E_p)^2}{[\exp (E_p/k_B T) - 1]} \quad \text{for } E_g - E_p < h\nu \leq E_g + E_p \quad (1.1.23)$$

In the case of indirect forbidden transitions, an extra factor $(h\nu - E_g \pm E_p)$ is involved into the expression for α_e and α_a . Therefore for forbidden transition, absorption coefficient α is given by

$$\alpha_{if} = \frac{B (h\nu - E_g \pm E_p)^3}{[\exp (E_p/k_B T) - 1]} \quad (1.1.24)$$

The plot of $(\alpha h\nu)^2$ versus $h\nu$ for direct allowed transition, $(\alpha h\nu)^{2/3}$ for direct forbidden transition, $(\alpha h\nu)^{1/2}$ for indirect allowed and $(\alpha h\nu)^{1/3}$ for indirect forbidden transition, should always be straight lines. By extrapolating these lines to $\alpha = 0$, we can obtain the band gap of the material.

It may be seen that a careful and systematic use of optical data can yield a wealth of information regarding the material under study. This include the band gap of the material and the relative position of conduction band and valence band maxima in K-space. The functional dependence of absorption coefficient on photon energy near a transition can tell whether the transition is forbidden or allowed. The nature of transition can give information about the electronic states from which the transition took place and this in turn can help to get a picture of the band structure of the semiconductor.

1.2. CURRENT INJECTION IN SOLIDS.

The study of electronic transport in semiconductors is becoming an increasingly important field. Metal-semiconductor contacts are very important in the semiconductor device technology. The electrical properties of the semiconductor crystals are governed by the combined effect of bulk and contacts. The current-voltage characteristic studies generally indicates the type of contact encountered in the system. The electron transport in a semiconductor will depend upon the nature of the contact as given below.

(a) Ohmic contact

An ohmic contact is one which supplies a reservoir of charge carriers to enter the material as needed. The energy band diagram for an ohmic contact of a metal to an n-type semiconductor is shown in figure 5a. In this case the metal work function Φ_m must be smaller than the semiconductor work function Φ_s . As the applied voltage is increased, electrons are injected into the bulk of the semiconductor. The carrier concentration near the contact is therefore increased due to the flow of current and carrier injection is said to take place. A consequence of the phenomenon of carrier injection is the formation of

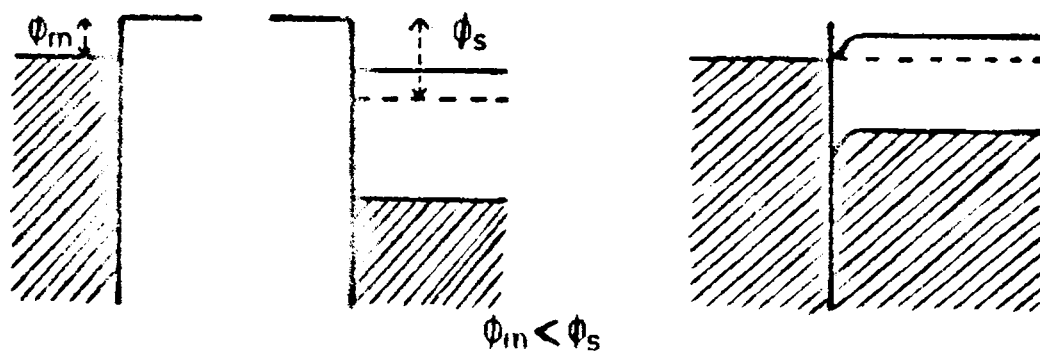


Fig.5.(a) Energy level diagram of an ohmic contact between a metal and an n-type semiconductor.

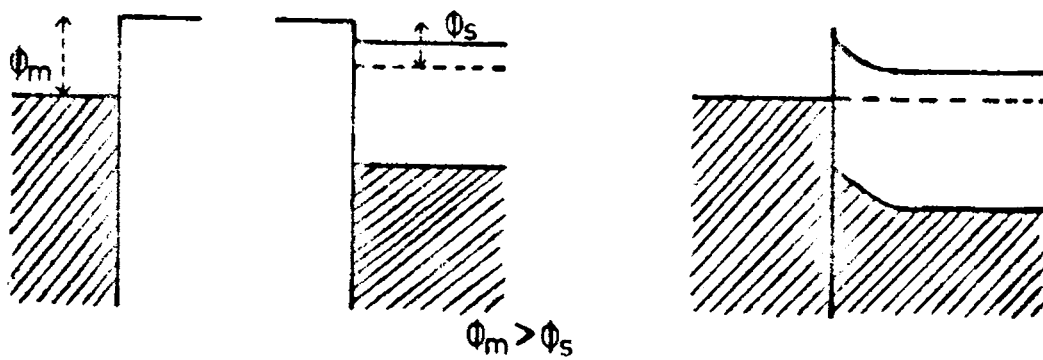


Fig.5(b) Energy level diagram of a blocking contact between a metal and an n-type semiconductor.

a space charge cloud of charge carriers in the vicinity of the contacts. Mutual repulsion between the individual carriers limits the total injected charge in the semiconductor and the resulting current is said to be space charge limited (SCL).

(b) Blocking contact

A blocking contact (Schottky barrier) occurs when $\phi_m > \phi_s$ and in this case electrons flow from the semiconductor into the metal to establish thermal equilibrium conditions. The energy band diagram for a blocking contact to an n-type semiconductor is shown in figure 5b. In this case the current is determined by the rate at which the contact can supply carriers. On the application of the field, a depletion region is created in the semiconductor and an equal negative charge resides on the metal electrode. Due to the electrostatic interaction between the oppositely charged regions, a local field exists within the surface of the semiconductor. This causes the bending of the bottom of the conduction band.

When contact is made to a p-type semiconductor the very opposite effects to those described above take place. That is, an ohmic contact is produced when ϕ_{ms} is positive and a blocking contact, when ϕ_{ms} is negative.

Space charge limited conduction.

When an ohmic contact is applied to a semiconductor or insulator, electrons will flow from the metal into the conduction band of the semiconductor and form a space charge. There is a close analogy between the equations governing space charge conduction in solids and those describing SCLC in a thermionic diode. The fundamental difference between the two cases lies in the fact that, in a vacuum, the electrons might be treated as obeying the laws of simple particle dynamics, whereas in a solid the mobile charge carriers are continually interacting with the crystal lattice.

Consider a perfect trap free insulator with no intrinsic carriers, of thickness d carrying a current J . Let the field at a distance x from the surface be $E(x)$ and $n(x)$ be the number of free electrons per unit volume. At equilibrium, the current is given by the difference between the drift current and the diffusion current.

$$J = ne \mu E - De (dn/dx) \quad (1.2.1)$$

where μ is the mobility and D is the diffusion coefficient. By using the Poisson's equation $dE/dx = ne/\epsilon$ in equation (1.2.1) we get

$$J = \epsilon \mu E (dE/dx) - \epsilon D (d^2E/dx^2) \quad (1.2.2)$$

where ϵ is the dielectric constant.

Integrating this equation using Einstein's relation

$\mu/D = e/k_B T$, taking $dE/dx \approx E/d$ and neglecting the last term, which is permissible if $k_B T \ll eEd$, we can obtain,

$$E = \sqrt{\left[\frac{2J}{\epsilon \mu} (x + x_0) \right]} \quad (1.2.3)$$

Since the diffusion term has already been neglected and if the space charge effect on the field near the injecting cathode is also neglected, x_0 can be calculated from the boundary condition that at $x = 0$, $n = N_0$.

$$N_0 \approx 2 \left(\frac{2\pi m_e^* k_B T}{h^2} \right)^{3/2} \exp -(W - \chi)/k_B T \quad (1.2.4)$$

where N_0 is the electron density at the metal-insulator interface, m_e^* is the electron effective mass, W is the metal work function and χ is the electron affinity of the insulator. From equations (1.2.1) and (1.2.3)

$$x_0 = \epsilon J / (\mu N_0^2 e^2) \quad (1.2.5)$$

Using the relation $V = \int_0^d E dx$, the potential across the insulator is given by

$$\begin{aligned} V &= \int_0^d \sqrt{\left[\frac{2J}{\epsilon \mu} (x + x_0) \right]} dx \\ &= \frac{2}{3} \sqrt{\left(\frac{2J}{\epsilon \mu} \right)} \left\{ (d + x_0)^{3/2} - x_0^{3/2} \right\} \quad (1.2.6) \end{aligned}$$

when $x_0 \ll d$

$$J = \frac{9}{8} \epsilon \mu \frac{V^2}{d^3} \quad (1.2.7)$$

This is the standard Mott and Gurney equation /1/ for one carrier injection.

If thermally generated free carriers with density n_0 are present, then at low voltages where the injected carrier density is less than n_0 , Ohms law will be obeyed.

$$J = en_0 \mu \frac{V}{d} \quad (1.2.8)$$

The transition from Ohms law to the Mott and Gurney law takes place at the transition voltage V_{tr} which is given by

$$\begin{aligned} en_0 \mu \frac{V_{tr}}{d} &= \frac{9}{8} \epsilon \mu \frac{V_{tr}^2}{d^3} \\ V_{tr} &= \frac{8 en_0 d^2}{9 \epsilon} \end{aligned} \quad (1.2.9)$$

The theory of space charge limited currents in the case of insulators or semiconductors with traps was due to Rose /2/. If the semiconductor contains traps, a large fraction of the injected space charge will condense therein, which will make the free carrier density much lower than that in a perfect one. Since the empty traps will remove most of the injected carriers, the presence of traps will reduce the space charge limited current. In thermal equilibrium the free electron density n_0 is given by

$$n_0 = N_c \exp \left[\frac{(E_F - E_c)}{k_B T} \right] \quad (1.2.10)$$

where N_c is the effective density of states in the

conduction band, E_F is the Fermi level and E_c is the bottom of the conduction band. The occupancy of a trap level at E_t in thermal equilibrium is given by

$$n_{t,0} = \frac{N_t}{1 + 1/g \exp \left[(E_t - E_F)/k_B T \right]} \quad (1.2.11)$$

where N_t is the trap density and g is the degeneracy factor. With no applied field, the equilibrium trap occupancy results from the balance of electron capture and thermal re-emission from the traps. When a field is applied, this balance is altered due to the change in free electron density accompanying the change in injection level. Therefore in the insulator, the balance between trapped and free carriers is reached as if the insulator were in thermal equilibrium with no applied field, only with a free carrier density $n(x)$ and the corresponding Fermi level known as the Electron steady state Fermi level (ESSFL).

$$n(x) = N_c \exp \left[(E_{Fn(x)} - E_c)/k_B T \right] \quad (1.2.12)$$

The trap occupancy

$$n_t(x) = \frac{N_t}{1 + 1/g \exp \left[(E_t - E_{Fn(x)})/k_B T \right]} \quad (1.2.13)$$

From the above equations

$$n_t(x) = N_t / \left(1 + \frac{1}{g} \frac{N}{n(x)} \right) \quad (1.2.14)$$

$$\text{where } N = N_c \exp \left[(E_t - E_c)/k_B T \right] \quad (1.2.15)$$

Shallow traps are at least $k_B T$ above the ESSFL and can be effective in capturing injected electrons. The ratio between the free to trapped carriers is given by

$$\frac{n(x)}{n_t(x)} = \frac{N}{\epsilon N_t} = \frac{N_c \exp \left[\frac{(E_t - E_c)}{k_B T} \right]}{\epsilon N_t} = \theta \quad (1.2.16)$$

where θ is a constant. If θ is small, the traps are more effective in immobilizing the injected carriers. Thus a higher injection level (applied field) will be required to produce an injected electron density greater than the thermal carrier density n_0 . Now the Mott and Gurney equation becomes

$$J = \frac{9}{8} \theta \epsilon \mu \frac{V^2}{d^3} \quad (1.2.17)$$

$$\text{and } V_{tr} = \frac{8 n_0 d^2}{9 \theta \epsilon} \quad (1.2.18)$$

In the presence of deep traps, $n_t(x) \simeq N_t$, the traps are full and have little influence on the free carrier density. When a field is applied to the semiconductor, the ESSFL moves up the energy gap towards the conduction band. When it moves through a trap level, the shallow traps become deep. When the applied field is so large that the ESSFL lies above the trap levels, all the traps are full and all the injected charge appears in the conduction band and the current increases rapidly back to the trap free

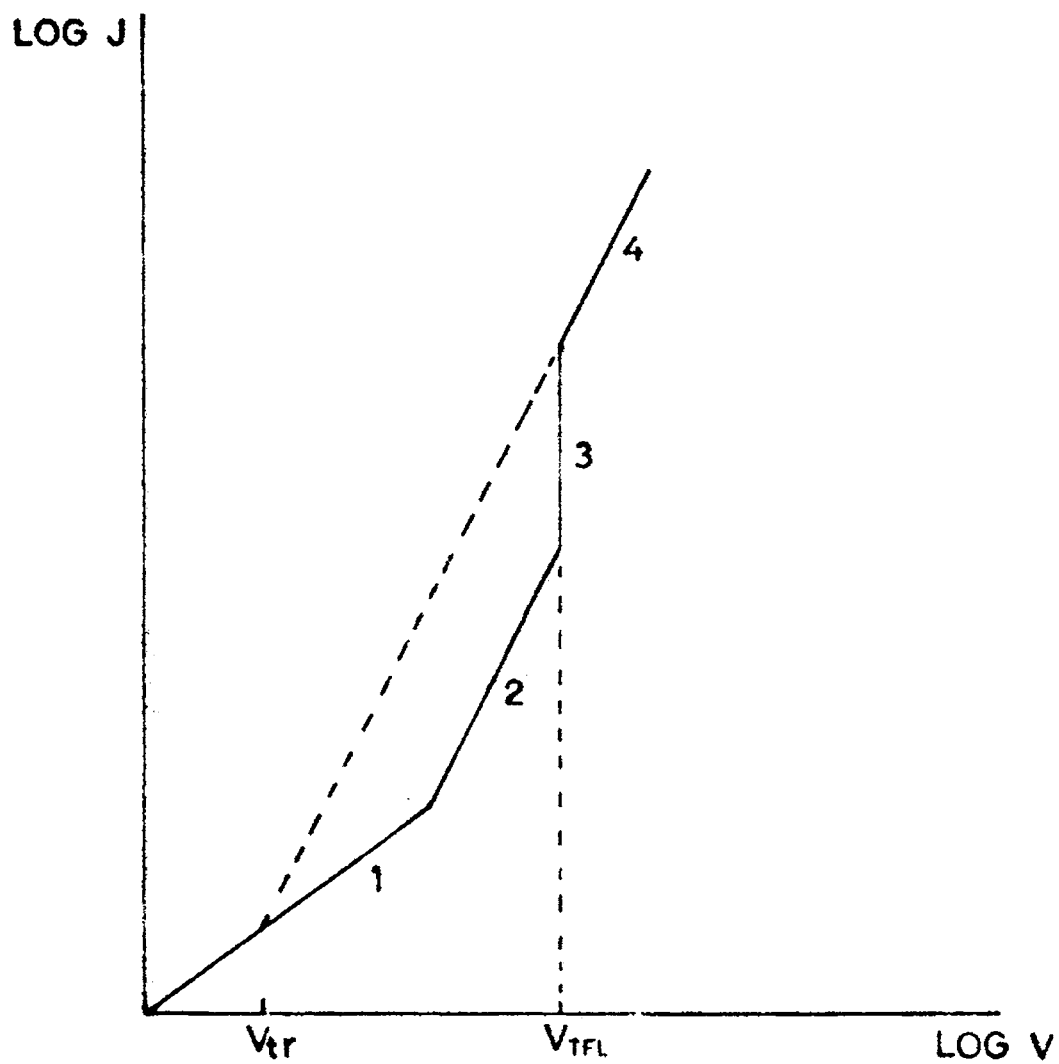


Fig.6. Space charge limited current-voltage characteristic for a semiconductor with a single trap level.
 (1) Ohm's law region (2) Trapped square law region
 (3) Trap-filled limit region (4) Trap free square law region.

curve. The voltage at which this occur is called the trap filled limit voltage.

$$V_{TFL} = e N_t d^2/\epsilon \quad (1.2.18)$$

Lampert /3/ has calculated the complete current-voltage curve for a single set of shallow traps and is shown in figure 6. At low voltages, the injected carrier density is less than the free carrier density and Ohm's law, is obeyed. This is the region 1. When the injected carrier density is greater than the free carrier density, the current becomes space charge limited and is modified by the traps in the semiconductor. This is the square law region (region 2). At the trap filled limit voltage all the traps are full and the current rises sharply in region 3 until it reaches the trap free square law region shown in region 4.

HALL EFFECT

Conductivity measurements are not sufficient for the determination of the number of charge carriers and their mobility, as the product of the two appears in the expression for conductivity. Moreover these measurements do not give any information about the sign of the prominent charge carrier. Hall effect may be used to separate out mobility and carrier concentration, as it directly gives the number of charge carriers. As a byproduct we get the sign of the prominent charge carrier also.

When a magnetic field is applied at rightangles to a conductor carrying electric current, an e.m.f. is developed across the conductor in a direction perpendicular to both the magnetic field and to the current. This is known as the Hall effect, and the developed voltage, Hall voltage.

Consider an n-type semiconductor having an electric current density J_x in the x-direction and a magnetic field in the z-direction as shown in figure 7a. If we consider the effect of the magnetic field on the drift velocity of the electrons in an electric field in the xy-plane, there must be a component of the field at rightangles to the current flow to balance the transverse force due to the magnetic field.

The drift velocity v_x is given by

$$v_x = -J_x/ne \quad (1.3.1)$$

where n is the electron concentration and e is the electronic charge. The average transverse force on an electron in the y-direction is equal to eBv_x where B is the magnetic induction. The balancing field E_y is given by

$$e E_y = ev_x B$$

$$E_y = v_x B \quad (1.3.2)$$

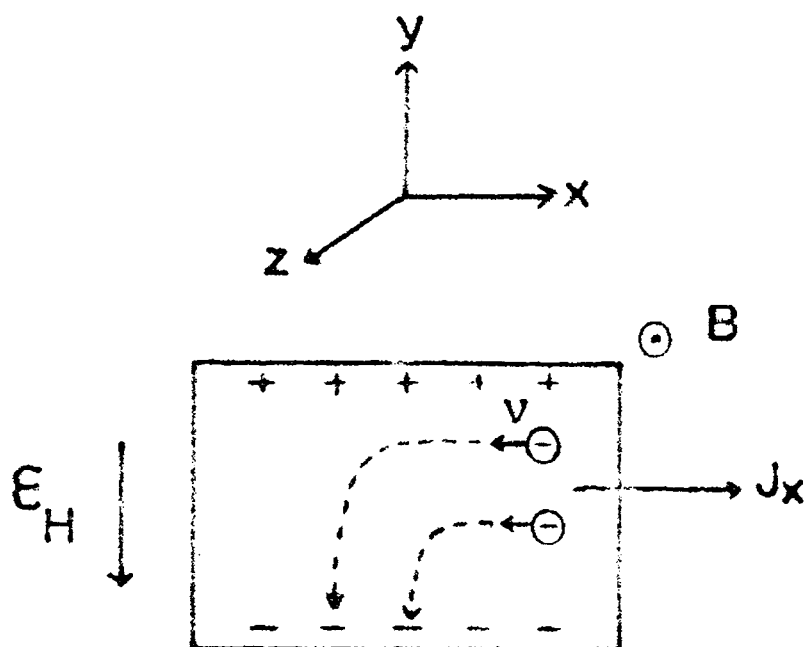


Fig.7.(a) Origin of the Hall field and Hall effect

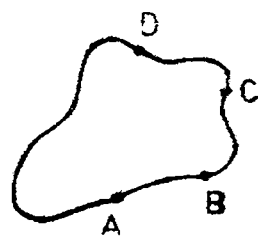


Fig.7.(b) Specimen with dot contacts for Hall effect measurement using van der Pauw's technique.

where E_y is the Hall field. By substituting the value of v_x from equation (1.3.1)

$$E_y = - J_x B / ne \quad (1.3.3)$$

The Hall field is proportional to the current density and magnetic induction. The proportionality constant is known as the Hall constant R_H .

$$R_H = - 1/ne \quad (1.3.4)$$

Hall constant is inversely proportional to the electron concentration. The sign of the equation depends on the sign of the charge carriers.

If the crystals are irregularly shaped, van der Pauw technique /4/ is the best method for the resistivity and Hall effect measurement. In this method four small ohmic contacts are made to the periphery of the specimen having uniform thickness. Let us consider a sample of a conducting material of arbitrary shape with successive contacts A, B, C and D fixed on arbitrary places along the circumference (figure 7b).

The resistance $R_{AB,CD}$ is defined as the potential difference $V_D - V_C$ between the contacts D and C per unit current through the contacts A and B. The current enters the sample through the contact A and leaves it through

the contact B. Similarly we can define the resistance $R_{BC,DA}$. In these cases the following relation holds.

$$\exp(-\pi R_{AB,CD} d/\rho) + \exp(-\pi R_{BC,DA} d/\rho) = 1 \quad (1.3.5)$$

From this expression, the resistivity ρ is obtained as

$$\rho = \frac{\pi d}{\ln 2} \frac{(R_{AB,CD} + R_{BC,DA})}{2} f\left(\frac{R_{AB,CD}}{R_{BC,DA}}\right) \quad (1.3.6)$$

where d is the specimen thickness and f is a function of the ratio $R_{AB,CD}/R_{BC,DA}$ only and satisfies the relation

$$\frac{R_{AB,CD} - R_{BC,DA}}{R_{AB,CD} + R_{BC,DA}} = f \operatorname{arccosh} \left\{ \frac{\exp(\ln 2/f)}{2} \right\} \quad (1.3.7)$$

The Hall mobility can be determined by measuring the change of the resistance $R_{BD,AC}$ when a magnetic field is applied perpendicular to the sample. Hall mobility is then given by

$$\mu_H = \frac{d}{B} \frac{\Delta R_{BD,AC}}{\rho} \quad (1.3.8)$$

where B is the magnetic induction and $\Delta R_{BD,AC}$ the change of the resistance $R_{BD,AC}$ due to the magnetic field.

References

1. N.F. Mott and R.W. Gurney, Electronic process in ionic crystals, (Oxford University Press, Oxford 1940).
2. A. Rose, Phys. Rev. 97 (1955) 1538.
3. M.A. Lampert, Phys. Rev. 103 (1956) 6.
4. L.J. van der Pauw, Philips. Res. Repts. 13 (1958) 1.

CHAPTER - II

THEORIES OF CRYSTAL GROWTH

The theory of crystal growth can be divided into two sections; the theory of the growth of an ideally perfect crystal and the theory of the growth of an imperfect crystal. Based on thermodynamical grounds, Gibbs /1/ gave the first crystal growth theory. Gibbs formulated the minimum free energy criterion and showed that the condition for the stability of an isolated drop of a fluid is that its surface free energy and hence its area be minimum. Thus for a crystal in equilibrium with its surroundings at constant temperature and pressure, the Gibbs free energy will be a minimum for a given volume. If the volume free energy per unit volume is taken as a constant throughout the crystal, then $\sum_{i=1}^n \sigma_i F_i = \text{minimum}$, where σ_i is the surface free energy per unit area of the i th face of area F_i on a crystal bounded by n faces. Thus those faces will develop which lead to a minimum total surface free energy for a given volume.

The theory was further developed by Curie /2/ and Wulff /3/. Wulff deduced that on a crystal, the velocities of growth of different faces in the directions of their normals are proportional to the appropriate specific surface free energies.

Bravais /4/ first advanced the theory of reticular density. According to this, the velocity of growth in a direction normal to a face would be the slowest for the planes of maximum density. The faster moving planes would grow out leaving only the slow moving planes of maximum reticular densities. The simple Bravais law, that the most densely packed planes will occur as crystal faces, was extended by Donn and Harker /5/ to take into account the effect of symmetry operations on the basis of Miller indices. Soehncke /6/ introduced the idea of surface energies by postulating that the faces which possess the greatest reticular densities are those with minimum surface energies and hence have minimum velocities of growth.

2.1 ATOMIC THEORY OF THE GROWTH OF A PERFECT CRYSTAL

For the growth of an ideally perfect crystal, Kossel /7/, Stranski /8/ and Volmer /9/ have developed an atomic theory. To illustrate the KSV theory, consider a simple cubic structure, in which each cube represents one molecule and also one unit cell. Each molecule is attracted equally by all its six neighbours and only the nearest neighbours attract one another. At absolute zero, at which there are no thermal vibrations, the flat crystal surface is partially covered by another

layer. The difference in level is the intermolecular spacing and is known as the "step". The reentrant corner where the step shifts through one lattice spacing, is the "kink". These kinks act as exchange sites where the molecules reach and leave the body of the crystal at finite temperatures.

When the temperature is raised from absolute zero, the component molecules will start vibrating relative to one another. Soon some molecules will have enough energy to overcome the energy that binds them to the crystal. They will then break away from the body of the crystal and fly about in the space surrounding it. These free molecules constitute the vapour. The molecules which are at the kink positions are more likely to leave the crystal and vapourize, though this will happen for some molecule at other positions. The energy required for a molecule to leave the kink position is the evaporation energy W . While some molecules are getting vapourized, other molecules from the vapour phase reach the crystal surface and are adsorbed there. An equilibrium will be reached when these two processes become equal, the step has acquired a number of kinks.

Based on thermodynamical considerations, Frenkel /10/ has calculated the concentration of kinks

in a monomolecular step at a finite temperature.

Burton, Cabrera and Frank /11/ showed that the concentration of kinks is larger than that given by Frenkel. According to them, in terms of the interatomic distance a , the mean distance x_0 between the kinks is given by

$$x_0 \sim 1/2 a \exp (w/k_B T) \quad (2.1.1)$$

where w is the energy necessary to form a kink, T is the absolute temperature and k_B is the Boltzmann constant. They found that for close packed crystals with homopolar binding w will be of the order of $W/12$, where W is the evaporation energy. In terms of the nearest neighbour interaction Φ , which is related to the evaporation energy by the equation

$$\Phi = 1/6 W$$

$$x_0 \sim 1/2 a \exp (\Phi/2 k_B T) \quad (2.1.2)$$

Migration of adsorbed molecules.

When the crystal is in equilibrium with its vapour, molecules join and leave the crystal at the same rate. The rate of leaving of the molecules from the crystal depends on the temperature and the rate of reaching of molecules on the surface is proportional

to the vapour concentration. When the vapour pressure in contact with the crystal is increased above the equilibrium value, more molecules join the crystal than leave it, and the crystal begins to grow.

Experiments indicated that in growth from vapour, the rate of direct arrival of molecules on the crystal surface is generally small compared to the rate of arrival by surface migration. Between the time a molecule hits the surface of a crystal and the time it evaporates again into the vapour, the adsorbed molecule diffuses a considerable distance.

According to BCF theory /11/ the mean displacement x_s of adsorbed molecules on the crystal surface is given by

$$x_s = a \exp \left[\frac{(W'_s - U_s)}{2 k_B T} \right] \quad (2.1.3)$$

where U_s is the activation energy for the surface diffusion. W'_s is the evaporation energy from the surface to the vapour and is given by $W'_s = 3\Phi$. Therefore,

$$x_s \sim a \exp (3\Phi/2 k_B T) \quad (2.1.4)$$

Rate of advance of a straight step.

The growth of a perfect crystal whose surface

has steps will be the result of (1) transport of molecules from the vapour phase to the surface to form the adsorbed layer (2) the diffusion of the adsorbed molecules on the crystal surface (3) the diffusion of such adsorbed molecules along the edge of the steps until they reach a kink.

The step at a particular temperature will go on receiving more molecules at its kinks than it loses from the kinks as long as the pressure of the vapour in contact with the crystal surface is above the equilibrium vapour pressure. The saturation ratio α_* and the supersaturation σ_* are defined as

$$\alpha_* = \frac{p}{p_0} \quad \text{and} \quad \sigma_* = \alpha_* - 1 = \frac{p-p_0}{p_0} = \frac{\Delta p}{p_0} \quad (2.1.5)$$

where p is the actual pressure and p_0 is the equilibrium vapour pressure. The straight step will continue to advance as long as Δp is positive. For a straight step, the rate of advance V_{∞} is proportional to the supersaturation and is given by /10/

$$V_{\infty} = 2 (\alpha_* - 1) x_s \mathcal{V} \exp(-W/k_B T) \quad (2.1.6)$$

where \mathcal{V} is the frequency factor.

Thus if a crystal face is covered partly by a

layer, this layer will grow with a speed proportional to the supersaturation. As long as the pressure of the vapour is kept above the equilibrium value, it will continue to grow until it covers the whole surface. All steps initially present on the crystal will move, during the process of growth, towards the edge of the crystal and disappear, forming a completed layer. This completed surface will now contain a few adsorbed molecules and some vacancies. Thus all the stepped surfaces will be eliminated during the growth process and low index surfaces will be left. Further growth will be possible only after the formation of new steps.

Surface nucleation.

On perfect crystal faces steps could be created by thermodynamic fluctuations in the same way as kinks are formed in a step. Calculation of BCF /11/ has shown that steps will not be created by thermodynamic fluctuations on a low index face unless the temperature of the crystal is raised almost to its melting point, when the surface rapidly becomes rough. Therefore for the growth to continue, steps must be formed gradually, if at all, at ordinary temperatures.

Gibbs /1/ showed that in the case of a perfect crystal surface, the rate of growth is limited by the production of new layers, which is a nucleation process. Hence before the formation of a new layer, a two dimensional nucleus has to be formed, on the edges of which growth can proceed. For a given degree of supersaturation, there is a critical radius of the nucleus and a nucleus of radius greater than this will grow and if less, it will evaporate.

BCF /11/ showed that the shape of the nucleus depends on the crystallographic symmetry. The rate of formation of nucleus is given by

$$Z (S/s_c) \exp (-\Phi^2/k_B^2 T^2 \ln \alpha) \quad (2.1.7)$$

where Z is the rate of arrival of fresh molecules at single surface sites, S is the area of the crystal face under consideration and s_c is the area per molecule in the layer. Below a critical supersaturation value of 25-50%, the formation of the nucleus is negligible. Above this critical supersaturation the growth process is not limited by nucleation, and a perfect crystal will therefore be able to grow layer by layer.

2.2 GROWTH OF REAL CRYSTALS.

Real crystals grow at supersaturations of

1% or lower. Frank /12/ proposed the mechanism for the growth of such imperfect crystals. In this case growth of the crystal takes place in the presence of a step provided by a screw dislocation. This step will have a large number of kinks. When the atoms are adsorbed on the crystal surface, they diffuse to the step and kinks, and the step advances. The step provided by the emergence of a screw dislocation, terminates at the dislocation point, where it remains fixed. Due to this, when growth takes place, the step can advance only by rotating round the dislocation point. After one revolution, a complete layer of molecules will have been added and the crystal thickened by one molecular layer, the step having been left in the initial angular position.

At a particular supersaturation each point of the straight step will advance with the same speed. Angular velocity of the step near the dislocation is very much greater than the parts farther out for the same linear velocity. During growth the step will wind itself into a spiral pattern around the dislocation point. The shape of the spiral depends on the rate of advance of a growth front in different crystallographic directions.

When the rate of growth is independent of crystallographic direction, spirals with circular symmetry will result. Such conditions are likely to occur in growth from vapour, so that the rate of advance of a straight step does not vary with orientation in the crystal face. When the distance between the kinks is small and the mean displacement of the adsorbed molecule is large, the molecules will have a high probability of adhering to the step if adsorbed near it, irrespective of the orientation of the step. Therefore, the rate of advance of the ledge will be independent of the crystallographic orientation and a rounded spiral will result. The shape of the spiral can be calculated using the BCF theory /11/.

A ledge which forms a portion of the spiral and has a radius of curvature r_* , will advance with a velocity V_{r_*} given by

$$V_{r_*} = V_{\infty} \left(1 - \frac{r_c}{r_*} \right) \quad (2.2.1)$$

where V_{∞} is the rate of advance of a straight step and r_c is the critical radius of curvature. If the supersaturation is not too high, r_c is given by

$$r_c = a \phi \left(2 k_B T \ln \mathcal{C} \right) \quad (2.2.2)$$

Let $\theta(r)$ represent the rotating spiral in polar coordinates (r, θ) . The radius of curvature at a point r will be

$$\rho = (1 + r^2 \theta'^2)^{3/2} / (2 \theta' + r^2 \theta'^3 + r \theta'') \quad (2.2.3)$$

where θ' and θ'' are the derivatives of $\theta(r)$. If the angular velocity of the whole spiral is ω^* , the normal velocity at the point r is

$$V(r) = \omega^* r (1 + r^2 \theta'^2)^{-1/2} \quad (2.2.4)$$

A good approximation is obtained by taking an Archimedean spiral

$$r = 2 \rho_c \theta > 0 \quad (2.2.5)$$

which has the proper central curvature. ω^* is then given by

$$\omega^* = V_\infty / 2 \rho_c \quad (2.2.6)$$

The spacing between the successive arms of the spiral will be constant and will be given by

$$dr = 4 \pi \rho_c \quad (2.2.7)$$

Polygonal spirals will arise from the dependence of the rate of advance of a growth front on its orientation, which will happen when V_∞ given by

equation (2.1.6) varies with the orientation on the crystal face. When the step is parallel to a close-packed direction, the step will have relatively few kinks, and the kink energy being high. Therefore, the kinks are few and far between and the distance moved by the adsorbed molecule is small, polygonal spirals will result.

For an unequivocal verification of the growth of crystals by the screw dislocation mechanism (1) the surfaces of the crystals should be minutely examined for microscopic growth features and their shapes should be shown to be in agreement with theory; (2) the molecular step heights of these spiral pyramids should be measured; and finally (3) unit cell parameters should be determined by X-ray diffraction methods, and it should be shown that the spiral step heights are equal to or are simply related to the appropriate lattice parameter.

The techniques that have been utilized for the observation of these growth spirals are (1) off-focus, bright-field microscopy with narrow pencil illumination (2) electron microscopic technique and (3) phase-contrast microscopy in reflection.

Soon after Frank /12/ put forward the spiral growth theory, Griffin /13/ presented the first direct observation of a growth spiral on the prism face of a natural beryl crystal. Dawson and Vand /14/ observed growth spirals on the basal planes of paraffin crystals. Simultaneously Verma /15/, Amelinckx /16/ and Bhide /17/ observed hollow cores at the centres of growth spirals having big step heights on SiC crystals. Forty /18/ studied the spiral growth and step heights of a large number of CdI_2 crystals. The smallest step height so far reported is 2.3 \AA , which was observed and measured by Sunagawa /19/ on the (0001) face of natural hematite crystals. Sunagawa and Bennema /20/ studied also the influence of stress fields around screw dislocations and the consequent change of shape of the spirals. They observed that depending on the stress field, the spiral step shows a change of curvature as it escapes from the centre of the spiral.

References

1. J.W. Gibbs, 'Collected works'. Vol.1 (Longmans, Green and Co., London, 1928) p-325.
2. P. Curie, Bull. Soc. Miner. France, 8 (1885) 145.
3. G. Wulff, Z. Krist. 34 (1901) 449.
4. A. Bravais, Entwicklung einer Theorie d. Krystallstruktur, (Leipzig, 1879).
5. J.D. Donnay and D. Harker, Amer. Min. 22 (1937) 446.
6. L. Soehncke, Entwicklung einer Theorie d. Krystallstruktur, (Leipzig, 1879).
7. W. Kossel, Nachr. Ges. Wiss. Gottingen, Math. Physik. K1; 11a (1927) 135.
8. I.N. Stranski, Z. Phys. Chem. 136 (1928) 259.
9. M. Volmer, Kinetic der Phasenbildung (Steinkopff Dresden and Leipzig, 1939).
10. J. Frenkel, J. Phys. USSR, 9 (1945) 392.
11. W.K. Burton, N. Cabrera and F.C. Frank, Phil. Trans. Roy. Soc. A 243 (1951) 299.
12. F.C. Frank, Disc. Faraday Soc. 5 (1949) 48.

13. L.J. Griffin, *Phil. Mag.* 41 (1950) 196.
14. I.M. Dawson and V. Vand, *Proc. Roy. Soc. A* 206 (1951) 555.
15. A.R. Verma, *Nature* 167 (1951) 939.
16. S. Amelinckx, *Nature* 167 (1951) 939.
17. V.G. Bhide, *Physica* 24 (1958) 817.
18. A.J. Forty, *Phil. Mag.* 42 (1951) 670.
19. I. Sunagawa, *Amer. Mineral.* 46 (1961) 1216.
20. I. Sunagawa and P. Bennema, *J. Crystal Growth* 53 (1981) 490.

CHAPTER - III

GROWTH OF CRYSTALS FROM VAPOUR

Crystallization from vapour is the method of choice for the preparation of many technologically important materials. Open tube vapour phase epitaxial processes are in wide spread use for the growth of thin films of Si and GaAs. Closed tube (ampoule) vapour growth is often used for the preparation of bulk samples, such as CdS. Crystal growth from vapour has certain advantages because it usually occurs at temperatures lower than those of other growth techniques, that might be used for the same material. For instance, materials that decompose before melting, have adverse melt/container reactions, or have a high temperature solid/solid phase transition, can often be grown at low temperatures. Also, the low atomic roughness of the vapour-solid interface implies strong morphological stability in the presence of heat and mass transfer non-uniformities. The main disadvantages of vapour growth are parasitic nucleation and low growth rates.

Vapour growth may be divided into four categories. Physical vapour transport (PVT) or sublimation-condensation, is a closed tube technique that

may be used to grow crystals if the material vapour pressure exceeds 10^{-2} Torr at some feasible temperature. If the vapour pressure is too low at convenient temperatures to allow effective transport by PVT, then growth by chemical vapour transport (CVT) may be possible. In this closed tube technique, a reversible chemical reaction, which yields only gaseous products, is used to volatilize the starting material.

Occasionally physical vapour deposition (PVD), i.e., open tube sublimation-condensation has been used to grow bulk crystals /1/. The most commonly used vapour growth technique however, is chemical vapour deposition (CVD). Here a chemical reaction is combined with open flow to effect transport. The reaction may either be reversible or irreversible at the deposition temperature.

The usefulness of these vapour grown materials often depends critically on their compositional uniformity. Local variations in dopant level or material stoichiometry can strongly influence the performance of an electronic or optical device.

The transport of chemical species in vapour phase growth occurs from the hotter source by different mechanisms such as diffusion, Stefan's flow, viscous flow, thermal convection etc. along the temperature gradient towards the colder condensation zone.

3.1 DIFFUSION

The general phenomena of diffusion, observed not only in gases and liquids but in all forms of matter, is a manifestation of the universal tendency of entropy towards a maximum. A system in which the components are initially segregated increases its entropy by mixing of the components. Diffusion is the motion of each component of a system from regions where the concentration is high to where it is lower, the motion involving individual atoms or molecules. Diffusion obeys a law named as Fick's law and it states that the flux of each component is proportional to the concentration gradient of that component.

$$J_i = - D_i \Delta n_i \quad (3.1.1)$$

The constant D_i is called the diffusion coefficient and it may be shown that it equals $(\lambda \bar{c}/2)$ where λ is the mean free path and \bar{c} the mean velocity of the

molecules and it depends on pressure and temperature as

$$D \propto \frac{T^{3/2}}{P} \quad (3.1.2)$$

Experimentally it may be shown that

$$D = D_0 \frac{P_0}{P} \left(\frac{T}{T_0} \right)^n \quad (3.1.3)$$

where n varies from 1.5 to 2.0 and D_0 is the measured value of D at a standard temperature T_0 and pressure P_0 .

The process of diffusion is statistical in nature. If there are more molecules of species A to the right of some imaginary reference surface than to the left, then because of the constant, random motion of the molecules, more A molecules cross the reference surface from right to left than in the reverse direction, resulting in a net current of species A. This is an irreversible process, because spontaneous separation of the different species to any appreciable degree is a very improbable event. The process of mixing is spontaneous as it increases entropy (second law of thermodynamics) while the reverse process may be carried out only by creating more entropy in the surroundings, for example, by imposing a thermal gradient and producing a certain amount of unmixing by thermal diffusion.

We will now consider diffusion in systems where a macroscopic motion is imposed. The velocities of the molecules of each species of the gas will cover the Maxwell-Boltzmann distribution. If the gas were stationary and uniform in composition, the average velocity u_i will be zero. If the gas were of a single component and moving at some macroscopic velocity v , then $u_i = v$. In a non-uniform gas each species will be having a different average velocity u_i and under these conditions, we can ascribe a macroscopic drift velocity to the gas as a whole in various ways.

In many chemical problems, the molar average velocity given by $U = \sum_i y_i u_i$ is the most useful, where y_i is the molar density. Whereas in hydrodynamical problems, the mass average velocity $u = \sum_i c_i u_i$, where c_i is the mass fraction, is chosen.

We may generalize the mean velocity V in terms of a general property β of the gas as $V = \sum_i \beta_i u_i / \sum_i \beta_i$ and may define the diffusion flux by

$$J_i = \beta_i (u_i - V) \quad (3.1.4)$$

If we take the summation of equation (3.1.4), over all the species in the gas, we obtain

$$\sum_i J_i = \sum_i u_i \beta_i - V \sum_i \beta_i = 0 \quad (3.1.5)$$

It follows that the sum of the diffusive fluxes over all species is zero. In consequence, it is not possible for diffusion to produce a net transport of property β , when diffusion fluxes are defined in terms of the β average velocity V .

3.2 STEFAN'S FLOW

Experiments of Stefan /2/ on the evaporation of liquids from pipes led him to conclude that the vapour is not transported away from the surface by diffusion alone. Stefan showed that the volume of gas passing through a unit cross-section of pipe in unit time is given by

$$V = \frac{D}{P-p} \frac{dp}{dx} \quad (3.2.1)$$

where P is the total pressure, p is the partial pressure of the vapour, and D its diffusion coefficient in the surrounding atmosphere.

The existence of flow velocity is necessary for transport, because diffusion alone will not give a net flux of molecules. The origin of flow velocity in the vapour of an evaporating substance lies in the

expansion on evaporation. A flow velocity will exist in the vapour from which a crystal is growing whenever the mechanism by which the vapour turns into a crystal involves a change in the number of vapour phase molecules, i.e., a change in volume or pressure. Thus for the simplest case.

solid \rightarrow vapour \rightarrow solid

there is a flow velocity away from the source material towards the growing crystal.

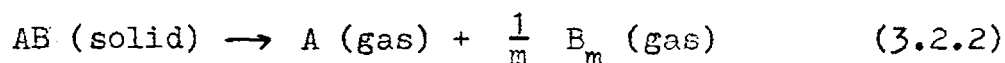
The direction of transport in a temperature gradient is determined, as in all vapour transport systems, by the sign of the enthalpy change for the transport reaction. An endothermic reaction results in transport from hot to cold and an exothermic reaction, in the other direction. Evaporation and sublimation (with and without dissociation) may be considered endothermic reactions and it is obvious that the transport there is from hot to cold.

The stefan flow velocity, where it exists, has been in the direction hot \rightarrow cold, irrespective of the direction of material transport. This is because the reaction taking place at the hot end of the system has

been accompanied by an increase in the number of vapour phase molecules.

Dissociative sublimation.

As an illustration of the process taking place in a crystal growth ampoule, we discuss the case of dissociative sublimation of a binary compound AB which dissociates according to the reaction



Our system consists of a source material AB at a point $x = l$ and our growing crystal at $x = 0$. We assume that the difference in temperatures $\Delta T = T(l) - T(0)$ is small compared with $T(l)$ and $T(0)$.

The flux of each component will be the sum of a flow velocity U which acts on the gas as a whole, and a diffusion term proportional to the concentration gradient of the particular component.

$$J_A = \frac{U}{RT} p_A - \frac{D}{RT} \frac{dp_A}{dx} \quad (3.2.3)$$

$$J_{B_m} = \frac{U}{RT} p_{B_m} - \frac{D}{RT} \frac{dp_{B_m}}{dx} \quad (3.2.4)$$

Addition of equations (3.2.3) and (3.2.4) causes the diffusion terms to disappear, leaving

$$J_A + J_{B_m} = UP / RT \quad (3.2.5)$$

Since we are growing a solid AB, we require the net flux of the component A and B_m to be in such a ratio as to give equal fluxes of atoms A and B, that is:

$$J_A = m J_{B_m} = J \quad (3.2.6)$$

where J is the growth rate of AB, and all fluxes are in molar units. Substituting, equation (3.2.6) becomes

$$\frac{UP}{RT} = J \left(1 + \frac{1}{m}\right) = Js \quad (3.2.7)$$

where s is a number. We may now rewrite the flow equations (3.2.3) and (3.2.4) as

$$J = \frac{Js}{P} p_A - \frac{D}{RT} \frac{dp_A}{dx} \quad (3.2.8)$$

$$J = \frac{mJs}{RT} p_{B_m} - \frac{mD}{RT} \frac{dp_{B_m}}{dx} \quad (3.2.9)$$

Integration of these equations neglecting the variation of P with x gives

$$p_A(x) - \frac{P}{s} = \left[p_A(1) - \frac{P}{s} \right] \exp\left(\frac{JsRT}{DP} (x-1)\right) \quad (3.2.10)$$

$$p_{B_m}(x) - \frac{P}{ms} = \left[p_{B_m}(1) - \frac{P}{ms} \right] \exp\left(\frac{JsRT}{DP} (x-1)\right) \quad (3.2.11)$$

There is a simple exponential variation in the quantities $(p_A - P/s)$ and $(p_{B_m} - P/ms)$, the strength of the exponential depending on the growth rate J . If the vapour were stoichiometric over the solid AB, the ratio $\sigma = p_A / p_{B_m}$ would be m . Hence these quantities which occur in equation (3.2.10) and (3.2.11) are the departures of stoichiometry in the vapour. They vary exponentially with x and always increase in magnitude as the distance from source material increases.

To see how this comes about, let us consider a capsule at a uniform temperature $T(1)$, containing source material at one end. The vapour in the capsule comes to equilibrium with the solid at a composition that depends on the composition of the solid and the ratio of the capsule volume to solid volume. In general, the vapour will not be stoichiometric, the ratio $\sigma = p_A / p_{B_m}$, will not have the value m . Now imagine a seed crystal introduced at the far end of the capsule from the source, and the temperature of that end lowered to $T(0)$. Now the seed grows by removing A atoms and B_m molecules from the vapour in the ratio $1:1/m$. A flow of vapour is caused, by the reduction in molar volume on condensation at seed and by the increase in molar volume on sublimation at the source.

This flow brings up vapour to the seed in the ratio \mathcal{d} . If \mathcal{d} is different from m , the vapour next to the seed becomes depleted in one component, while an excess of the other component accumulates. The change in vapour composition developing at the seed end of the capsule produces diffusion currents which carry the excess component away, and bring up more of the minority component. In the steady state, the flow of vapour and the diffusion currents of the component species combine to give net fluxes of A and B_m in the ratio m , in spite of the non-stoichiometry of the vapour.

The growth rate J may be expressed in terms of the vapour compositions over the source material and crystal by

$$\begin{aligned} J &= \frac{DP}{RTsl} \ln \left\{ \frac{p_A(1) - P/s}{p_A(0) - P/s} \right\} \\ &= \frac{DP}{RTsl} \ln \left\{ \frac{p_{B_m}(1) - P/ms}{p_{B_m}(0) \cdot P/ms} \right\} \end{aligned} \quad (3.2.12)$$

The growth rate may be calculated if values for $p_A(1)$ and $p_A(0)$ are known.

For a given ratio $\mathcal{d}(1)$ of the components in the vapour at the source end of the capsule, the growth rate J varies very rapidly with temperature difference ΔT between the source and the crystal

while ΔT is fairly small. As ΔT becomes larger, the growth rate approaches a maximum value. The rapid rise in growth rate as ΔT increases from zero is brought about by a rapid fall in the partial pressure of the minority component over the crystal, and a corresponding rapid rise in the partial pressure of the majority component.

3.3 VISCOUS FLOW OF GAS

Viscosity is an important phenomenon in crystal growth from the vapour phase because in most crystal growth systems, there is some movement of the gas as a whole, and this movement of the gas as a whole will be subject to viscous forces. According to the laws of viscosity, the volume flow of gas in a tube is given by

$$V \propto \frac{a^4}{l} (P_1 - P_2) \quad (3.3.1)$$

where P_1 and P_2 are the pressures at the inlet and outlet ends of the tube, a its radius and l its length. The constant of proportionality is characteristic of the particular gas, and turns out to be a function of temperature but independent of pressure except at very low and very high pressures.

In a crystal growth system, diffusion is taking place at the same time as flow of the gas as a whole. This diffusion is the result of concentration gradients brought about by a change in equilibrium concentrations between two parts of the system at different temperatures. Let us consider the behaviour of a gas mixture flowing over a solid surface such as the walls of the apparatus or a substrate on which some material is to be deposited. Each component of the gas stream is travelling at a mean molecular velocity u_i specific to that component. When molecules of component i strike the apparatus walls, they are scattered randomly, and hence lose any net velocity. The number of molecules i leaving the wall is equal to the number arriving at the wall, and in consequence proportional to the mole density n_i . The diffusion flux at the wall causes a net momentum flow, unless the different components have the same molecular weight, since equal numbers of molecules leave the wall with a positive component parallel to it as with a negative component. This diffusion flux is the only flux at the wall, that the mole average velocity U is zero at the wall.

When a gas flows down a tube, work is done on the gas by the external pressure, and this work is partly dissipated by viscous drag at the walls of the tube and

is partly taken up as increased kinetic energy of the gas stream. The volume flow is given by

$$V = \frac{\pi a^4 (P_1 - P_2)}{8\eta l} \quad (3.3.2)$$

For the radial variation of the velocity

$$v = v_0 \left(1 - \frac{r^2}{a^2} \right)$$

where v_0 is the velocity at the centre of the tube. This shows that the velocity profile across the tube is parabolic, being zero at the wall.

3.4 CONVECTION

Convection is the motion of macroscopic regions or parts of a fluid, and is to be contrasted with diffusional motion, in which individual atoms or molecules are concerned.

Consider a sealed ampoule system in a vertical furnace. Heat is applied to the vapour in the ampoule by electrical heating elements and heat is lost from the furnace down the middle towards the cold ends. Let there be a small lateral temperature gradient in the furnace, as well as primary vertical gradient which is imposed to provide the driving force for growing the crystal. This lateral gradient can of course, be reduced by the use of heat reflectors. If conditions

are so arranged that convection sets in, the lateral temperature gradient may determine the flow pattern, with the slightly hotter gas near the perimeter rising, and the cooler gas in the middle of the ampoule falling. The convective velocities will be determined by a balance of the work done by buoyancy forces and work done against viscous forces.

In horizontal furnaces, there is usually no driving force for convection except for the small temperature gradient across the furnace tube. This arises because heat is fed in from the perimeter and lost down the middle to the ends.

The effect of convection on transport in a sealed, vertical ampoule or similar system depends on the relative magnitude of the convective velocity and the Stefan velocity. The Stefan velocity is proportional to the transport rate, and for a given temperature difference ΔT we can make the rate large (by reducing the amount of inert gas or stoichiometric excess) or small (by the reverse processes). If the Stefan velocity is very large compared with the convective velocity, the effect of convection on the velocity distribution and on the variation of composition in the vapour can be ignored. If the transport is very slow, the convection effects will dominate.

3.5 GROWTH BY PHYSICAL VAPOUR TRANSPORT (PVT)

Physical vapour transport (PVT) method of growth is applicable to materials which have appreciable vapour pressure at the concerned growth temperature. In this method, the compound to be grown is vapourized from a polycrystalline or elemental source which is kept at a high temperature. The vapours are transported down a temperature or pressure gradient and deposited at the comparatively cold growth end of the ampoule or on the substrate or the seed crystal. Single crystals obtained from the physical vapour transport have much purity than that grown using transporting agent. Obvious examples of vapour transport method for the preparation of thin films are the vacuum evaporation and sputtering techniques.

By PVT method single crystals can be grown directly from solid to vapour and back again to solid. The growth is performed in vacuum. The temperatures of the growth zone and the source zone should be controlled accurately to minimise surface irregularities of the growing crystal. To obtain large and good quality crystals, a linear temperature gradient should be ensured along the length of the ampoule. In most cases horizontal two zone furnaces are used. Temperatures of each zones are controlled separately using programmable temperature controllers.

Travelling containers or heaters have also been used satisfactorily for the growth of bulk crystals by PVT method. This is the Piper and Polich /3/ method. In this method, the charge is placed in one end of a silica tube and slowly pulled through a horizontal furnace whose temperature profile has a single peak. The ampoule can either be sealed off prior to growth or, can have a loose fitting plug in the end or a small orifice in the side. In order to prevent ingress of any undesirable impurities, the outside of the open capsules must be purged with an inert gas. Once transport takes place the capsule generally seals itself off. This can be prevented by having the orifice hotter than the charge and therefore remaining open throughout the run. The orifice can then either act as a sink for volatile material that comes off or it can act as a source of excess of one of the constituents. This can help to grow the crystal under known partial pressures /4,5/. If there is not a significant over pressure of one of the constituents, the capsule should be back-filled with an inert gas to introduce a diffusion limiting step in the reaction to prevent too rapid growth.

According to Nitsche et al /6/ the following rules must be obeyed for the successful growth of crystals by vapour transport techniques.

1. The rate of transport must not exceed the rate of growth of the seeds.
2. The crystallization chamber should be large in order to prevent inter growth between adjacent seeds.
3. The temperature distribution in the crystallization chamber should be as uniform as possible to avoid partial re-evaporation of already grown crystals.
4. Well developed crystals form more easily in large diameter tubes, where transporter convection determines the rate of transport.
5. The temperature difference between the reaction and growth chambers can be made smaller when wider tubes are used, since the gas flow is here the rate determining parameter.

References

1. M. Krulfeld, Mater. Res. Bull. 2 (1967) 337.
2. J. Stefan, Annalen der Physik und Chem. 17 (1890) 550.
3. W.W. Piper and S.J. Polich, J. Appl. Phys. 32 (1961) 1278.
4. L. Clark and J. Woods, J. Crystal Growth 3/4 (1968) 127.
5. P.D. Fochs, W. George and P.D. Augustus, J. Crystal Growth 3/4 (1968) 122.
6. R. Nitsche, H.U. Bolsterli and M. Lichtensteiger, J. Phys. Chem. Solids 21 (1961) 199.

CHAPTER - IV

EXPERIMENTAL TECHNIQUES4.1 FABRICATION OF THE FURNACE

For the growth of crystals by vapour transport method, a horizontal linear gradient two zone furnace was used. The furnace core consisted of a ceramic tube of about 50 cm length and 4 cm inner diameter. Two specially made 15 cm long ceramic tubes with regularly spaced inner grooves for the heater winding, which will go over the furnace tube, was used as the heater. This allowed the adjustment of the relative positions of the zones, so that a linear temperature gradient could be maintained between the high temperature and low temperature zones. Kanthal A1 wire of 22 SWG was used for the heater windings. The length of the kanthal heating element was so chosen that 230 V AC could be applied to the coils without the coils getting damaged. The furnace tube and the independent heater assemblies were insulated using a 3 cm thick asbestos rope winding. The whole assembly was covered using a MS outer jacket. This protected the asbestos rope windings and also acted as a heat reflector. When approximately 4 amps of current was flowing through the heaters, a maximum temperature of 1000° C was achieved.

4.2 TEMPERATURE CONTROLLER

To control the temperature of each zones of the furnace with $\pm 1^\circ\text{C}$ accuracy, proportional temperature controllers were used. The details of the temperature controller fabricated for this purpose are given below.

The proportional temperature controller was constructed by combining an integrated circuit (IC) differential amplifier with a triangular wave generator, and a microvoltmeter. The circuit diagram of the temperature controller is shown in figure 1. A chromel-alumel thermocouple which gives $40\ \mu\text{V}/^\circ\text{C}$ is used as the sensor. The thermocouple voltage V_{TC} is mixed with a standard DC voltage V_{SP} , whose magnitude is equal to the output of the thermocouple at the required temperature. The resultant error signal is amplified by the microvoltmeter. The recorder/meter output of the microvoltmeter is usually floating and hence a differential amplifier with a high input impedance is used for further amplifying the signal as shown in the figure. The amplification of the differential amplifier is given by

$$V_E = (R_3/R_1) \frac{(R_1 + R_F)}{(R_2 + R_3)} V_2 - (R_F/R_1) V_1 \quad (4.2.1)$$

where V_E is the output voltage of the differential amplifier, V_2 is the input voltage at the non-inverting

input and V_1 is the input voltage at the inverting terminal. When $R_1 = R_2$, $R_3 = R_F$, then the amplifier output V_E is given by

$$V_E = (R_F/R_1) (V_2 - V_1) = (R_F/R_1) V_R \quad (4.2.2)$$

where $V_2 - V_1 = V_R$ is the meter output.

The amplified output is passed through a voltage follower for isolating the amplifier from the next stage, which is a comparator. The output of the voltage follower together with a triangular wave of frequency 0.1 Hz, 1.2 V peak to peak is fed to the negative input of the comparator. The heater is ON when the resultant of the input to the comparator is positive and OFF when the resultant is negative.

The set point voltage V_{SP} is generated using a highly stable voltage given by 7805 IC. This voltage is divided by a chain of resistors and a 10 turn helical potentiometer. By this means, it is possible to obtain any voltage between 0 and 50 mV with an accuracy of $5 \mu V$. A standard circuit is used for generating the triangular wave. The period of the wave in seconds is given by

$$T = 4C R_{10} R_9/R_{11} \quad (4.2.3)$$

Working of the temperature controller.

V_{TR} is the triangular wave generated. When the set point voltage V_{SP} is turned up, V_E goes positive, so $V_E > V_{TR}$ and the power to the heater is completely ON. As V_{TC} rises, V_E decreases and when V_E is slightly less than the positive peak of V_{TR} , the average power to the load is t_{ON}/T , where t_{ON} is the ON time of the heater and T is the period of the triangular wave. The temperature stabilizes for a value of V_E within the proportional band

$$V_{TR \max} < V_E < V_{TR \min} \quad (4.2.4)$$

D_1 , D_2 , R_6 and R_8 form a limiting circuit to keep V_{OUT} in the range permissible for switching the transistors. The value of R_5 may be varied to control the width of the proportional band. When $R_5 > R_4$, the proportional band is increased and when $R_5 < R_4$, the proportional band is decreased.

The temperature can be set by setting the standard voltage V_{SP} equal to the output of the thermocouple at the desired temperature and this can be read on the appropriate range of the microvoltmeter. As the temperature of the furnace is increased, the sensitivity of the microvoltmeter is increased in steps and when the

temperature of the furnace is close enough to the set point, the microvoltmeter is put into its most sensitive range. An Anadigi precision microvoltmeter model AD 7020 is used. This meter has $100\ \mu\text{V}$ as full scale in its most sensitive range and a floating recorder output of 100 mV. The accuracy of the temperature controller is better than $\pm 1^\circ\text{C}$ in the 1000°C range of temperature.

4.3 AMPOULES AND PRE-TREATMENT

For the sample preparation, evacuated closed ampoules of fused quartz of 18 mm inner diameter and about 17 cm length were used. One end of the ampoule was closed and the other end was uniformly constricted to allow for sample introduction and easy sealing. In order to reduce the large number of nucleation sites in the ampoule, the quartz tubes were cleaned thoroughly by washing first with detergent soap solution, then kept in aquaregia for two to three hours, and then washed and cleaned ultrasonically several times with doubly distilled water and acetone.

Fusing of ampoules.

In physical and chemical transport methods of crystal growth, the transporting of the reactants from the hot zone to the cold zone is done at a low pressure

of $\sim 10^{-5}$ Torr in a closed ampoule. Prior to the sealing of the ampoule containing the reactants, the ampoule must be evacuated to this low pressure and also the low pressure should be maintained at the time of sealing the ampoule. For this an adaptor with provision for connecting the neoprene tube to the ampoule and a penning gauge head for pressure measurement was fabricated and was fixed to the base plate of a vacuum coating unit. This assembly is shown in figure 2.

The initially cleaned quartz tube was connected to the vacuum system and evacuated to $\sim 10^{-5}$ Torr. The ampoule was then flame heated from outside to red hot for 30 minutes. This was to remove surface impurities from the growth end of the ampoule and to reduce surface irregularities of the quartz wall. After cooling, the ampoule was disconnected from the vacuum system and the ampoule was filled with the stoichiometric amount of the reactant materials. The ampoule with the elements was reevacuated to a pressure of 10^{-5} Torr. The lower end of the ampoule was kept in a freezing mixture to avoid the sublimation of materials during fusing. After attaining the final pressure, the ampoule was sealed at the constriction.

The sealed ampoule was then placed in the two zone linear gradient horizontal furnace. Prior to

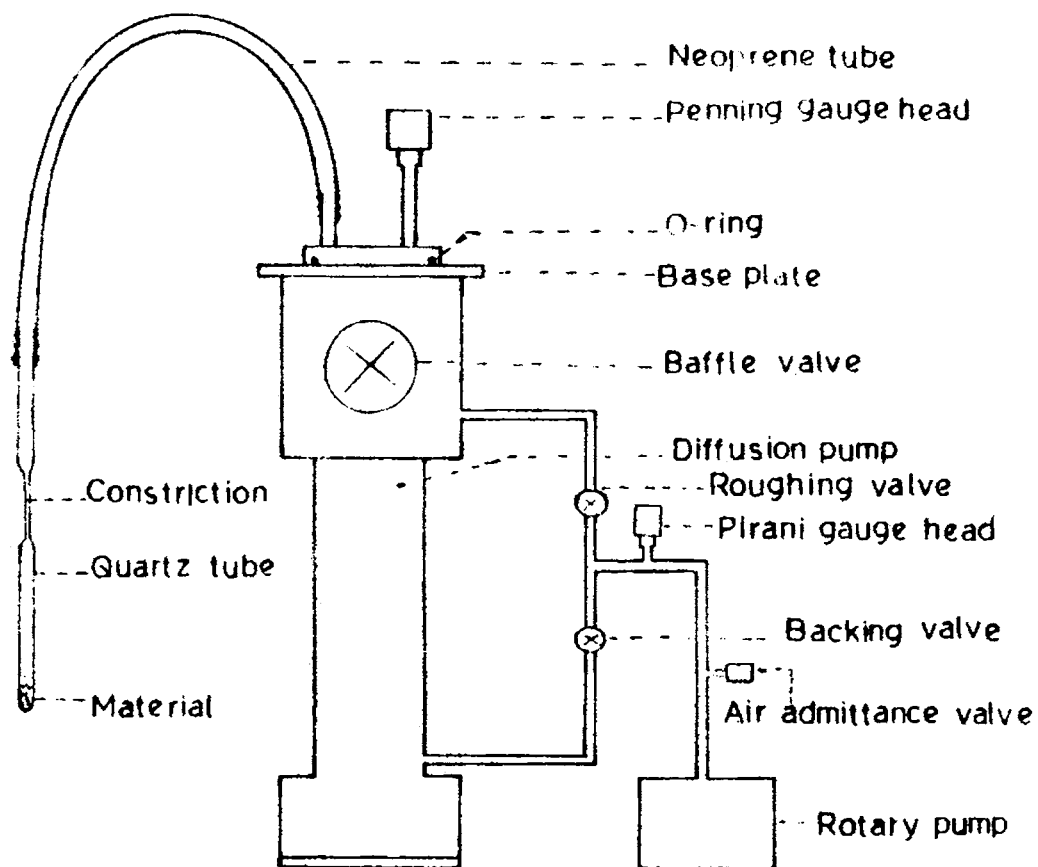


Fig.2. Vacuum system for fusing the ampoule.

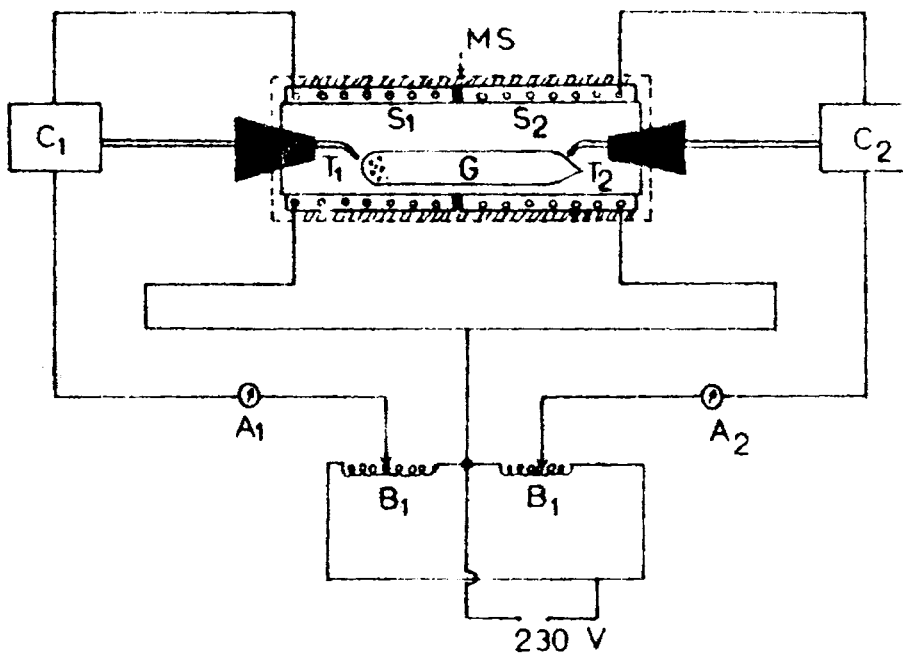


Fig.3. Experimental setup for the growth of crystals by PVT method. C₁, C₂ - Temperature controllers, T₁, T₂ - Thermocouples, S₁ - Source zone, S₂ - Growth zone, G - Ampoule, MS - Mild steel outer jacket, A₁, A₂ - Ammeters, B₁, B₂ - Autostats.

the actual growth, a reverse temperature gradient was applied such that the source region was at a temperature lower than the condensation zone. After two to six hours of this reverse transport, the traces of starting material at the growth zone would be removed. The system used for the crystal growth is shown in figure 3. For the growth process, the charge and was at the higher temperature side and the growth end at the lower temperature side. The temperatures of each zones were controlled with an accuracy of $\pm 1^{\circ}\text{C}$ using independent temperature controllers. After a growth time of 50 - 200 hours, platelet like crystals were obtained.

4.4 OPTICAL MICROSCOPY

The elementary molecular growth features are the ideally simple features which are easily interpreted by theory and reveals considerable information about the mechanism of crystal growth. Optical microscopy is one of the best suited method for observing crystal surfaces. From the growth patterns observed, the dislocation mechanism involved in crystal growth can be obtained.

For the observation of the as grown surfaces of the crystal under reflection, a Carl-Zeiss epityp II metallurgical microscope was used. Crystals with good

plane surfaces were used for the morphological studies. Thin and very small specimens were mounted on microscopic slides by small dots of adhesive. The disadvantage of this method is that only one side of the specimen can be observed. For observing both surfaces of the crystal, a plate was made with a circular hole and the crystal was placed above this hole. By using this technique, both sides of the crystal could be observed. For observing faint features on the crystal surface, the surface was given a reflecting coating of aluminium by vacuum evaporation.

4.5 DETERMINATION OF OPTICAL CONSTANTS

The determination of refractive index and absorption coefficient as a function of wavelength can give considerable information about the band structure of a solid. The usual methods used to measure the optical constants as a function of wavelength are transmission measurements, normal incidence reflectance accompanied by the use of dispersion relations and spectroscopic ellipsometry. Since ellipsometric measurements are applicable only in the regions of wavelength where polarisers and analysers are available, reflection and transmission measurement is the best practical method to obtain refractive index and absorption coefficient.

If the specimens under study are in platelets or in thin film form, it is possible to determine the spectral dependence of refractive index in the region of transparency by observing interference fringes by transmission or reflection.

At normal incidence, the fraction T of the incident light intensity of wavelength λ , transmitted through a plane parallel crystal of thickness d and refractive index n is given by /1/

$$T = \frac{(1-R)^2 (1 + k^2/n^2)}{\exp(\mathcal{C}d) - R^2 \exp(-\mathcal{C}d) - 2R \cos 2(\Psi + \Upsilon)} \quad (4.5.1)$$

where the absorption coefficient \mathcal{C} is related to the absorption index k by

$$\mathcal{C} = \frac{4\pi k}{\lambda} ; \quad R = \frac{(n-1)^2 + k^2}{(n+1)^2 + k^2}$$

$$\Upsilon = \frac{2\pi nd}{\lambda} , \quad \Psi = \tan^{-1} \left(\frac{2k}{n^2 + k^2 - 1} \right)$$

On the long wavelength side of the absorption edge, where \mathcal{C} is small, the spectral variation of T (equation 4.5.1) shows successive maxima and minima due to interference. The condition for a transmission maximum is $2nd = p\lambda$, where p is the fringe order. If the fringe

number can be unambiguously determined by detecting the first fringe, the refractive index of the crystal for different wavelengths can be calculated using the equation $n = p\lambda/2d$. Thickness of the crystal may be accurately measured using a micrometer. On the other hand if refractive index is known, thickness can be determined from the interference spectra using the relation $d = \frac{(\Delta m \lambda_1 \lambda_2)}{2n (\lambda_1 - \lambda_2)}$, where Δm is the number of fringes in between two maxima (minima) λ_1 and λ_2 .

In the absorption edge region where $n^2 \gg k^2$, $1 + k^2/n^2$ can be approximated to unity. If no interference fringes are present, equation (4.5.1) reduces to

$$T = \frac{(1 - R)^2}{\exp(\alpha d) - R^2 \exp(-\alpha d)} \quad (4.5.2)$$

and from this expression, absorption coefficient can be calculated.

For the measurements in the UV - Vis. region, a Hitachi 200 - 20 UV - Vis. spectrophotometer was used. This instrument can cover the wavelength range from 900 nm to 200 nm with a light source change at 370 nm. For the measurements in the NIR region, a Cary 17D double beam spectrophotometer which could cover the range from 200 - 3500 nm was used. For the IR measurements a

Beckmann IR - 20 spectrophotometer was used. Measurements were made in the transmission mode. After switching on the spectrophotometer, 15 minutes were given for warm up of the instrument before taking the spectra. For the high resolution absorption edge measurements a spectral band width of 0.1 nm was used. Data was taken manually at 1 nm interval with an accuracy of 0.1% in transmission. Base line of the spectrophotometer was also recorded manually and the ratio between the observed transmission and the base line was taken as the true transmission. For other measurements a spectral band width of 1 nm was used. A computer (ECIL, micro 78) was used to process the data.

4.6 DETERMINATION OF CONDUCTIVITY TYPE

Hot probe method is a simple and convenient test to identify the type of carriers present in a semiconductor. This is based on the thermoelectric properties of a semiconductor. This method is practicable even when Hall effect measurements are difficult to make.

The distribution of thermal velocities of the charge carriers in a small region of the semiconductor will depend on the temperature of that region. If the crystal is heated with the hot probe, charge carriers near the hot probe have higher velocities than those

near the cold probe. This disturbance in the equilibrium distribution of charge carriers produces an electric field. The field will be positive with respect to the cold end if the charge carriers are electrons (n-type) and negative if the carriers are holes (p-type).

To test the type of conductivity of the crystals grown, one probe of a digital multimeter was heated, and both probes were made to touch the crystal. The deflection of the meter was noted to determine the type of the conductivity of the crystal.

4.7 MEASUREMENT OF HALL VOLTAGE

Hall effect measurement give the carrier concentration and the type of current carriers present in the crystal. These results together with the knowledge of the conductivity of the specimen can be used to determine the mobility of the charge carriers. If the crystal is small and the shape is irregular, ordinary Hall effect measurement techniques are impracticable. In such cases van der Pauw's technique /2/ is very effective.

For the measurement of resistivity and Hall effect perpendicular to c-axis by van der Pauw's technique, current through the specimen was kept below 1 mA and was measured using a digital multimeter

(Pla, model DM - 14B). A Hewlett-Packard 3465 A digital multimeter which has a resolution of $1\ \mu\text{V}$ was used to measure the voltage developed across the specimen. A magnetic field of 0.3 tesla was used for the measurements.

The specimens were mounted on an etched PCB. The contacts made to the specimen should be ohmic in nature. Four contacts were pressed to the crystal using tin or indium. The whole setup is then heated to the melting point of the contact metal and kept at that temperature for some time and then the system is allowed to cool. Because of this temperature treatment, alloying of the metal with the crystal take place, which ensures good ohmic contacts.

4.8 MEASUREMENT OF ELECTRICAL PROPERTIES USING MIM STRUCTURES

Conductivity measurements as a function of temperature can give informations about the levels in the forbidden gap and also the value of the band gap in certain cases (in the intrinsic region). Since the thickness of layered platelet like crystals was usually a few microns, MIM structures were used to measure the conductivity parallel to c-axis (perpendicular to the layers). Using MIM structures, the conduction mechanism involved in the crystals, trap concentration, carrier

concentration, position of the Fermi level etc. can be evaluated.

To study the electrical properties parallel to c-axis, a specially made jig and an evacuated all-metal cell was used. The setup is shown in figure 4. The measurements were made in a vacuum of 10^{-2} Torr and all the electrical insulations in the cell and the jig were made of teflon. The cell has provisions for heating and temperature measurements. Chromel-alumel thermocouples were used to measure the temperature.

The contacts made on the crystal should be ohmic in nature and these were made by vacuum evaporation of suitable metals (Al or Sn). For this, crystals were placed over suitable masks in the vacuum system. The metal to be evaporated as the electrode was taken in a molybdenum boat or tungsten filament and evaporated on to the specimen at a vacuum of 10^{-5} Torr. The resulting metal-semiconductor-metal system was placed in the jig and measurements were made. Current was measured using a digital picoammeter (ECIL, model EA 5600) and the voltage using a digital multimeter (HP, model 3465 A).

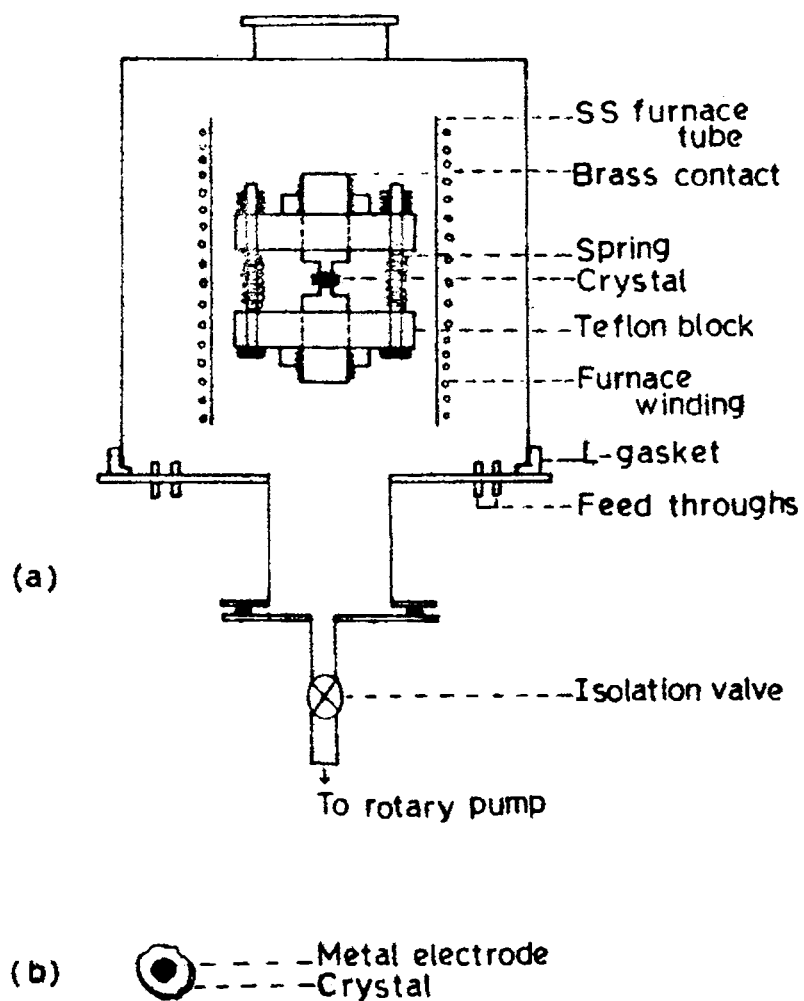


Fig.4.(a) Cell for electrical measurements.

(b) A typical specimen.

Current and voltage were measured with an accuracy of 0.5%. Sufficient time was given for the current reading to stabilize and extreme care was taken to avoid specimen heating due to current flow.

References

1. J.A. Stratton, Electromagnetic theory, (New York; McGraw Hill) 1941.
2. L.J. van der Pauw, Philips. Res. Repts. 13 (1958) 1.

CHAPTER - V

GROWTH AND MORPHOLOGY OF TIN DISULPHIDE CRYSTALS

Crystals of tin disulphide are usually grown by vapour transport methods /1-9/. The technique for growing single crystals with layered structures have been described by Levy /9/ and he has grown SnS_2 crystals with and without using the transporting agent. Mikkelsen /10/ has grown these crystals by Bridgmann-Stockbarger method and has obtained bulk crystals with higher purity. For the growth of tin disulphide by chemical transport method, all of the investigators had used iodine as the transporting agent. Crystals grown using transporting agent are usually contaminated by the incorporation of transporting agent. It has been found that the growth conditions of the crystals have a marked influence on their properties. Good quality crystals are obtained when growth is performed without using the transporting agent. One of the most striking features of crystals with layered structures is the existence of screw dislocations with Burgers vector perpendicular to the plane of the layers giving rise to growth spirals. Bletskan /6/ and Mitchell /8/ have reported growth spirals on SnS_2 crystals but no systematic study of their growth morphology have been made. In this

chapter the growth of tin disulphide by physical vapour transport method and their morphological studies are presented.

5.1 CRYSTAL GROWTH

Tin disulphide single crystals were grown by the physical vapour transport method. For the growth process quartz ampoules of 17 cm length and 1.6 cm diameter were used. Stoichiometric amount of tin (99.999%) and sulfur (three times recrystallised from solution) were sealed in pre-cleaned ampoules at a final pressure of 10^{-5} Torr. The ampoules were placed in a two zone linear gradient furnace. Before starting growth, a reverse temperature gradient was applied such that the source region is at a lower temperature than the condensation zone. After one to three hours in a reverse temperature gradient, any traces of starting material in the growth zone are removed. Figure 1 shows the temperature profile of the furnace used for the crystal growth. The source temperature was maintained at $T_1 = 700^\circ \text{C}$ and the growth temperature at $T_2 = 630^\circ \text{C}$. Temperature of the zones were controlled with an accuracy of $\pm 1^\circ \text{C}$ using temperature controllers as described in chapter IV. After a growth period of 40 - 150 hrs., golden yellow platelet like crystals of 2 cm^2 area and 10 - 60 μm thickness were obtained.

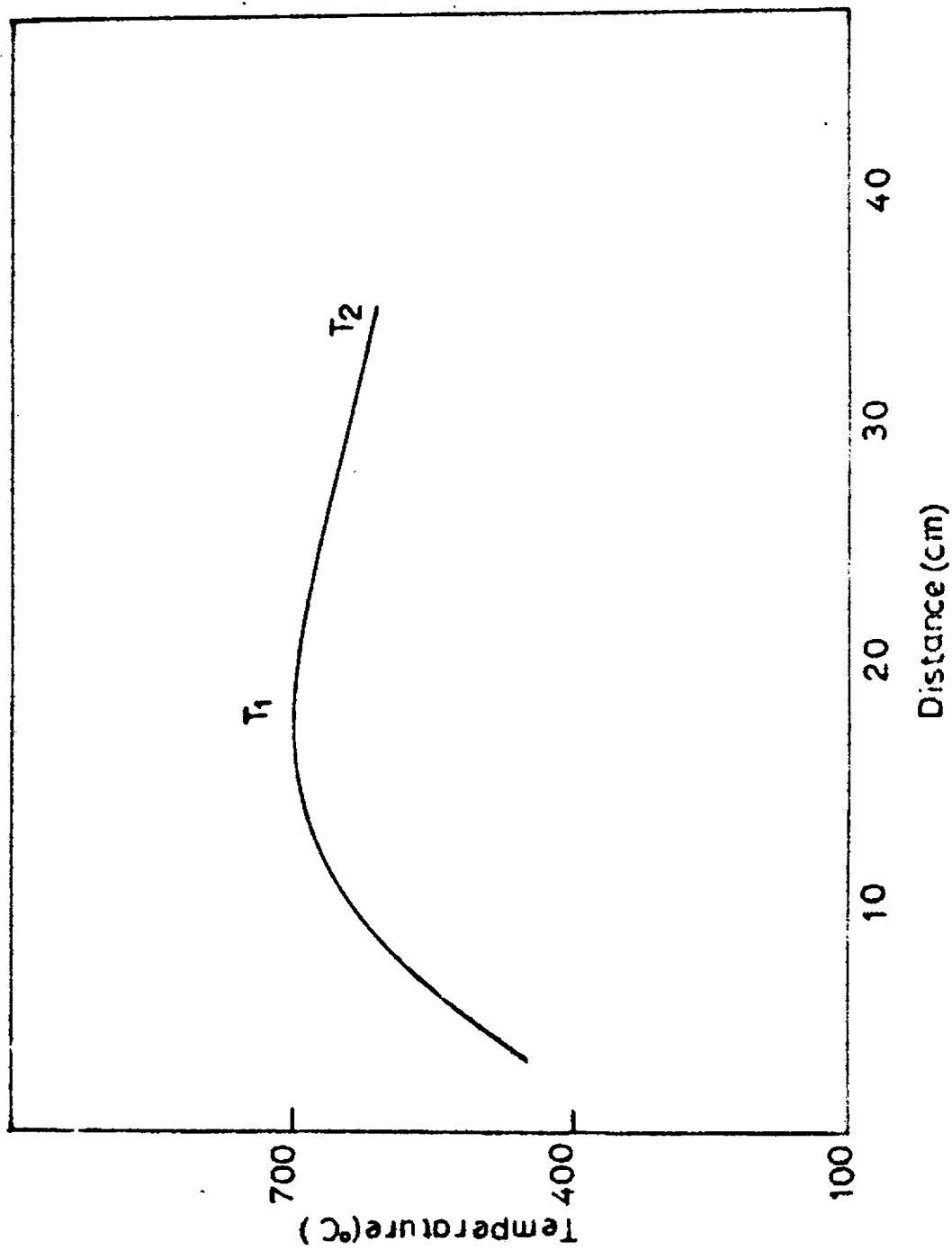


Fig.1. Temperature profile of the furnace used for the growth of SnS_2 crystals.



Crystals with good plane surfaces were used for the morphological studies. The as grown surfaces of the crystals were observed in reflection as described in Chapter-IV.

5.2 RESULTS AND DISCUSSIONS

The theory of crystal growth in presence of screw dislocation mechanism has been developed by Burton, Cabrera and Frank /11/. When a single screw dislocation emerges on the face of the crystal, a molecular ledge will run from the point of emergence on the crystal surface, to the boundary of the face. When the supersaturation of the vapour in contact with the crystal is raised to a certain critical value, growth will start and the ledge will curl up and form a spiral. Frank /12/, Cabrera and Levine /13/ have shown that if a Burgers vector of a dislocation becomes relatively high, a cylindrical hollow core will be developed around the dislocation. Cabrera and Levine generalised the BCF theory by introducing the influence of the strain energy around the dislocation. According to this a hollow core could develop due to the stress and from the hollow core a spiral step emerges. Hollow cores are developed in the centre of dislocations with Burgers vector larger than 10 \AA . Hollow core at the centre of a growth spiral had been reported by many authors /14.17/.

Beautiful circular and hexagonal spirals have been observed on all the tin disulphide crystals grown by the physical vapour transport method establishing that these crystals grow from the vapour phase by the screw dislocation mechanism. In vapour growth when the rate of advance of the ledge is independent of the crystallographic orientation, a rounded spiral will result. When the displacement velocity of the straight growth front varies with the orientation on the crystal face, polygonal spirals will result. A typical hexagonal spiral pattern with a central core is shown in figure 2. The hexagonal spiral pattern exhibits the symmetry of the tin disulphide crystal face. The distance between the successive turns of the spiral is constant. The step separation in this case is obtained as $30\ \mu\text{m}$. Since the step height of the spiral is very large, the spiral can be observed easily under ordinary reflected light.

Sunagawa and Bonnema /15/ have shown that when the step height of the spiral is very high, a hollow core is formed at the centre of the spiral and from the core, the step escapes with a change of curvature depending on the stress field. In figure 3 such a spiral pattern with a hollow core showing a clear change of curvature as the step leaves from the hollow core, observed on tin disulphide crystal is shown. The degree of the change of

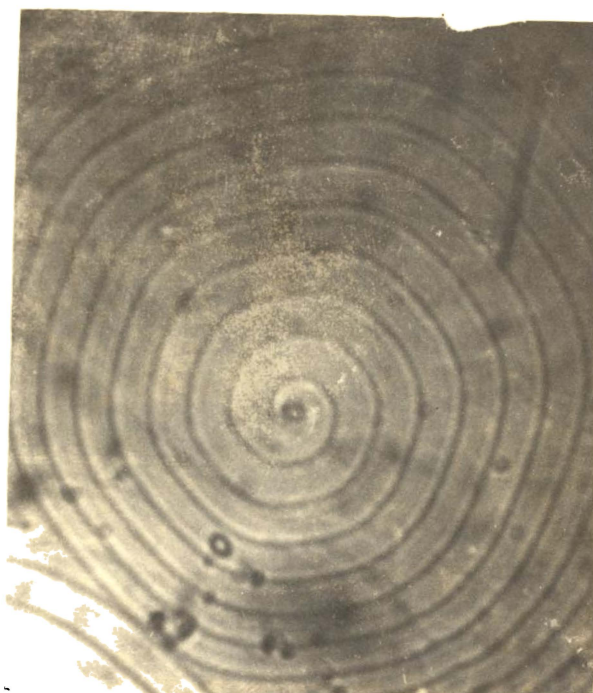


Fig.2. Hexagonal spiral observed on the as grown face of SnS₂ crystal. (x190)

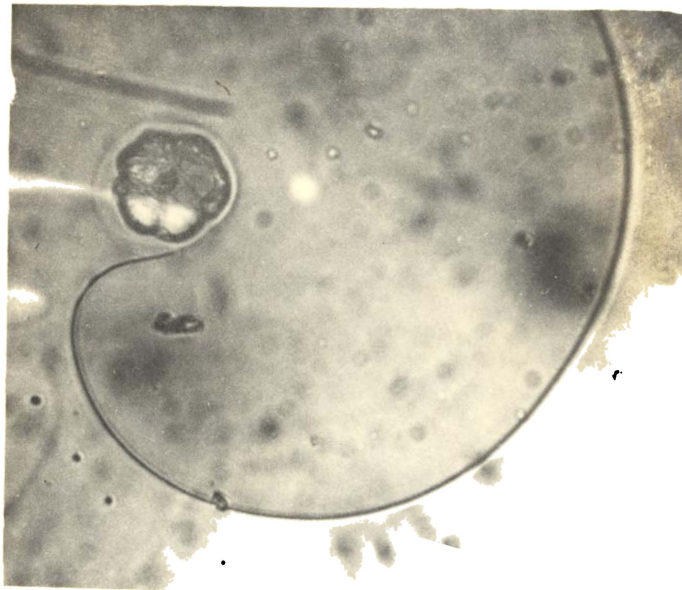


Fig.3. Spiral with hollow core at the centre showing a change of curvature of the spiral step. (x1000)

curvature varies depending on the stress field. Growth spirals showing such change of curvature at the centre has been observed on SiC and hematite crystals by Sunagawa and Bennema /15/. Figure 4 shows two growth spirals of opposite sign originating from two screw dislocations. It can clearly be seen that a spiral start from the centre of the hollow core marked A in the figure and another outer spiral layer originates from the point where the inner spiral meets the surface.

A hollow core with a closed loop around the central core is shown in figure 5, the spiral starting from the closing point of the loop. This closed loop may be the result of the interaction of two independent screw dislocations with their emergence points very close to each other. Figure 6 is a case where the hollow tube is partly closed. This may be created not as a result of the spiral growth but by an unfilled portion during growth. It can also be seen that this act as a source of screw dislocation resulting in spiral growth. Growth spirals without a central core have also been observed in SnS_2 crystals (figure 7). Here neither a hollow core nor a change of curvature is observed at the centre. This may be due to the higher supersaturation value which dominates the stress effect at the centre of the growth spiral. Figure 8 is a case in which three dislocation

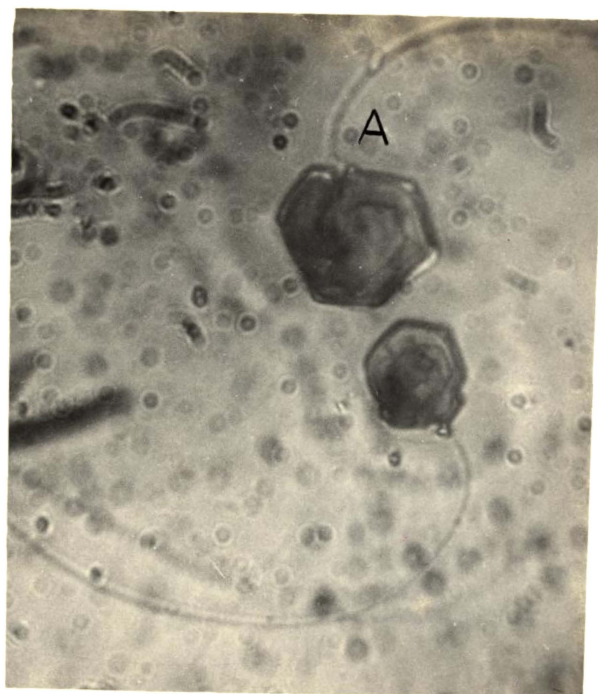


Fig.4. Inner spiral originating from the centre of the hollow core. (x 1500)



Fig 5. Spiral with a hollow core and a closed loop
around the core. (x1500)



Fig.6. Spiral with a partly filled hollow tube. (x1500)

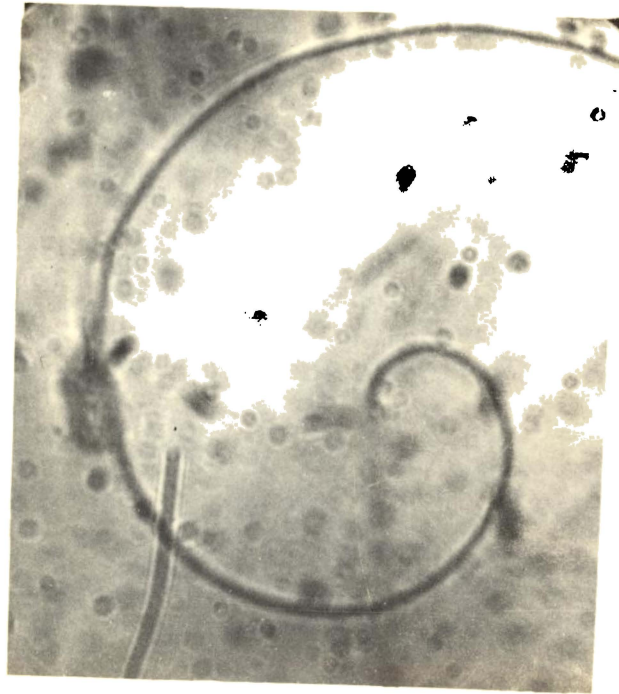


Fig.7. Spiral without a central core. (x1500).

of same strength and same sign originate from different emergence points. Two spirals show central cores at the emergence points of the dislocation. In this case, the ledges meet together, they fuse and annihilate each other over the common portion and successive closed loops are formed. The hyperbolic curve of intersection between the spirals are clearly seen.

Figure 9 shows the eccentric growth spirals observed on the basal plane of tin disulphide crystals. Originating from a single screw dislocation, this shows increasing wider separation towards the centre portion and narrower towards the base. The direction in which step separation becomes narrower is the direction towards the sides of the ampoule. At this portion, the temperature is higher than the centre portion and hence at a low supersaturation. The supersaturation increases towards the centre portion of the ampoule because of the lower temperature there, and the spiral step becomes more wider. Thus the reason for the eccentric shape of the spiral must be the anisotropy of environmental conditions such as supersaturation gradient over the surface.



Fig.8. Three spirals of same sign, originating from different screw dislocations. (x 190)



Fig. 9. Eccentric spiral due to the supersaturation gradient over the surface. (x190)

CONCLUSION

The growth spirals observed on basal surface of SnS_2 crystals indicate that the crystals are grown by the screw dislocation mechanism. The hexagonal spiral exhibits the symmetry of the unit cell of the tin disulphide crystals. Hollow core at the centre of the spirals are due to the stress field around the dislocation. The eccentric shape of the spirals observed are due to the supersaturation gradient over the surface.

References

1. D.L. Greenaway and R. Nitsche : J. Phys. Chem. Solids, 26 (1965) 1445.
2. G. Domingo, R.S. Itoga and C.R. Kannewurf, Phys. Rev. 143 (1966) 536.
3. P.A. Lee, G.Said, R. Davies and T.H. Lim, J. Phys. Chem. Solids 30 (1969) 2719.
4. M.J. Powell, J. Phys. C. **Solid State Phy.** 10 (1977) 2967.
5. S.G. Patil and R.H. Tredgold, J. Phys. D : Appl. Phys. 4 (1971) 718.
6. D.I. Bletskan, I.F. Kopinets, I.M. Migolinets and S.V. Mikulaninots, Neorgenicheskie Materially 12 (1976) 2142.
7. S. Acharya and O.N. Srivastava, Phys. Stat. Solidi (a) 56 KI (1979).
8. R.S. Mitchell, J. Crystal Growth 57 (1982) 273.
9. F. Levy, IL. Nuovo Cimento 38B (1977) 359.
10. Mikkelsen Jr., J. Crystal Growth 49 (1980) 253.

11. W.K. Burton, N. Cabrera and F.C. Frank, Phil. Trans. Roy. Soc., London A. 243 (1951) 299.
12. F.C. Frank, Acta. Cryst. 4 (1951) 497.
13. N. Cabrera and M.M. Levine, Phil. Mag. 1 (1956) 450.
14. A.R. Verma, Crystal Growth and Dislocations (Butterworths, London, 1953).
15. I. Sunagawa and P. Bennema, J. Crystal Growth 53 (1981) 490.

CHAPTER - VI

OPTICAL PROPERTIES OF TIN DISULPHIDE CRYSTALS

Optical absorption studies of tin disulphide have been reported by many authors. Optical studies were first reported by Greenaway and Nitsche /1/. They reported that tin disulphide is an indirect band gap semiconductor and the transition leading to fundamental absorption is an indirect allowed one at 2.21 eV. Domingo et al /2/ reported an indirect forbidden band gap value of 2.07 eV and a direct gap of 2.88 eV. Lee et al /3/ studied the optical properties of the solid solutions of tin disulphide and tin diselenide. They reported an indirect allowed transition at 2.22 eV. From the pressure dependence of absorption edge, Powell /4/ reported an indirect transition at 2.29 eV and a direct transition at 2.44 eV. From the electrical measurements, Acharya and Srivastava /5/ reported band gap values for different polytypes of SnS_2 crystals. It was found that band gap varied with polytype periodicity. Nozaki and Imai /6/ reported an indirect allowed transition at 2.14 eV. Absorption edge measurements of tin disulphide in thin film form has been carried out by George and Joseph /7/ and they also reported indirect allowed transitions at 2.21 eV and 2.31 eV.

In all these studies, the reported value of the band gap and the nature of the absorption edge transitions are found to be different. Such differences can possibly occur due to the presence of impurities, imperfections and the consequent free carrier absorption in the crystals used in the studies.

Theoretical band structure calculations have been made for tin disulphide crystals by the empirical pseudopotential method /8,9/. Murray and Williams /10/ calculated the band structure using the semi empirical tight binding method. The first principles pseudopotential band structure calculation was made by Mula and Aymerich /11/ and Powell et al /12,13/. These calculations showed similar features of the energy bands, but gave different results in the detailed ordering of energy levels and in the band profiles.

Photoconductivity measurements of SnS_2 crystals was reported by Domingo et al /2/, Patil and Tredgold /14/, Nakata et al /15/ and Bletskan et al /16/. All of them have reported a photoconductive peak at 2.30 eV. Generally the band gap value coincides with the photoconductive peak value. But in the case of SnS_2 , there is a disagreement in these two values. Only George and Joseph /7/ have correlated their band gap value obtained at 2.31 eV with the photoconductivity peak at 2.30 eV.

Optical absorption studies made by the previous workers have used a spectral band width of about 5 nm which gives an energy resolution of about 0.02 eV. This chapter presents high resolution absorption edge measurements of tin disulphide single crystals. For these measurements a spectral band width of 0.1 nm which gives an energy resolution better than 0.0005 eV was used.

6.1 EXPERIMENTAL

Single crystals of tin disulphide grown by vapour transport method were used for absorption edge measurements. The crystals were platelets of 0.5 x 0.5 cm and thickness around 100 microns. Cleaved crystals with good plane surfaces were selected for transmission measurements. For transmission measurements a Cary 17 D double beam spectrophotometer and a Hitachi 200 - 20 UV - Vis. spectrophotometer were used. All the measurements were carried out parallel to c-axis and at room temperature. Refractive index and absorption coefficient of the crystal was determined using equations as discussed in Chapter IV.

6.2 RESULTS AND DISCUSSIONS

The transmission spectra of a typical tin disulphide crystal is shown in figure 1. From the

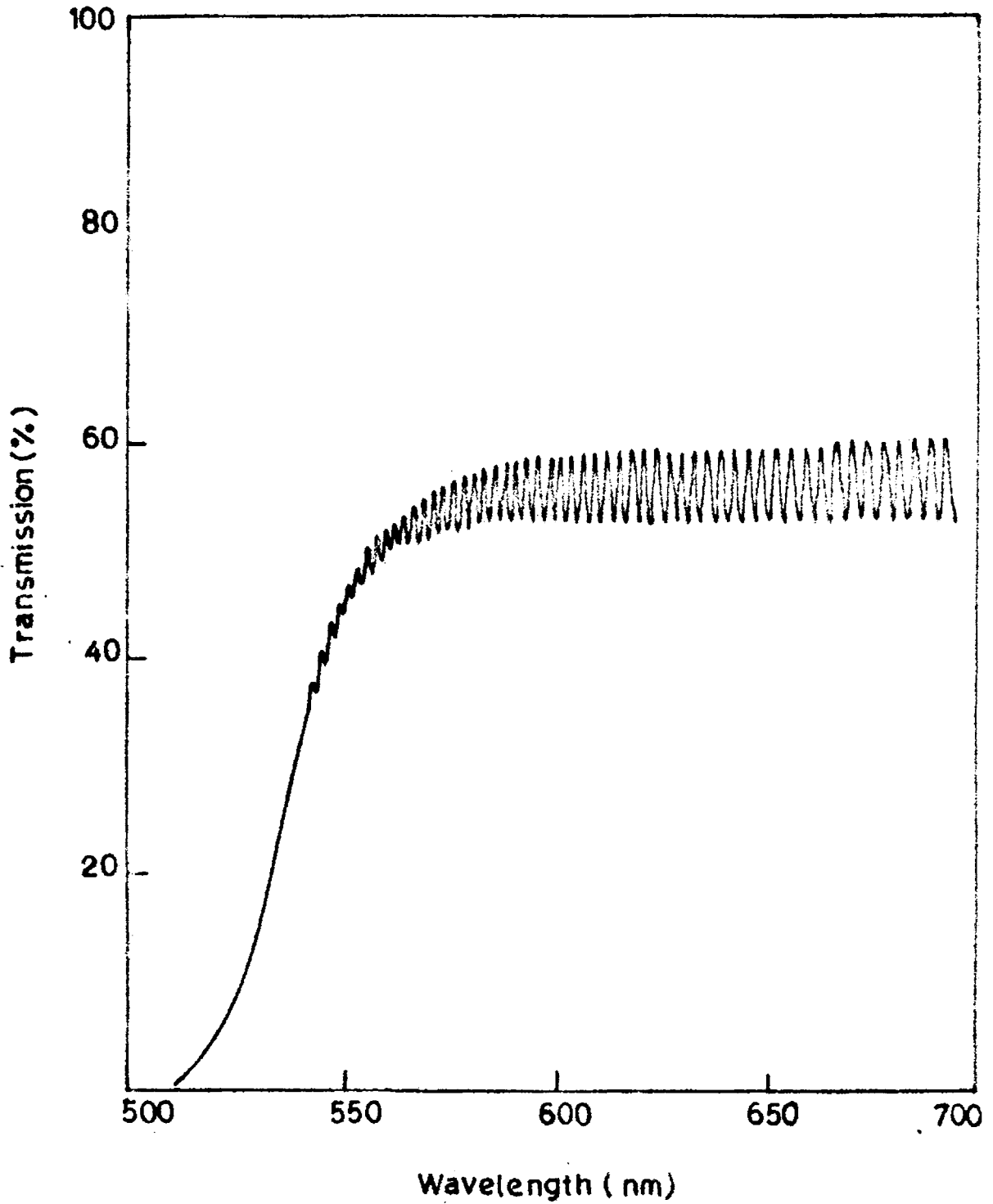


Fig.1. Transmission spectra of a typical tin disulphide crystal.

interference fringes obtained, refractive index was calculated and the variation of refractive index with wavelength is shown in figure 2. Although the value obtained by Domingo et al /2/ are slightly higher than the present value, there is good agreement with that of Lee et al /3/.

The crystals exhibit a wavelength independent absorption ($\alpha = 15 \text{ cm}^{-1}$) before the onset of band to band transitions. This wavelength independent part of the absorption coefficient was subtracted from the total absorption to obtain the absorption coefficient due to fundamental absorption. The variation of absorption coefficient with photon energy is shown in figure 3. It can be seen that the absorption begin around 1.90 eV, shows a shoulder and then increases rapidly. This shoulder is due to the presence of ionized donor impurity levels just below the conduction band. Unlike the exciton absorption which occurs between a discrete level and the well defined edge of a band, a transition between an impurity and a band should manifest themselves by a shoulder in the absorption edge. This occurs at a threshold value lower than the energy gap by an amount E_i , where E_i is the energy value of the impurity level /17/. The absorption coefficient for transitions involving the impurity levels covers a much smaller range than the transitions

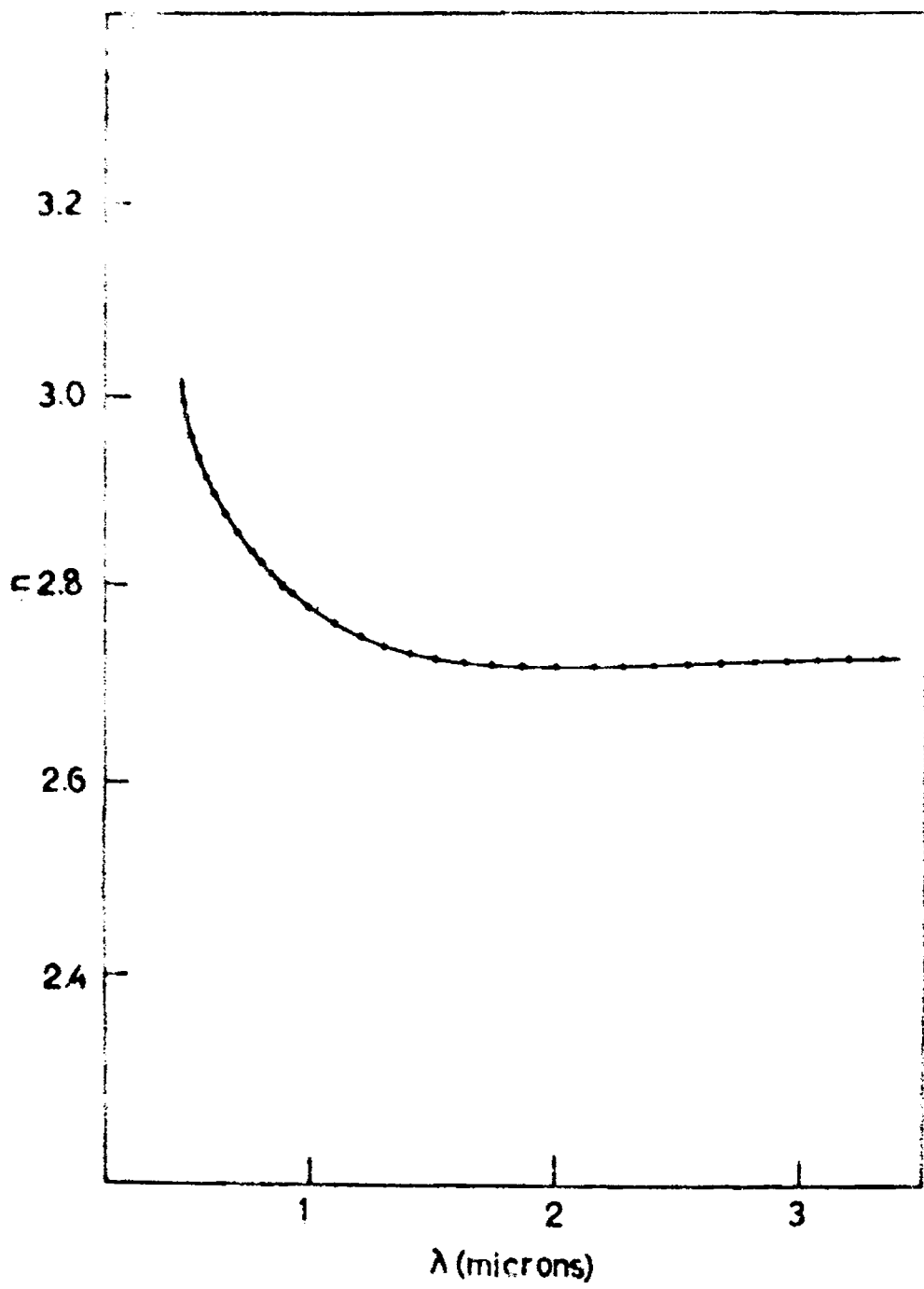


Fig. 2. Variation of refractive index with wavelength.

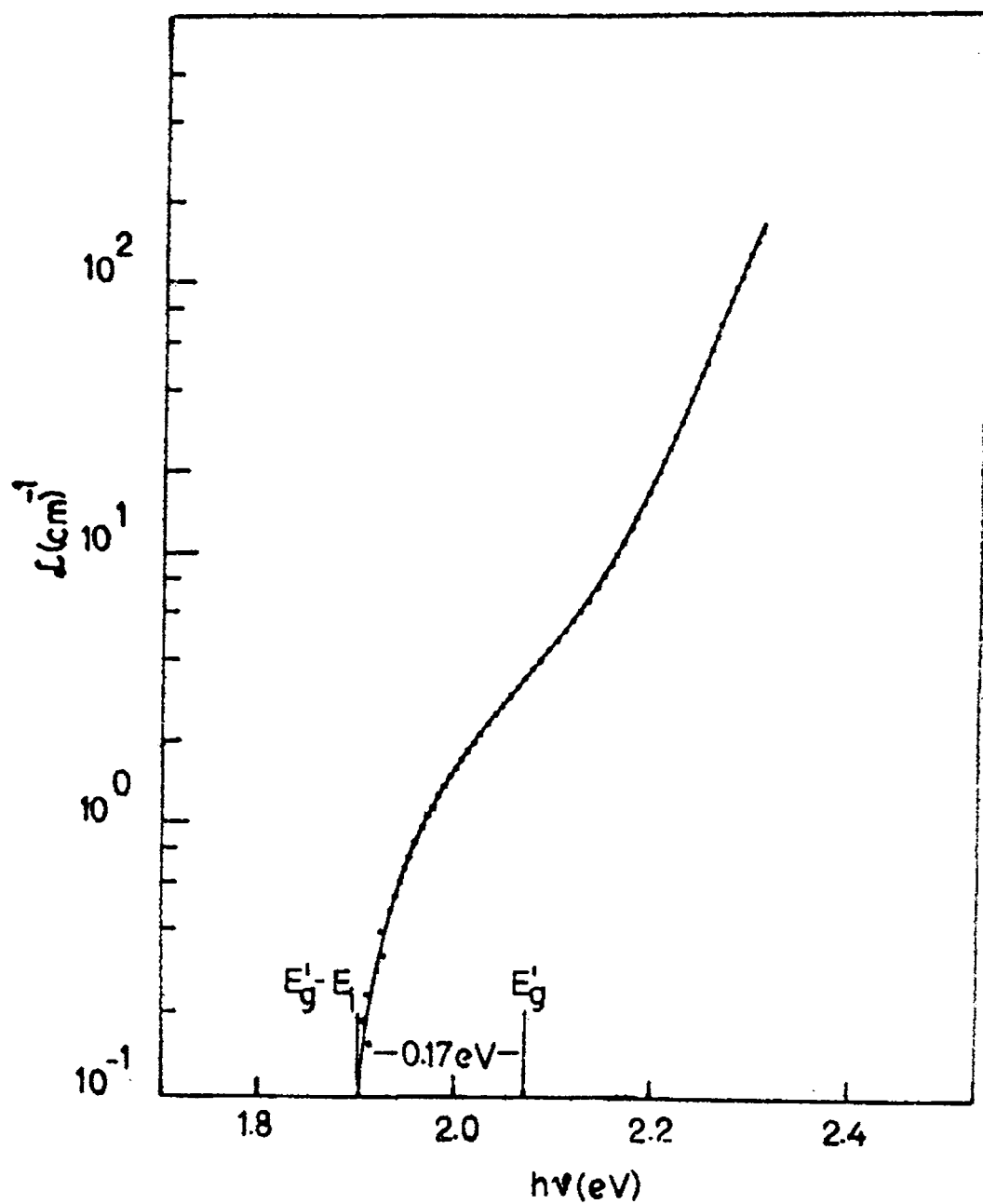


Fig.3. Absorption coefficient α versus photon energy $h\nu$. E_g^i is the indirect band gap and E_i is the impurity level.

between valence band and conduction band because the density of impurity states is much lower than the density of states in the bands. From the absorption data (see figure 3) the energy value for the impurity level is obtained as 0.17 eV. From the electrical conduction studies, Said and Lee /18/ reported the values of impurity levels in tin disulphide as 0.40 eV, 0.11 eV and 0.05 eV. Recently George and Joseph /19/ has reported that in tin disulphide thin films, two donor levels exist at 0.20 eV and 0.25 eV below the conduction band. These are due to the presence of doubly ionizable sulphur vacancies in the films. The crystals we studied also exhibit n-type conductivity and it may possibly due to the presence of sulphur vacancies which act as donor impurities as in the case of thin films.

Exciton spectra at room temperature was observed before the fundamental absorption in GaSe by Bassani et al /20/ and in InSe by Piacentini et al /21/ which are layer compounds like tin disulphide. In order to distinguish between exciton absorption and impurity absorption, the infrared spectra of the crystals by the KBr pellet process was taken. This, as expected showed a broad absorption band starting from 7 microns (0.177 eV) to 16 microns which was the limit of the IR spectrophotometer used. This is certainly due to transitions from

unionized donor impurity levels to the conduction band. It can be seen that the impurity level obtained from the IR spectra (0.177 eV) agrees very well with that obtained from the fundamental absorption data (0.17 eV).

The fundamental absorption data was analyzed in terms of the theory of Bardeen et al /22/ which gives for an indirect transition

$$\alpha = \frac{A (h\nu - E_g' + E_p)^r}{h\nu}$$

where E_g' is the indirect band gap; $h\nu$ is the photon energy and E_p is the energy of the absorbed (+) or emitted (-) phonons. If $r = 2$, the transition is allowed and if $r = 3$, the transition is forbidden.

The plot of $(\alpha h\nu)^{1/3}$ versus $h\nu$ is given in figure 4. Absorption coefficient was obtained after subtracting the impurity contribution assuming that it obeys a law of the form

$$\alpha = B (h\nu - E_g' - E_i)^{1/2}$$

where B is a constant /23/. It has been previously reported that both $(\alpha h\nu)^{1/3}$ and $(\alpha h\nu)^{1/2}$ gives a straight line /1-4/. The previous authors have not subtracted out the wavelength independent part of the

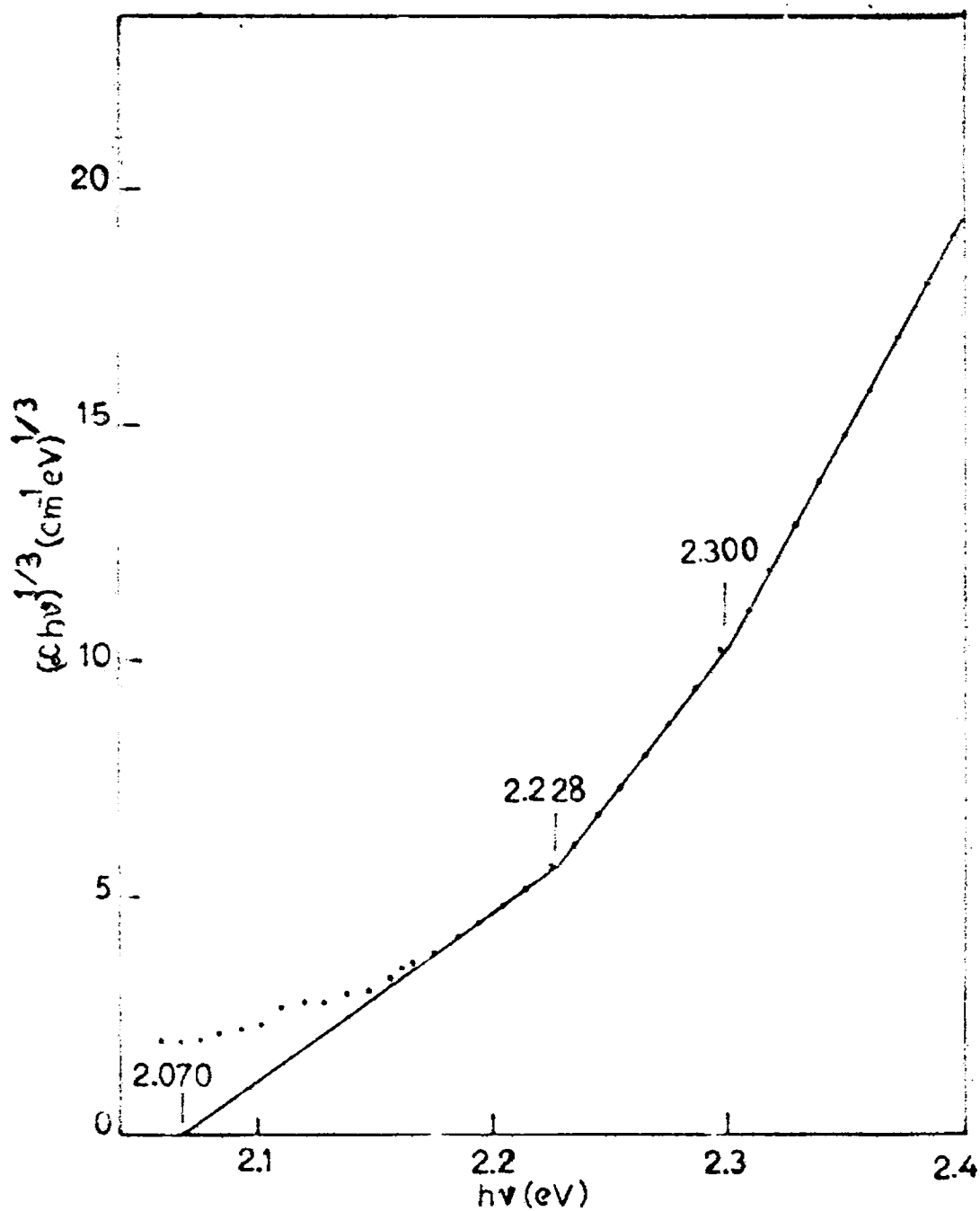


Fig.4. $(\epsilon h\nu)^{1/3}$ versus photon energy.

absorption coefficient and also the impurity contribution. It may be the reason for the above discrepancy.

From the plot of $(\alpha h\nu)^{1/3}$ versus photon energy, the value of the band gap obtained is 2.070 ± 0.001 eV. Three straight line portions are clearly seen in the figure. This may be due to the presence of three valence bands. This is highly probable because in tin disulphide the valence band is roughly divided into two groups, the lower two bands being split off from the upper six bands /12/. Lower valence band originate from sulphur s-states and the upper bands from sulphur p-states. The six sulphur p-states from the two sulphur atoms in the unit cell are split under the action of the crystal field into four p_x , p_y states and two p_z states. These states then combine to form bonding and antibonding bands. The final ordering of the states could give either a p_z state or p_x , p_y degenerate state for the valence band maximum. The degenerate p_x , p_y states can be further split due to spin orbit interaction.

Figure 4 gives the energy difference between the first valence band and conduction band as 2.070 ± 0.001 eV, for the second valence band 2.228 ± 0.001 eV and for the third valence band

2.30 ± 0.001 eV. From these values, assuming that the first two bands are the degenerate p_x , p_y bands split by spin-orbit interaction, we get 0.158 eV as the spin orbit interaction energy. This value agrees quite well with the spin-orbit splitting in sulphur atom, which is 0.157 eV /24/. Greenaway and Nitsche /1/ also observed this three line structure, but they arbitrarily took the mean of the extreme ones to get the band gap. The present value and the nature of transition is the same as that given by Domingo et al /2/.

The ordering of the valence band agrees with the pseudopotential band structure calculation of Powell et al /13/. It is shown that the top most valence band is doubly degenerate and the lowest conduction band is non-degenerate. Phonon energies reported in tin disulphide are 0.40 eV and 0.25 eV /25/ and it can be seen that the structure observed in the $(\alpha\text{Chv})^{1/3}$ plot is not due to the emission or absorption of the phonons. The photoconductivity maxima observed at 2.3 eV by the earlier workers /2, 14-16/ was not explained satisfactorily because the absorption edge data at that time gave the indirect band gap value at 2.07 eV and the direct gap value at 2.88 eV. It can now be explained from the present observations, that the transition from the third valence band should be responsible for the reported photoconductivity peak at 2.3 eV.

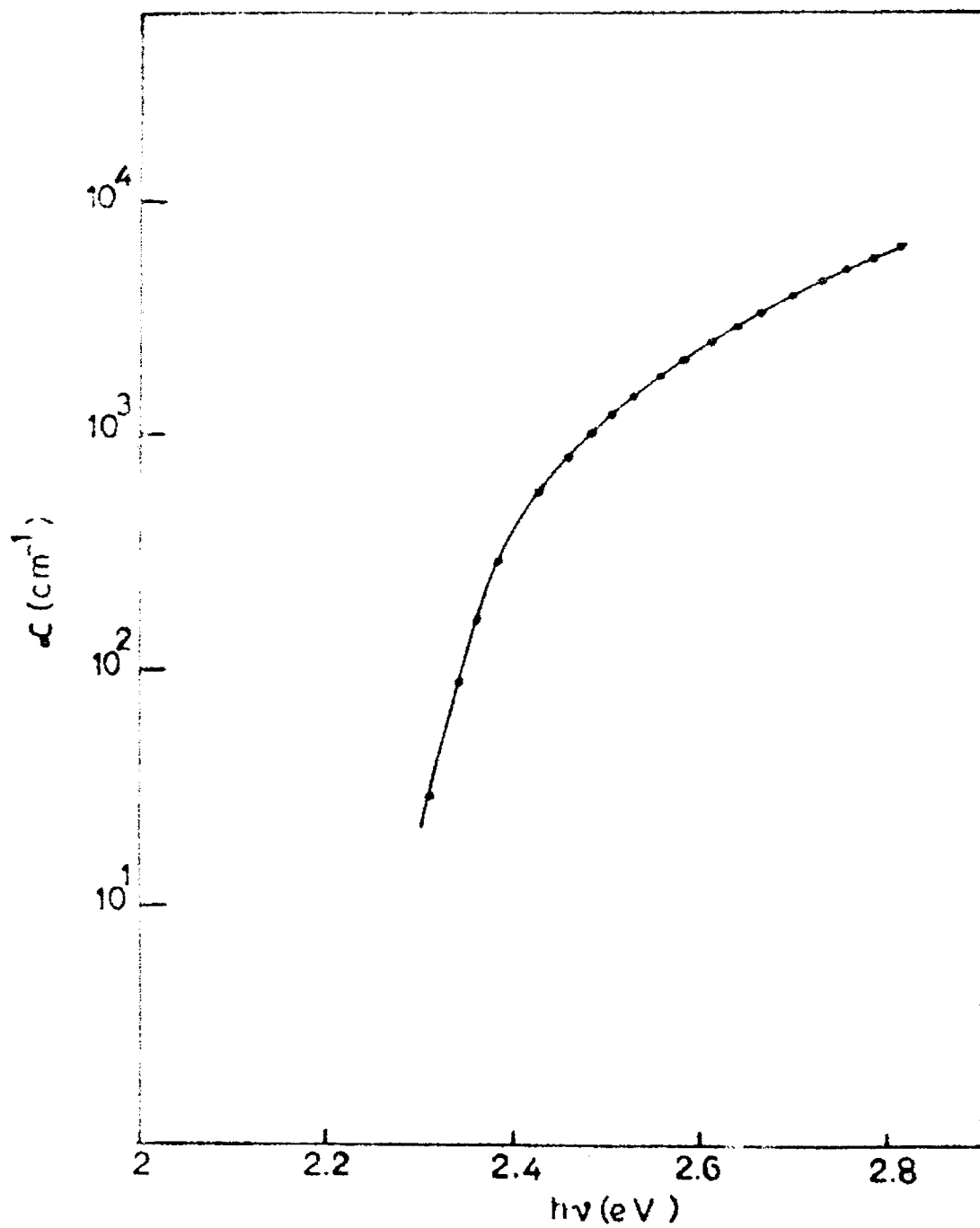


Fig. 5. Absorption coefficient versus photon energy for a thin SnS_2 crystal.

Thin crystals of tin disulphide were used to detect the direct transition in this material. Figure 5 shows the variation of absorption coefficient with photon energy obtained for a crystal of thickness $< 15 \mu\text{m}$. From the figure it can be seen that the absorption coefficient exhibits a shoulder around 2.4 eV, which is due to the onset of the direct transitions. According to Bardeen's theory /22/, for a direct transition

$$\mathcal{L} = \frac{B (h\nu - E_g)^r}{h\nu}$$

where E_g is the direct band gap. If $r = 1/2$, the transition is allowed and if $r = 3/2$, the transition is forbidden.

The plot of $(\mathcal{L}h\nu)^{2/3}$ versus $h\nu$ is given in figure 6. The energy intercept gives a direct forbidden band gap of 2.40 ± 0.002 eV. Powell /4/ has reported the direct band gap of tin disulphide crystals (2H) as 2.44 ± 0.05 eV from the pressure dependence measurements and the present value is in agreement with this. The reported values of band gap for tin disulphide are given in table 1.

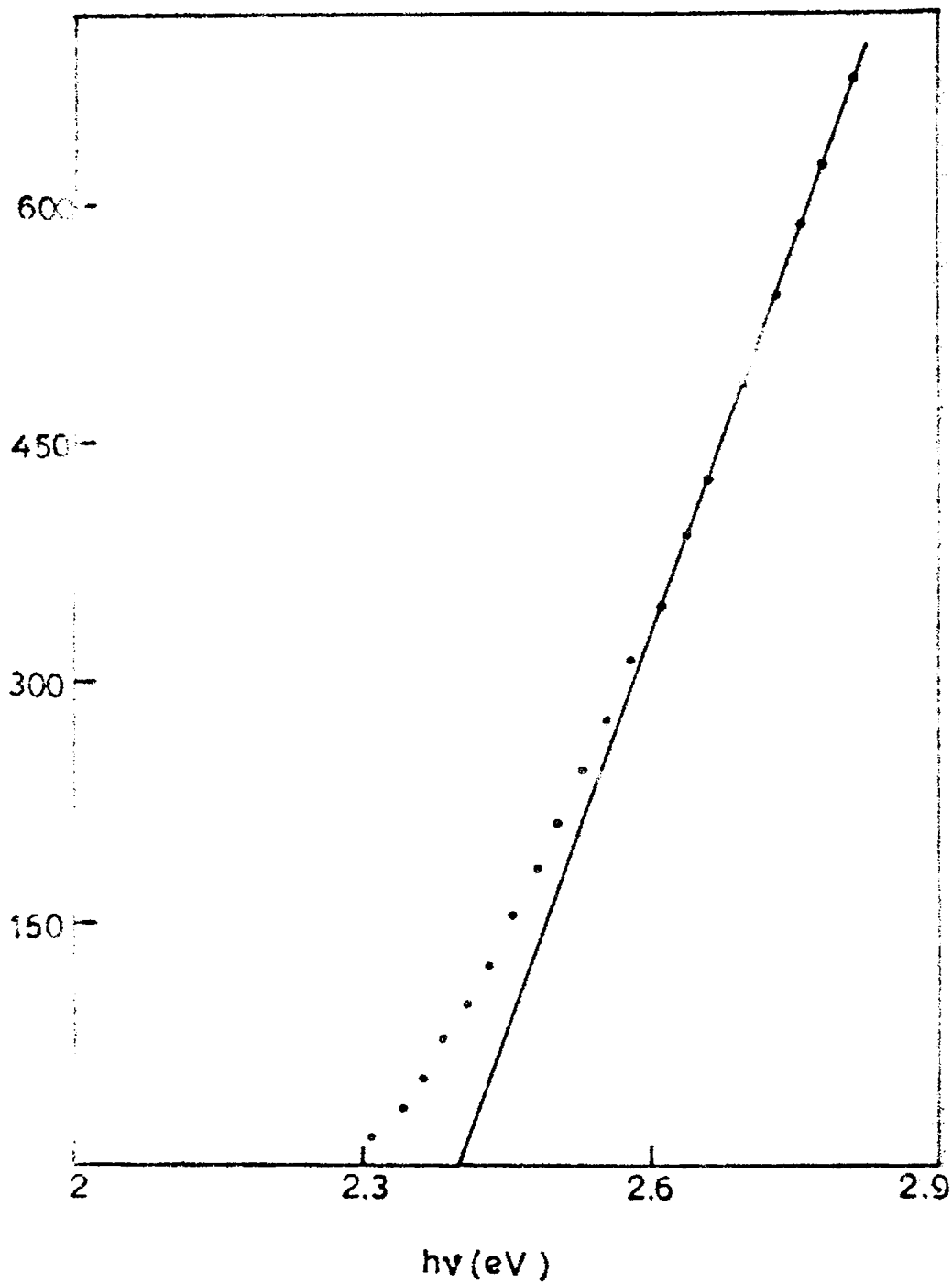


Fig.6. $(\sigma h\nu)^{2/3}$ versus photon energy.

Table 1
Reported values of band gap for tin disulphide

Authors with reference	Energy gap (eV)				Photo-conductivity methods	Electrical methods
	Indirect allowed	Indirect forbidden	Optical methods	Direct forbidden		
Greenaway & Nitshe /1/	2.21					
Domingo et al /2/		2.07		2.88	2.3	
Lee et al /3/	2.22					
Patil & Tredgold /14/					2.3	
Nakata et al /15/					2.3	
Bletskan et al /16/					2.296	
Powell /4/	2.29 (2H)			2.44 (2H)		
Acharya & Srivastava /5/	2.14					2.18 (2H)
Nozaki & Imai /6/	2.21					
George & Joseph /7/	2.31					
Present work		2.07 2.228 2.30		2.40		

CONCLUSION

High resolution absorption edge measurements of tin disulphide single crystals have shown that there is a shoulder in the absorption caused by the presence of donor levels **s**ituated just below the conduction band. It is found that there are three valence bands which originate due to spin-orbit interaction and crystal field splitting. Indirect forbidden transitions at 2.07 eV, 2.228 eV, 2.30 eV and a direct forbidden transition at 2.40 eV have been detected. The photoconductivity maxima at 2.30 eV reported by earlier workers agrees with the present observations.

References

1. D.L. Greenaway and R. Nitsche, J. Phys. Chem. Solids 26 (1965) 1445.
2. G. Domingo, R.S. Itoga and C.R. Kannewurf, Phys. Rev. 143 (1966) 536.
3. P.A. Lee, G. Said, R. Davies and T.H. Lim, J. Phys. Chem. Solids 30 (1969) 2719.
4. M.J. Powell, J. Phys. C. Solid State Phys. 10 (1977) 2967.
5. S. Acharya and O.N. Srivastava, Phys. Stat. Solidi(a) 56 (1979) K1.
6. H. Nozaki and I. Imai, Physica 105 B (1981) 74.
7. J. George and K.S. Joseph, J. Phys. D : Applied Phys. 15 (1982) 1109.
8. C.Y. Fong and M.L. Cohen, Phys. Rev.(B) 5 (1972) 3095.
9. C. Schluter and M. Schluter, Phys. Stat. Solidi (b) 57 (1973) 145.
10. R.B. Murray and R.H. Williams, J. Phys. C : Solid State Phys. 6 (1973) 3643.
11. G. Mula and F. Aymerich, Phys. Stat. Solidi (b) 51 (1972) K. 35.

12. M.J. Powell, W.Y. Liang and D.J. Chadi, J. Phys. C : Solid State Phys. 11 (1978) 885.
13. M.J. Powell, E.A. Marseglia and W.Y. Liang, J. Phys. C : Solid State Phys. 11 (1978) 895.
14. S.G. Patil and R.H. Tredgold, J. Phys. D : Applied Phys. 4 (1971) 718.
15. R. Nakata, M. Yamaguchi, S. Zembutsu and M. Sumita, J. Phys. Soc. Japan 32 (1972) 1153.
16. D.I. Bletskan, I.F. Kopinets, I.M. Migolinets and S.V. Mikulaninets, Neorganicheskie Materialy 12 (1976) 2142.
17. J.I. Pankove, Optical Processes in Semiconductors (Prentice-Hall, New Jersey 1971).
18. G. Said and P.A. Lee, Phys. Stat. Solidi 15 (1973) 99
19. J. George and K.S. Joseph, J. Phys. D : Applied Phys. 16 (1983) 33.
20. F. Bassani, D.L. Greenaway and G. Fischer, Proceedings of the 7th international conference on the physics of semiconductors (Dunod, Paris, 1964) p-51.
21. M. Piacentini, E. Doni, R. Girlanda, V. Grasso and A. Balzaotti, IL Nuovo Cimento 54 B (1979) 269.

22. J. Bardeen, F.J. Blatt and L.H. Hall, Proceedings of Photoconductivity Conference, Atlantic City (New York, Wiley 1956) p-146.
23. R.A. Smith, Semiconductors (Cambridge University Press, London) p-146.
24. R.C. Gibbs and H.E. White, Phys. Rev. 33 (1929) 157.
25. D.J. Mead and J.C. Irwin, Solid State Commun. 20 (1976) 885.

CHAPTER - VII

ELECTRICAL PROPERTIES OF TIN DISULPHIDE CRYSTALS

Gowers and Lee /1/ studied the electrical properties of tin disulphide crystals and reported a value of 10^{-4} $\text{cm}^2/\text{V. sec.}$ for the mobility of electrons parallel to c-axis and 30 $\text{cm}^2/\text{V. sec.}$ for the perpendicular direction. They conjectured that when conduction is perpendicular to the layers (parallel to c-axis), electrons have to tunnel between the layers and hence the low mobility. Patil and Tredgold /2/ studied the conductivity parallel and perpendicular to the c-axis by a probe method and their measurements showed an anisotropy ratio $\sigma_{\perp} / \sigma_{\parallel}$ of the order of 10^4 . They interpreted that this is due to the different mechanisms of charge transport in the direction along and perpendicular to the layers. From the Hall effect measurements, Ishizawa and Fujiki /3/ reported mobility perpendicular to c-axis (6.4 $\text{cm}^2/\text{V. sec.}$) and carrier concentration (6×10^{16} cm^{-3}) of n-type SnS_2 crystals. Patil /4/ investigated AC conductivity in tin disulphide over the temperature range -100° C to 120° C, and from the frequency dependence of AC conductivity in the low temperature region suggested that perpendicular to the c-axis, electron transport is by a hopping mechanism.

Electrical conduction mechanism in tin disulphide crystals have been reported by Said and Lee /5/ using Sn-SnS₂-Sn structures. They measured the conductivity parallel to c-axis and found that the conduction mechanism in these crystals is space charge limited. Acharya and Srivastava /6/ studied the activation energy for conduction for different polytypes of tin disulphide crystals and reported that activation energy decreases with increasing polytype periodicity.

All the above mentioned investigations were on crystals grown using iodine as transporting agent. Crystals grown by the use of transporting agents are highly contaminated and this usually has a pronounced effect on the electrical properties. Resistivity and mobility generally decreases with increasing iodine content.

This chapter contains the electrical properties of tin disulphide crystals grown by physical vapour transport method. The current-voltage characteristics of the crystals in the direction parallel to the c-axis have been investigated at different temperatures using MIM structures and the trap depth, trap concentration, free carrier mobility etc. have been determined.

7.1 EXPERIMENTAL

The crystals were grown by PVT method as already described in Chapter IV. To study the current voltage characteristics, aluminium electrodes of area 0.1256 cm^2 was deposited by vacuum evaporation on the opposite faces of the crystals. The Al-SnS₂-Al sandwich was placed in between a jig and the measurements were made in an evacuated all-metal cell as described in Chapter IV. Current was measured using a digital pico-ammeter and the voltage using a digital multimeter. During the measurements, temperature of the crystal was controlled by the current applied to the heater from a low voltage stabilized DC source. The specimens were held at the desired temperature for a sufficiently long time before the measurements were made. Temperature of the specimen was measured using a chromel-alumel thermocouple kept close to the specimen. Thickness of the crystals used in the study were in the range of 10 - 60 μm .

7.2 RESULTS AND DISCUSSIONS

The current-voltage characteristic of a typical MIM structure is shown in figure 1. It can be seen that at low voltages the current is proportional to the applied voltage, indicating that the current is controlled by thermally generated charge carriers.

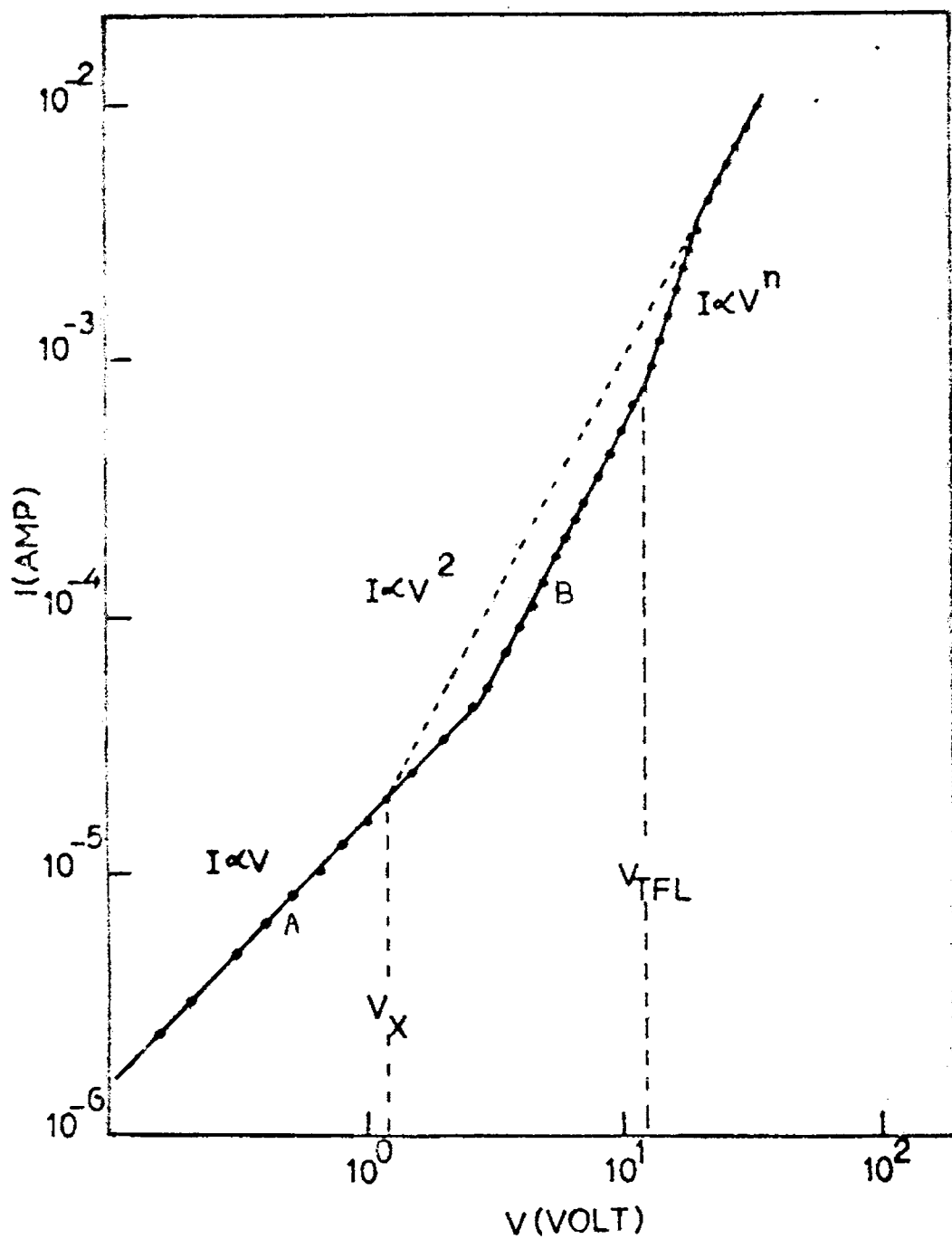


Fig.1. I-V characteristic for a typical Al- SnS_2 -Al structure. Thickness $d = 20 \mu\text{m}$, $T = 293 \text{ K}$, electrode area = 0.125 cm^2 .

This region A is called the ohmic law region. The ohmic law region is followed by a square law region at high fields as shown in region B. This is the shallow trap square law region. The square law region is followed by another region where current increases sharply with voltage ($I \propto V^n$; $n \geq 3$) and this is due to the filling up of the traps. This region is followed by yet another square law region called trap free square law region. These observations, where an ohmic region is followed by a square law region, indicate a charge injection into the semiconductor with trapping centres, which may be interpreted in terms of space charge limited conduction /7-9/ and the current obeys a law of the form

$$J = (9/8) \theta \mu \epsilon \frac{V^2}{d^3} \quad (7.2.1)$$

where J is the current density, θ is the fraction of total carriers which are free, μ is the charge carrier mobility, ϵ is the dielectric constant, V is the voltage and d is the specimen thickness. Figure 2 shows a plot of the current I in the trapped square law region as a function of thickness d on a log-log scale at 300 K. This straight line graph shows the d^3 dependence establishing that the conduction mechanism in tin disulphide is space charge limited.

θ in equation (7.2.1) is the ratio between the free electrons n_c in the conduction band to the

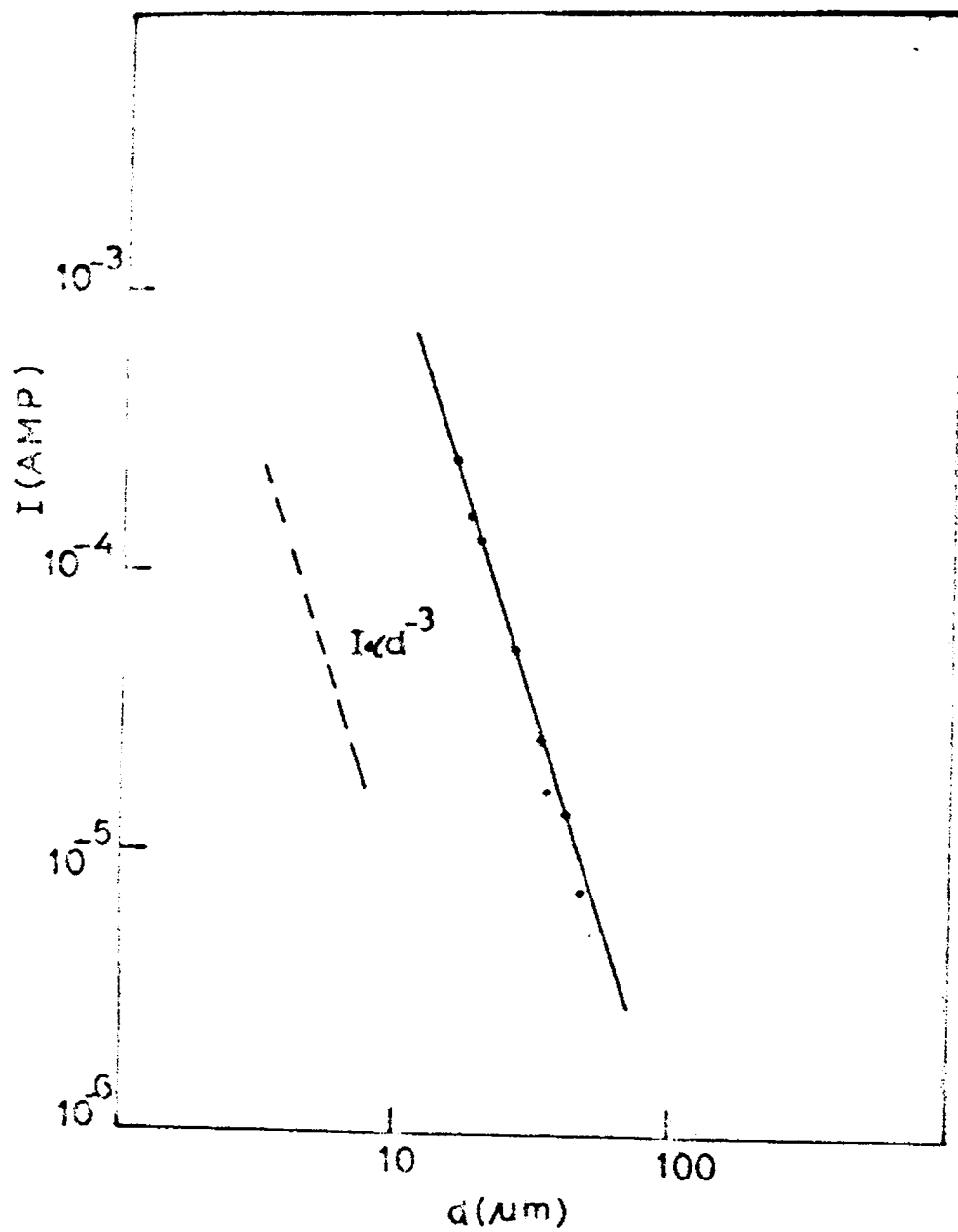


Fig.2. Current versus thickness in the space charge limited region; slope = -3, $V = 5$ volt, $T = 298$ K.

total electron density ($n_o + n_t$), n_t being the density of the trapped electrons. Experimentally θ is determined from the equation

$$\theta = \frac{n_o}{n_o + n_t} = J_1/J_2 \quad (7.2.2)$$

where J_1 and J_2 are the current densities at the start and end of the sharp rise of the current (figure 1). Using the experimentally determined value of $\theta = 0.205$ and $\mu = 7.2 / 10^4$, the average value of the free carrier mobility was obtained as $6 \text{ cm}^2/\text{V. sec.}$ But Gowers and Lee /1/ reported the free carrier mobility parallel to c-axis in SnS_2 crystals grown by chemical transport method as $10^{-4} \text{ cm}^2/\text{V. sec.}$ This extreme low value may be due to the contamination of their crystals by the transporting agent.

The threshold voltage V_x where the ohmic current crossover to the space charge limited current in the absence of traps is obtained by extrapolating the trap free square law region to meet the ohmic law region. The thermally generated free carrier density n_o can be calculated from the crossover voltage V_x using equation

$$n_o = \frac{\theta \epsilon}{1.8 \times 10^{-6} d^2} V_x \quad (7.2.3)$$

The average value of the density of thermally generated free carriers was found to be equal to $2.3 \times 10^{11} \text{ cm}^{-3}$. Using the values of n_0 and θ in equation (7.2.2), the density of the trapped carriers n_t was calculated as $9.1 \times 10^{11} \text{ cm}^{-3}$.

The conductivity σ is given by $\sigma = n_0 e \mu$ where e is the electronic charge. Using the values of n_0 and μ , σ was found to be equal to $2.2 \times 10^{-7} \Omega^{-1} \text{ cm}^{-1}$. This calculated value of σ agrees very well with the experimental value of σ obtained from the ohmic regions. All the specimens studied shows n-type conductivity. The sharp increase in current value after the shallow trap square law region was due to the filling of the traps (fig. 1). The trap filled limit voltage measures the fraction of the total concentration of traps that is empty in thermal equilibrium. The trap concentration is calculated using the equation

$$N_t = \frac{1.1 \times 10^6 \times \epsilon}{d^2} V_{\text{TFL}} \quad (7.2.4)$$

where V_{TFL} is the trap filled limit voltage. Using the experimentally determined value of V_{TFL} , the trap concentration was obtained as $2.3 \times 10^{13} \text{ cm}^{-3}$.

The temperature dependence of current-voltage characteristics for a typical crystal is shown in figure 3.

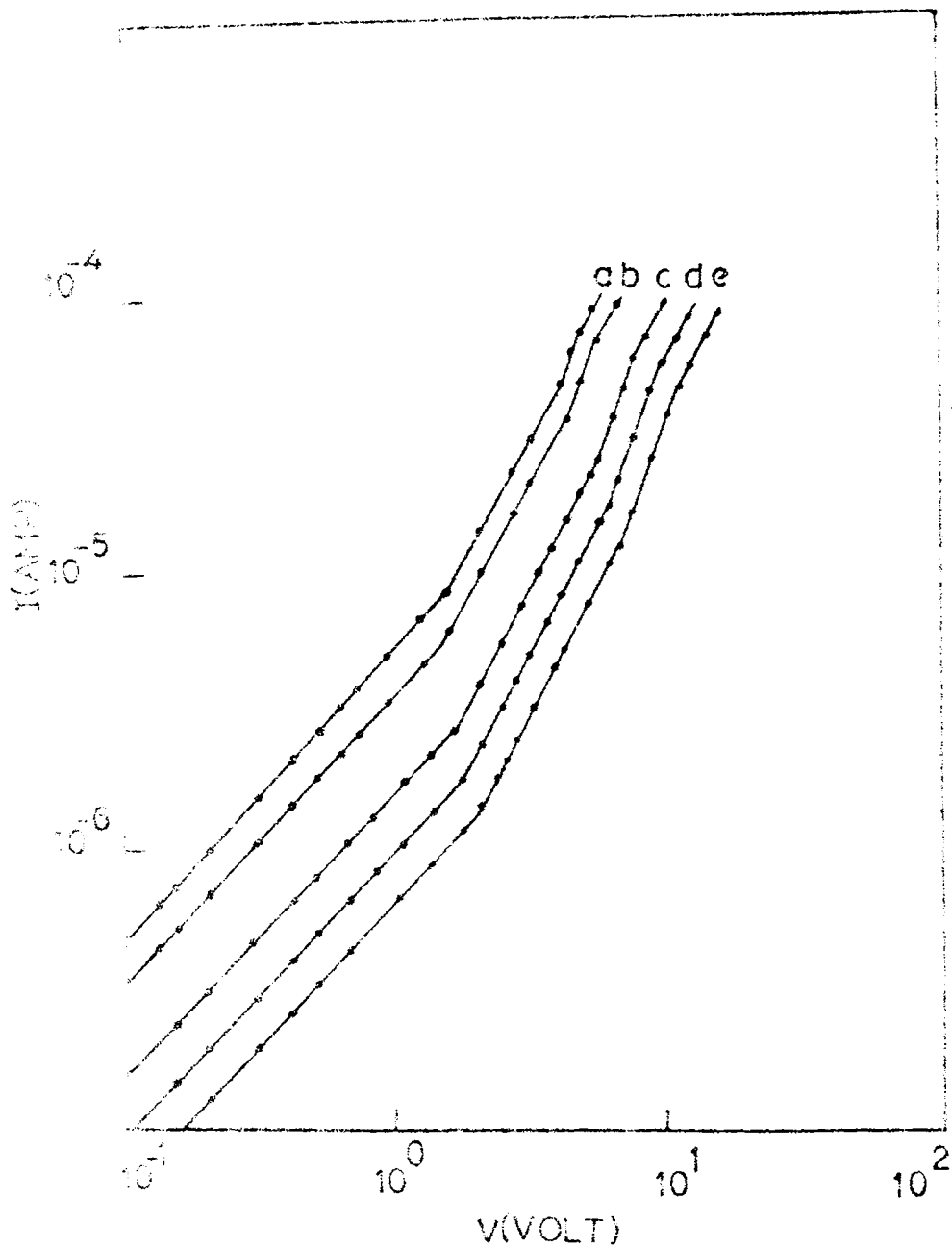


Fig. 1.

Fig. 2. (a) 40% (b) 40% (c) 40%

(d) 40% (e) 40%

Fig. 1.

Fig. 2. (a) 40% (b) 40% (c) 40% (d) 40% (e) 40%

It can be seen that the current increases with the increase of temperature for the same applied voltage. At high temperatures, the current rises sharply even at the ohmic law region and hence care was taken to avoid specimen damage.

$$\theta = \frac{N_c}{N_t} \exp(-E_t/k_B T) \quad (7.2.5)$$

where N_c is the effective density of states in the conduction band, E_t is the trap depth, k_B is the Boltzmann constant and T is the absolute temperature. From the temperature dependence of the I-V characteristics, the values of θ for various temperatures were calculated and the $\log \theta$ versus $1/T$ plot is shown in figure 4. From the slope of the straight line, the value of the trap depth E_t was found to be equal to 0.10 ± 0.01 eV. This trap level may be due to the presence of doubly ionizable sulphur vacancies in SnS_2 crystals. High resolution absorption edge measurements (discussed in Chapter VI) in these crystals gave an impurity level at 0.17 eV. Said and Lee /5/ has also reported a trap depth at 0.14 eV in tin disulphide. All these confirm that there exists an impurity level in tin disulphide crystals around 0.10 eV. The effective density of states in the conduction band can be obtained by extrapolating the $\log \theta$ versus $1/T$ curve. From the intercept at $T^{-1} = 0 \text{ K}^{-1}$, N_c was found to be equal to $5.1 \times 10^{17} \text{ cm}^{-3}$.

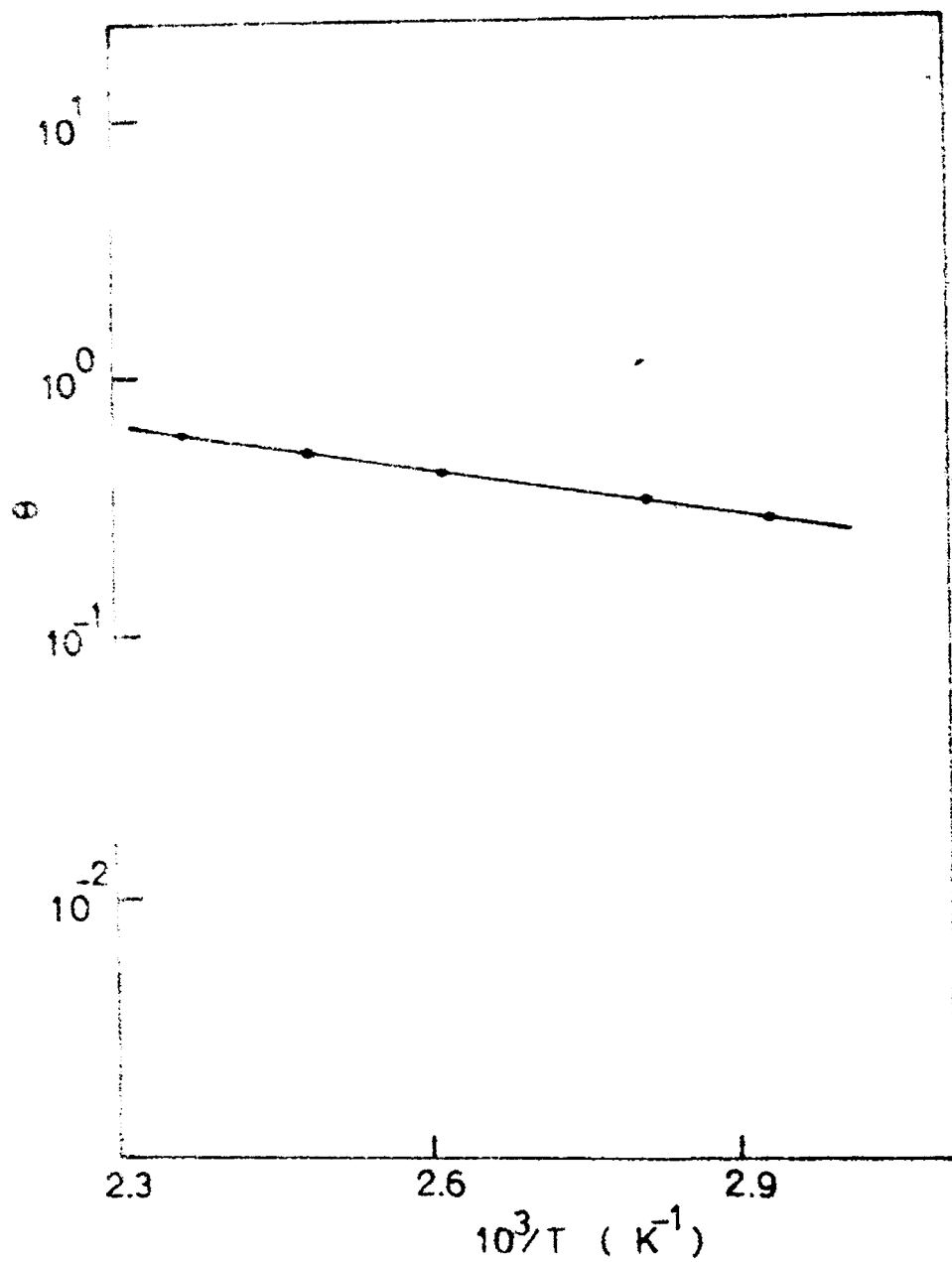
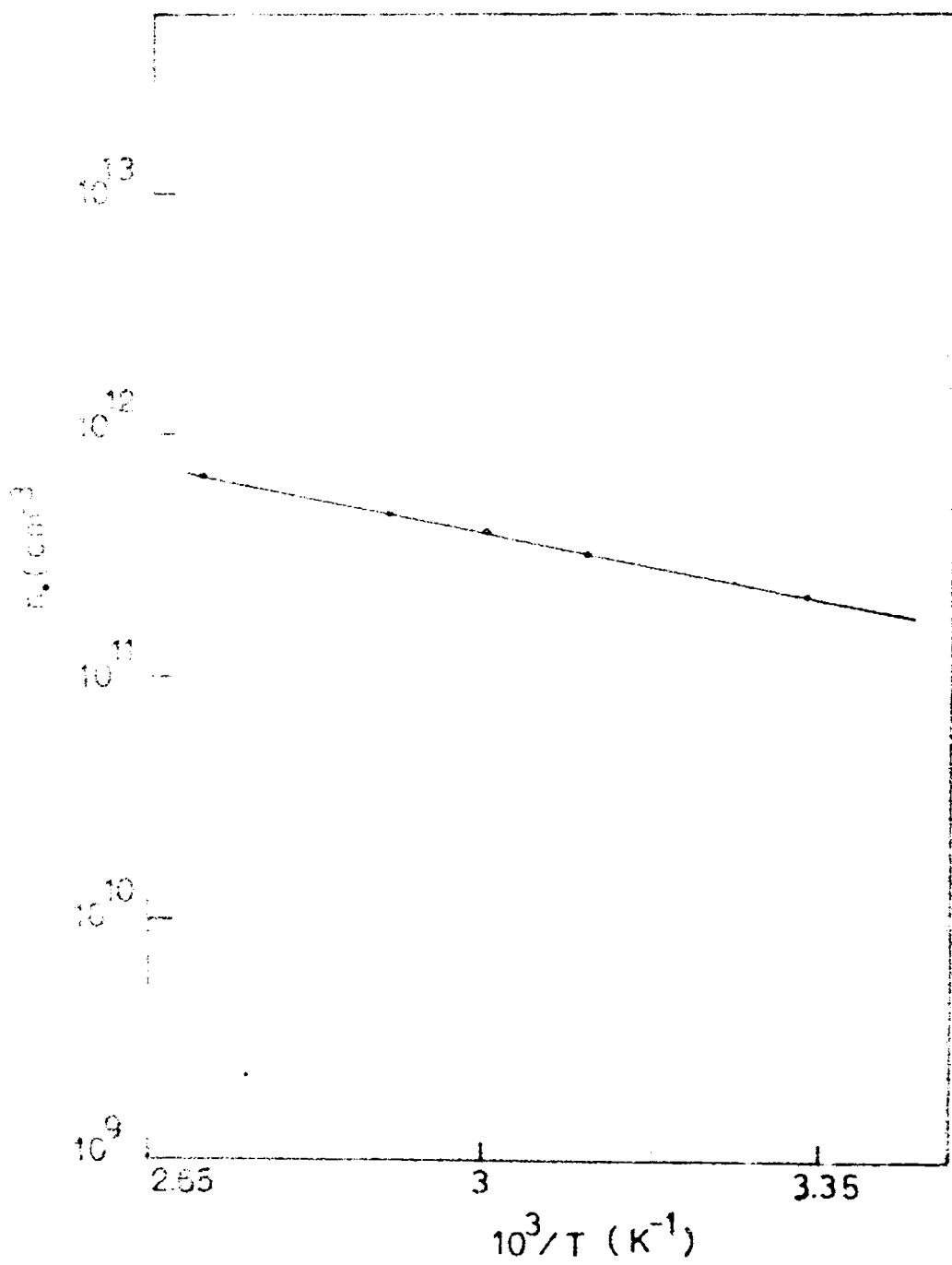


Fig. . . $\log \theta$ versus $1/T$; $E_g = 0.10$ eV.



... 9. $1/T$ for typical specimen;

The Fermi level E_F measured from the bottom of the conduction band is given by

$$n_0 = N_c \exp (- E_F/k_B T) \quad (7.2.6)$$

Log n_0 versus $1/T$ plot is shown in figure 5. The plot is a straight line with a slope 0.15 eV. Thus it may be seen that the position of the Fermi level in tin disulphide is at 0.15 eV below the conduction band.

The thermally activated electrical conductivity is

$$\sigma = \sigma_0 \exp (- E_a/k_B T) \quad (7.2.7)$$

where σ_0 is a constant and E_a is the activation energy. The plot of the temperature dependence of current in the ohmic law region ($V = 800$ mV) for different temperatures is shown in figure 6. From the slope, the value of the activation energy for conduction was obtained as 0.40 ± 0.05 eV. Said and Lee /5/ has also reported an activation energy of 0.40 eV in tin disulphide crystals.

The electrical parameters reported for tin disulphide crystals are given in table 1. From the table, it may be seen that carrier concentration of the crystals grown by physical vapour transport is much lower than that grown by chemical vapour transport method.

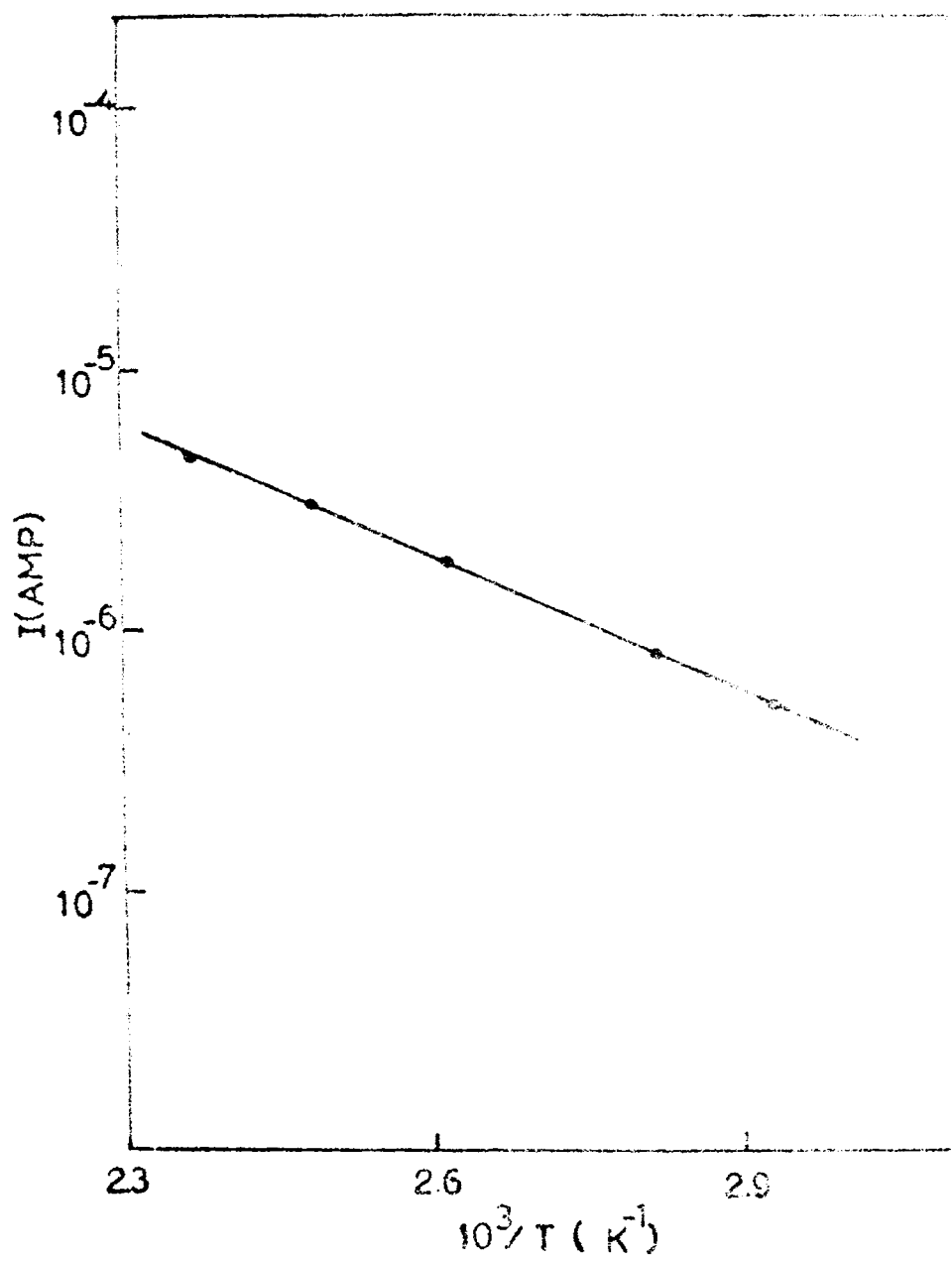


Fig.6. $\log I$ versus $1/T$ state
 $V = 800$ mV, $E_a = 0.7$ eV.

Table 1
Reported electrical parameters of SnS₂

Authors	Method of growth	Technique used	Activation energy eV		Mobility cm ² /V.sec.		Resistivity Ω cm		Carrier concentration cm ⁻³	Trap depth eV
			1/4-c	1/2-c	1/4-c	1/2-c	1/4-c	1/2-c		
Gowers and Lee /1/	Chemical transport	Hall effect	0.18		10 ⁻⁴	20				
Patil and Tredgold /2/	Chemical transport	Electrical conductivity	0.50-0.70	0.4-0.61			10 ¹² -10 ¹⁴	10 ⁷ -10 ⁹		
Ishizawa and Fujiki /3/	Chemical transport	Hall effect	-	0.19		6.3		3	4x10 ¹⁶	
Said and Lee /5/	Chemical transport	MIM	0.40 0.11 0.05				0.35 7x10 ⁵ 4x10 ⁷			0.14
Present work	Physical transport	MIM	0.40		6		5x10 ⁶		2.3x10 ¹¹	0.10

This shows that crystals grown by PVT have much purity than that grown by CVT.

CONCLUSION

Electrical conduction mechanism is studied using Al-SnS₂-Al structures in single crystals of tin disulphide grown by physical vapour transport method and it is established that the conduction is space charge limited. The higher mobility value parallel to c-axis and the low carrier concentration exhibited by the crystals shows that these crystals are more pure than the crystals grown using the transporting agent. The trap level situated at 0.10 eV below the conduction band may be due to the presence of doubly ionizable sulphur vacancies. The trap concentration is found to be $2.3 \times 10^{13} \text{ cm}^{-3}$.

References

1. J.P. Gowers and P.A. Lee, Solid State Commun. 8 (1970) 1447.
2. S.G. Patil and R.H. Tredgold, J. Phys. D : Appl. Phys. 4 (1971) 718.
3. Y. Ishizawa and Y. Fujiki, J. Phys. Soc. Japan 35 (1973) 1259.
4. S.G. Patil, J. Phys. C : 5 (1972) 2881.
5. G. Said and P.A. Lee, Phys. Stat. Solidi (a) 15 (1973) 99.
6. S. Acharya and O.N. Srivastava, Phys. Stat. Solidi (a) 56 (1979) K1.
7. A Rose, Phys. Rev. 97 (1955) 1538.
8. M.A. Lampert, Phys. Rev. 103 (1956) 1648.
9. M.A. Lampert and P. Mark, Current injection in solids, Academic press, New York (1970).
10. Joy George, C.K. Valsala Kumari and K.S. Joseph, J. Appl. Phys. 54 (1983) 5347.

CHAPTER - VIII

GROWTH AND MORPHOLOGY OF TIN DISELENIDE CRYSTALS

Tin diselenide is a layered semiconductor isostructural to tin disulphide and these crystals have been grown by chemical vapour transport method /1-5/. Garg et al /6/ have reported the growth of these crystals from vapour using synthesised charge. The most prominent features of crystals with layered structures is the existence of screw dislocation, giving rise to growth spirals. None of the earlier reported workers have studied the growth morphology of tin diselenide crystals. But Acharya and Srivastava /5/ reported that they were not able to observe any evidence of growth spirals on the as grown faces of these crystals.

In this chapter is described the growth of tin diselenide crystals by physical vapour transport method and their morphology. Growth spirals have been observed on the as grown faces of tin diselenide crystals for the first time.

8.1 EXPERIMENTAL

Tin diselenide crystals were grown by the physical vapour transport method. Quartz ampoules

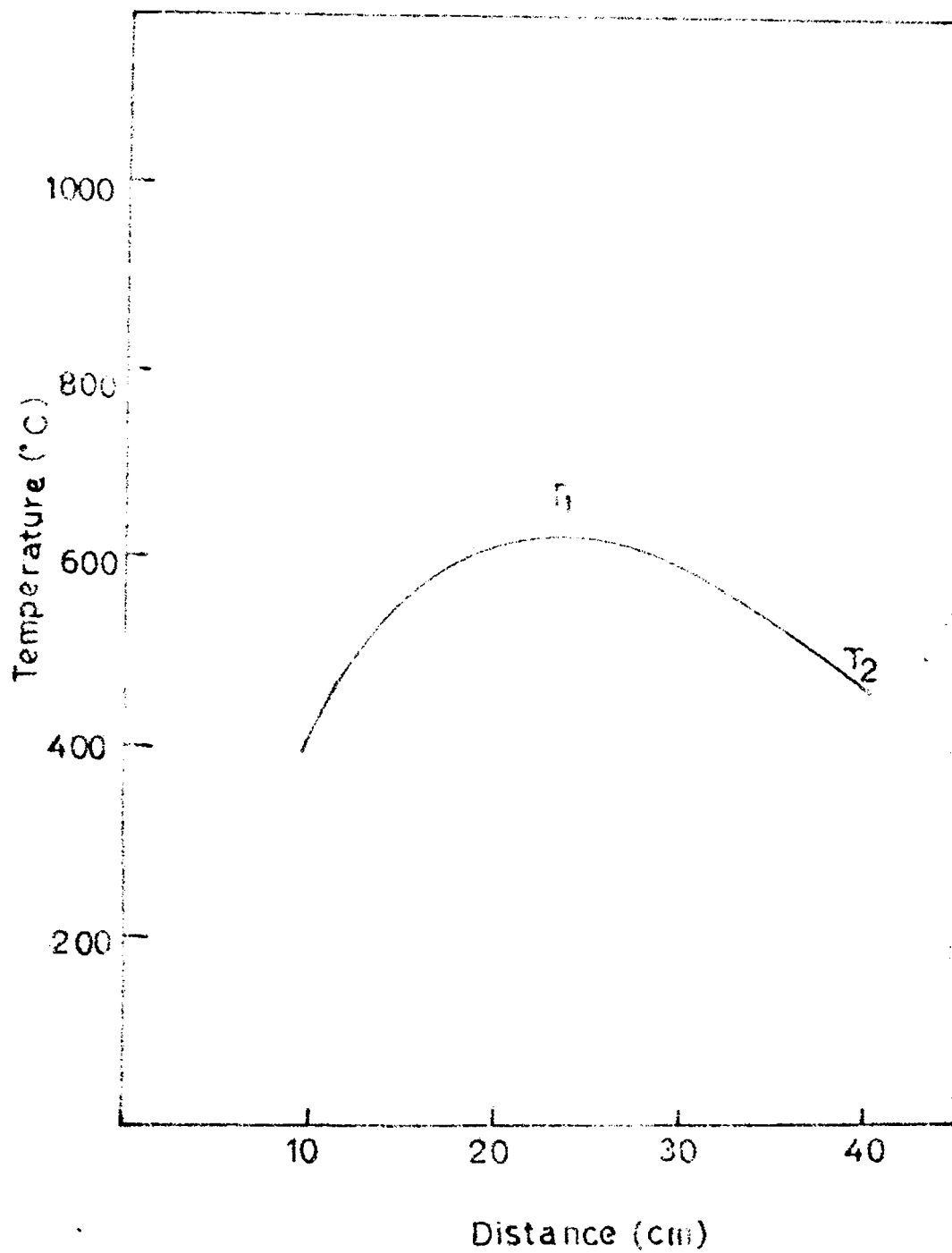


Fig.1. Temperature profile of the furnace used for the growth of SnSe_2 crystals.

of 15 cm length and 1.6 cm inner diameter were used for the crystal growth. Ampoules were cleaned as described in Chapter IV. Stoichiometric composition of tin (99.999%) and selenium (99.999%) were filled in the ampoule and was sealed at a final pressure of 10^{-5} Torr. The sealed ampoules were then placed in the horizontal two zone furnace. The temperatures of the zones were controlled with an accuracy of $\pm 1^\circ\text{C}$ using temperature controllers as described in Chapter IV. Figure 1 shows the temperature profile of the furnace used for the growth of tin diselenide crystals. The source temperature was maintained at 640°C (T_1) and the growth temperature at 475°C (T_2). The transport time was around 100 hours. Crystals obtained were metallic coloured platelets having a thickness of $150\ \mu\text{m}$ and surface areas upto $1.5\ \text{cm}^2$. As grown surfaces of the crystals were observed using metallurgical microscope.

8.2 RESULTS AND DISCUSSION

According to Burton, Cabrera and Frank /7/, Cabrera and Levine /8/, Muller - Krumbhar et al /9/, when a spiral originating from an isolated single screw dislocation is formed under a steady growth condition and is not perturbed by spiral layers from other

sources, the spiral will take regular shape. Ideal spirals originating from isolated screw dislocations are not commonly observed on crystal faces. If the growth conditions are so controlled and perturbations are not present, the whole surface will be covered by a single spiral. Figure 2 shows a single growth spiral observed on as grown face of the tin diselenide crystal. Several hexagonal spirals were also observed on the as grown faces and these growth spirals confirms that the growth of SnSe_2 crystals is due to the screw dislocation mechanism.

Based on the theoretical predictions by Frank /10/, Cabrera and Levine /8/, if the Burgers vector of a dislocation becomes relatively high, a cylindrical hollow core will develop around the dislocation. Hollow cores at the centre of growth spirals were first observed by Verma on SiC /11/ and Forty /12/ on CdI_2 crystals. From the experimental evidence obtained from faces of haematite crystals, Sunagawa and Bennema /13/ reported that if the step height of the spiral is very high, the spiral step escapes with a change of curvature from the hollow core depending on the stress field. Figure 3 shows such a spiral pattern. Both spirals having the same sign are originating from the single screw dislocation with a clear change of curvature as they escape from the central core.

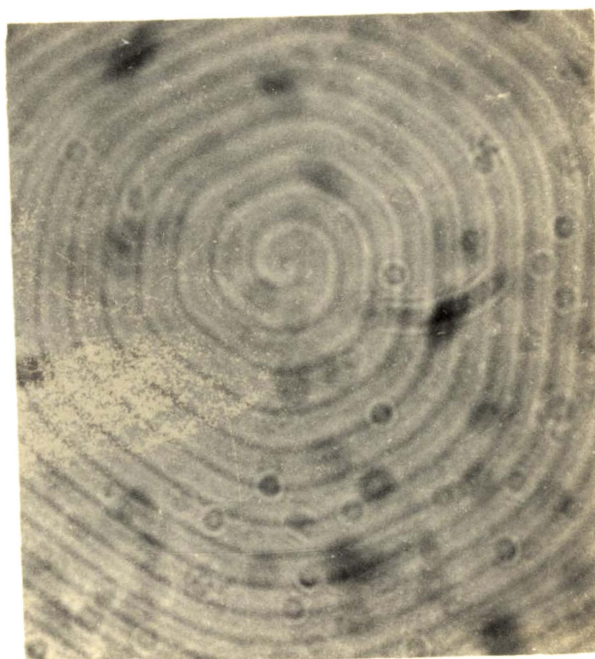


Fig.2. A circular spiral originating from a single screw dislocation. (x 300)

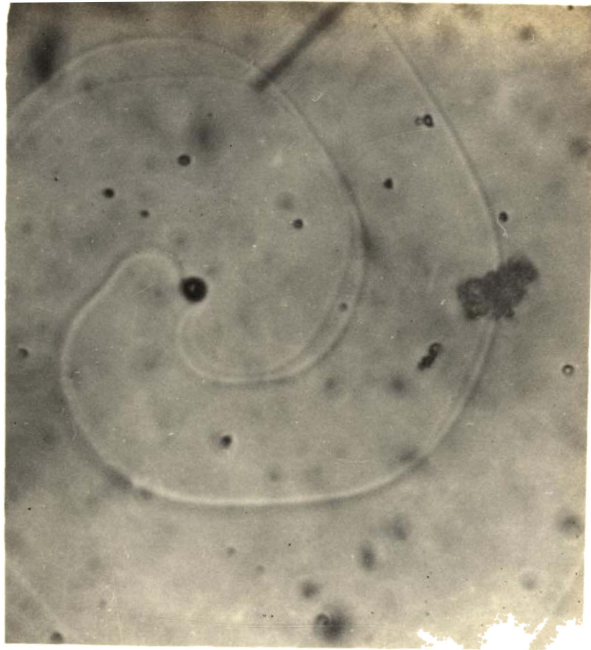


Fig.3. Two spirals of same sign with central core and change of curvature. (x1000)

When two screw dislocations of the same sign are closer together than $2\pi r_c$ where r_c is the radius of curvature of the two dimensional nucleus, they will generate a pair of non-intersecting growth spirals. Such an example is shown in figure 4. Here the spiral is doubled and will behave like one dislocation of double strength. A group of spirals observed on the basal plane of the tin diselenide crystal is shown in figure 5. All the spirals are originating from the central core of the same dislocation and have same sign and strength of dislocation. Eccentric spirals originating from a single screw dislocation were also observed on the as grown faces of these crystals (Figure 6). During the growth process a supersaturation gradient is over the surface of the growing crystal. Hence at the higher supersaturation side, the spiral step advance more rapidly and form wider step separation. At the lower supersaturation side, step separation becomes narrower and the spiral as a whole take the eccentric shape.

Another interesting feature observed was the interlaced spirals. A typical example is shown in figure 7. In this spiral pattern, interlacing appears along the six corners of the hexagon and the dissociation of the

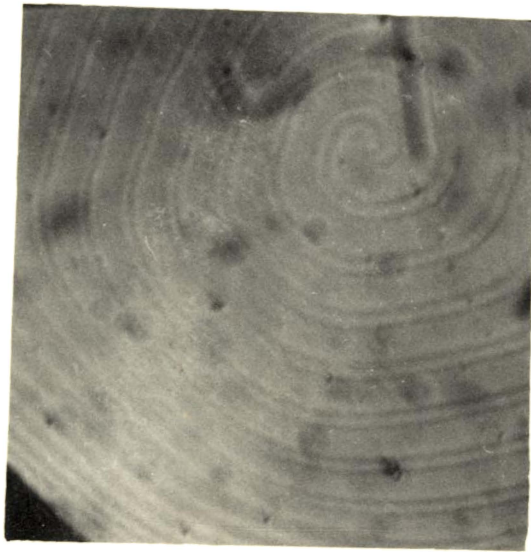


Fig.4. Two screw dislocations of the same sign at a distance of separation less than f_c , cooperating with one another. (x 300)

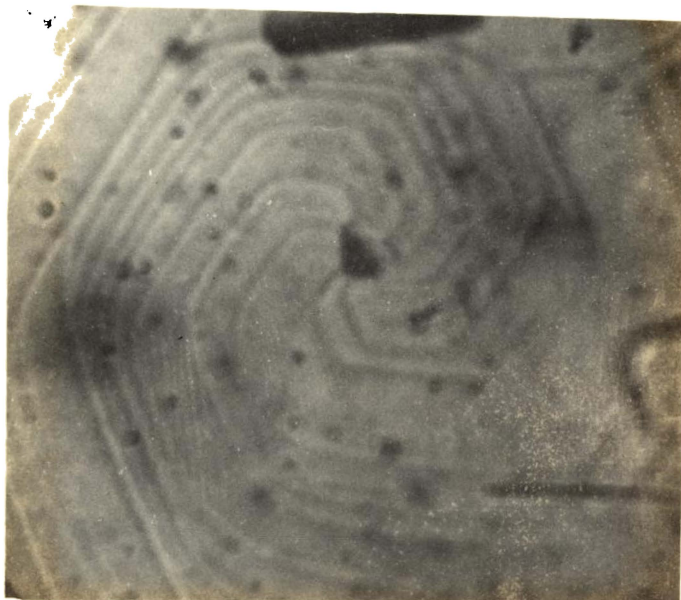


Fig.5. A group of spirals originating from the centre of the same screw dislocation. (x1000)

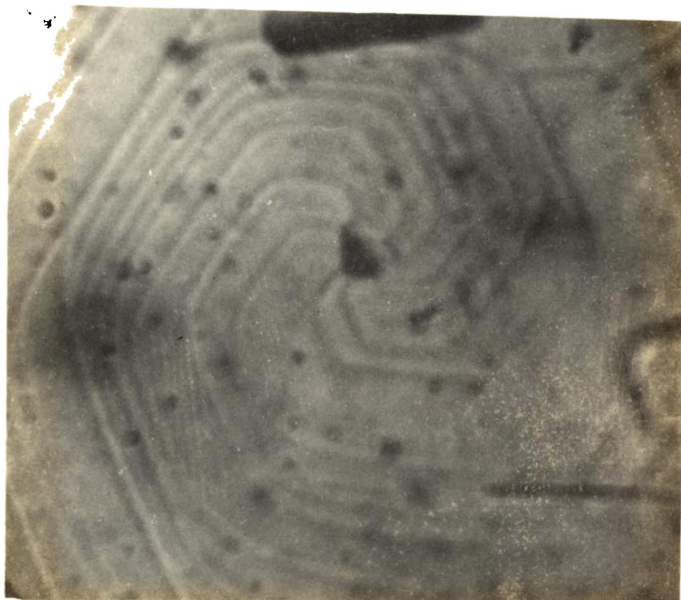


Fig.5. A group of spirals originating from the centre of the same screw dislocation. (x1000)

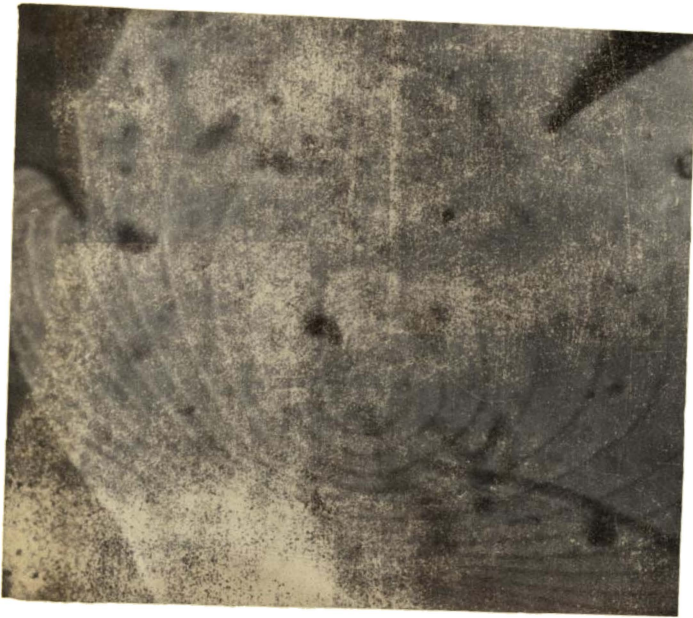


Fig.6. Eccentric spiral. (x 300)

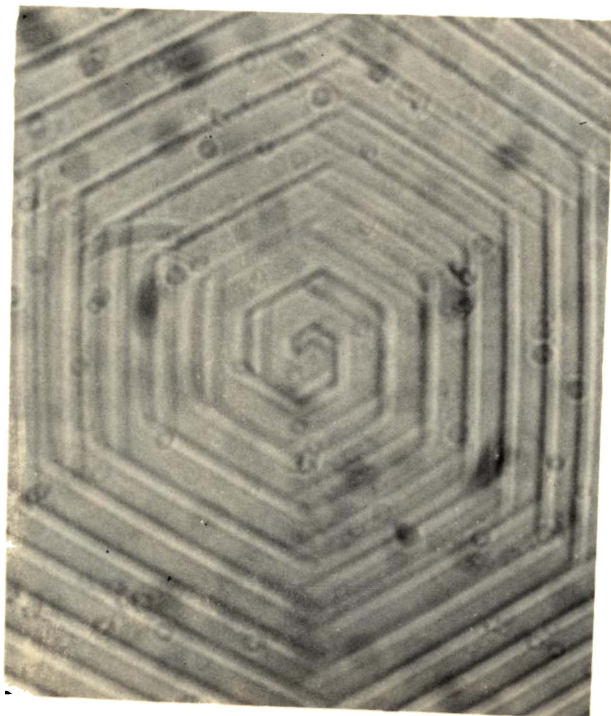


Fig.7. Interlaced spiral. (x 300)

spiral step into its components can be seen. The splitting have occurred in orientations parallel to the three alternate edges of the hexagonal spiral. Tin diselenide is a polytypic crystal which exhibit 2H, 4H and other higher order structures. In the crystal, for each successive monolayer in the repetition sequence, the force field is slightly different. In a given orientation of the step, one of these monolayers will have the slowest rate of growth. The other faster moving monolayer will overtake it and pile up behind it /14,15/. Therefore on alternate edges of the hexagon, the growth layers form alternate groupings. Thus the interlacing pattern results from the dependence of the growth rates on crystallographic directions and the change of the growth rate of the monolayers in different orientations of the crystal.

CONCLUSION

Circular and hexagonal growth spirals observed on the basal plane of tin diselenide single crystals revealed that they grew from the vapour phase by the screw dislocation mechanism. The change of curvature of the spiral step as it escape from the centre core is due to the increase in strain at the dislocation centre. Interlaced spirals are the result of the change in growth rate of the monolayers in different orientations

of the crystal. Almost all growth spirals observed on the as grown face of SnSe_2 crystals are similar to that observed on SnS_2 crystals.

References

1. G. Domingo, R.S. Itoga and C.R. Kannewurf, Phys. Rev. 143 (1966) 536.
2. P.A. Lee, G. Said, R. Davis and T.H. Lim, J. Phys. Chem. Solids 30 (1969) 2719.
3. B.L. Evans and R.A. Hazelwood, Brit. J. Appl. Phys. 2 (1969) 1507.
4. F. Levy, IL Nuovo Cimento 38 B (1977) 359.
5. S. Acharya and O.N. Srivastava, J. Crystal Growth 55 (1981) 395.
6. A.K. Garg, O.P. Agnihotri, A.K. Jain and R.C. Tyagi, J. Appl. Phys. 47 (1976) 997.
7. W.K. Burton, N. Cabrera and F.C. Frank, Phil. Trans. Roy. Soc. London A 243 (1951) 299.
8. N. Cabrera and M.M. Levine, Phil. Mag. 1 (1956) 450.
9. H. Muller - Krumbhaar, T.W. Burkhardt and D. Kroll, J. Crystal Growth 38 (1977) 13.
10. F.C. Frank, Acta. Cryst. 4 (1951) 497.

11. A.R. Verma, Phil. Mag. 42 (1951) 1005.
12. A.J. Forty, Phil. Mag. 43 (1952) 377.
13. I. Sunagawa and P. Bennema, J. Crystal Growth 53 (1981) 490.
14. F.C. Frank, Phil. Mag. 42 (1951) 1014.
15. A.R. Verma, Crystal Growth and Dislocations (Butterworths, London 1953).

CHAPTER - IX

OPTICAL AND ELECTRICAL PROPERTIES OFTIN DISSELENIDE CRYSTALS

Optical and electrical properties of tin diselenide single crystals have been investigated by many workers. Domingo et al /1/ studied the optical properties and reported that the fundamental absorption occurs due to an indirect forbidden transition. A direct transition was also observed at higher photon energies. Lee et al /2/ reported the ordinary and extraordinary refractive indices and from the measurement of absorption coefficient they also found that the transition leading to the fundamental absorption is an indirect allowed one. Evans and Hazelwood /3/ studied the optical properties at 290 K and 77 K and reported a direct allowed and an indirect forbidden transition. Garg et al /4/ also reported a direct allowed transition and an indirect forbidden transition. From the pressure dependence of absorption edge Powell and Grant /5/ reported a direct and an indirect allowed transition.

Asanabe /6/ studied the resistivity and Hall coefficient of SnSe_2 crystals grown by melting the elements together, at temperatures above 700 K.

These crystals showed a rapid decrease in resistivity with rise in temperature. This behaviour being attributed to the onset of intrinsic conduction. From the plot of resistivity versus inverse temperature, the energy gap was estimated to be about 1.0 eV. Domingo et al /1/ reported the resistivity perpendicular to c-axis and Hall effect measurements. Lee and Said /7/ studied the Hall effect and reported the mobility perpendicular to c-axis and carrier concentration. Likhter et al /8/ studied the pressure dependence of the electrical resistivity and Hall effect and found that the activation energy and band gap decreases with pressure. Perluzzo et al /9/ also studied the electrical properties of SnSe_2 crystals perpendicular to c-axis.

Not much data is available in the literature on the electrical resistivity parallel to c-axis. Also all the studies mentioned above were made on crystals grown by the iodine transport method. Such crystals may be contaminated by the incorporation of the transporting agent and this may have a pronounced effect on their properties. Optical properties of tin diselenide crystals grown by physical vapour transport method and their electrical properties parallel and perpendicular to c-axis are reported in this chapter.

9.1 EXPERIMENTAL

Crystals used in the present investigation were grown by physical vapour transport method as described in Chapter IV. As grown crystals were in the form of platelets having a thickness of $\leq 150 \mu\text{m}$ and surface area upto 1 cm^2 . Crystals with good plane surfaces were selected for optical measurements. Thickness of the crystals were accurately measured using a micrometer. Transmission measurements were made using a Hitachi 200 - 20 double beam UV - Vis. spectrophotometer. To find the refractive index of the material, very thin crystals were used and for these measurements, a Cary 17 D double beam spectrophotometer was used. From the interference fringes obtained, refractive index was calculated as described in Chapter IV. All the optical measurements were made parallel to c-axis at room temperature.

Electrical resistivity parallel to c-axis was studied by evaporating tin contacts on opposite faces of the crystals. The contact area was $.0415 \text{ cm}^2$. The resulting Sn-SnSe₂-Sn structure was placed in between the jaws of the jig described in Chapter IV and was heated in vacuum upto the maximum temperature of measurement prior to the actual measurement of the

temperature variation of resistance. This ensured good alloying of the contacts and was found necessary for good noise free ohmic contacts. During the measurement sufficient time was given for the current reading to stabilize and very reproducible results could be obtained on all the specimens studied. Electrical resistivity and Hall effect measurements in the plane of the crystal (i.e., perpendicular to c-axis) was studied using van der Pauw's technique /10/. Indium and tin were used as the contact materials since both of them give ohmic contact to tin diselenide crystals.

9.2 RESULTS AND DISCUSSIONS

The variation of refractive index with wavelength is shown in figure 1. Earlier workers reported a slightly higher value of refractive index in their crystals. They reported that interference fringes in the transmission spectra of SnSe_2 was not well defined due to various sample imperfections. Hence they calculated refractive index from the reflectivity data and this may be the reason for the high values of the refractive index obtained for their studies.

The optical absorption data was analyzed in terms of the theory of Bardeen et al /11/ and for an

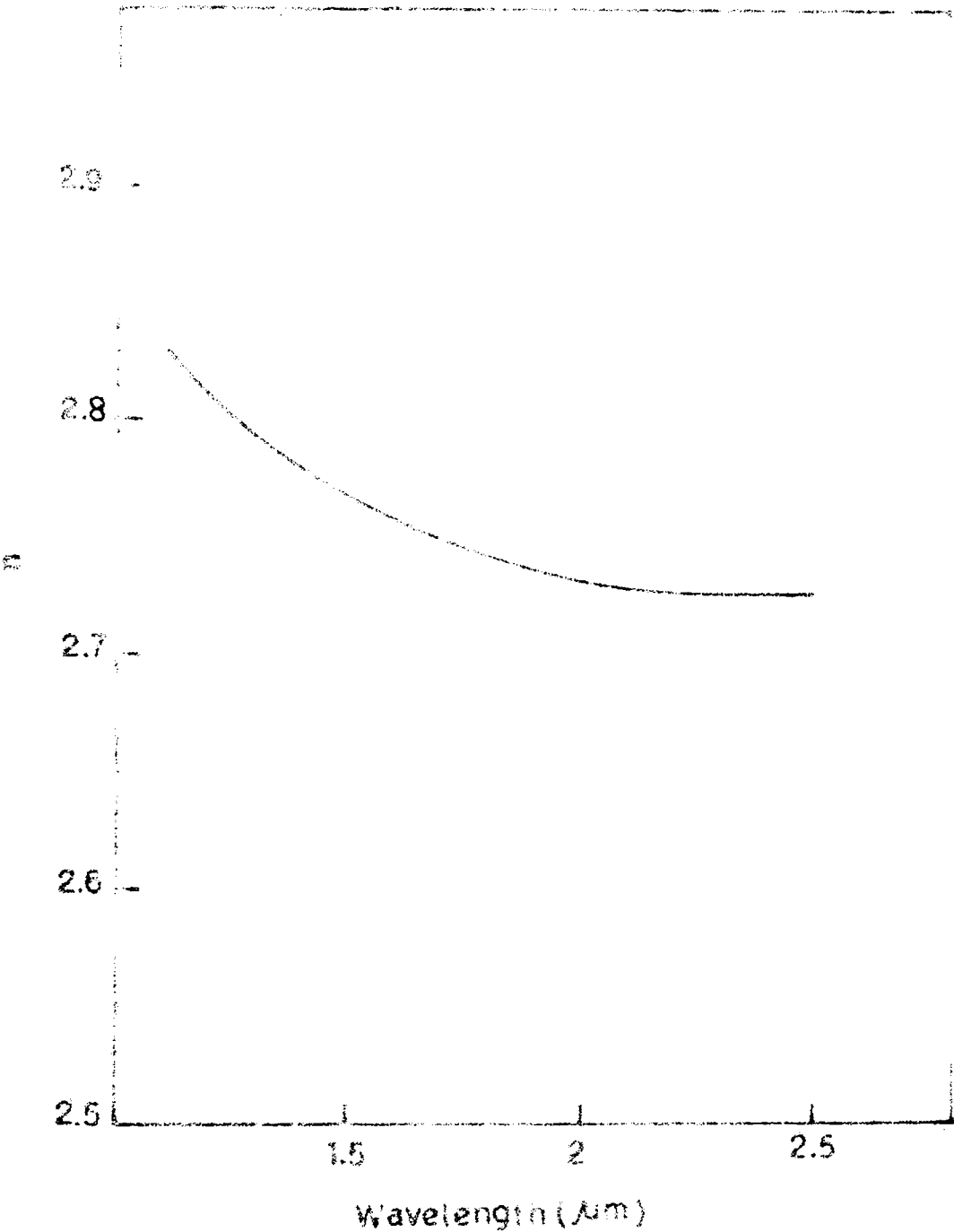


Fig. 1. Refractive index vs. wavelength.

indirect transition

$$\mathcal{L} = \frac{A (h\nu - E_g \pm E_p)^r}{h\nu}$$

where $r = 2$ for allowed indirect transitions and $r = 3$ for forbidden indirect transitions, $h\nu$ is the photon energy, E_g is the indirect band gap and E_p is the absorbed (+) or emitted (-) phonon energy. Absorption coefficient \mathcal{L} was calculated using equations as described in Chapter IV and the variation of $(\mathcal{L}h\nu)^{1/2}$ with photon energy is shown in figure 2. The intercept of the straight line along the energy axis gives a band gap of 1.03 ± 0.02 eV. From the functional dependence obtained for the absorption coefficient on photon energy, it may be seen that the transition is an indirect allowed one. The reported values of band gap for tin diselenide single crystals are given in table 1. Only Lee and Said /2/ and Powell and Grant /5/ have reported indirect allowed transition. But in other reported cases, the transition leading to the fundamental absorption is indirect in nature, but their functional dependence of \mathcal{L} on $h\nu$ shows that the transition is forbidden one. The discrepancy in functional dependence of \mathcal{L} on $h\nu$ may be caused by the presence of impurity absorption in the crystals.

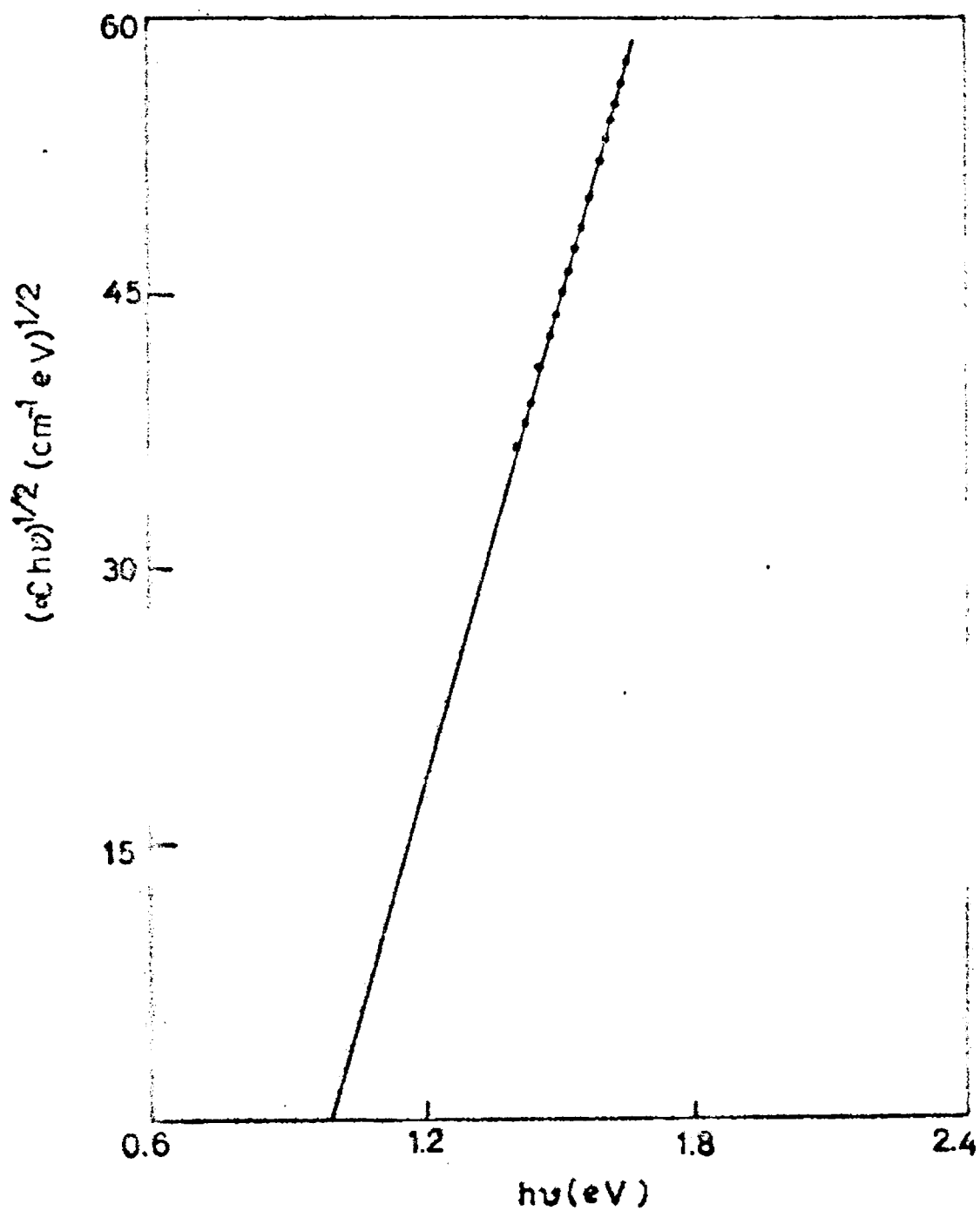


Fig. 2. $(\alpha Ch\nu)^{1/2}$ versus photon energy.

Table 1
Reported values of band gap of SnSe_2 crystals

Reference	Energy gap (eV)				Electrical methods
	Direct allowed	Direct forbidden	Indirect allowed	Indirect forbidden	
Domingo /1/		1.62		0.97	
Lee et al /2/			1.09		
Evans and Hazelwood /3/	1.97			1.03 1.30	
Gary et al /4/	2.1			.98	
Powell & Grant /5/			1.16		
Asanabe /6/					1.0
Present work			1.03		

9.3 ELECTRICAL PROPERTIES

Thermal probe measurements indicated that the crystals are n-type. Resistivity and Hall mobility of tin diselenide crystals perpendicular to c-axis was obtained using van der Pauw's technique /10/. The measurements were made on several samples taken at random from different growth runs and the average resistivity value obtained is $\approx 17\Omega\text{cm}$ and the corresponding carrier concentration is $\sim 10^{16}\text{cm}^{-3}$. Results obtained from the present investigation along with the earlier reported electrical parameters are given in table 2. From the table it is clear that the crystals grown by physical vapour transport are less contaminated (carrier concentration $\sim 10^{16}$) than crystals grown by iodine vapour transport (carrier concentration $\sim 10^{18} - 10^{19}$). It may also be seen from the table that the resistivity obtained in the present case is much greater than that obtained by other workers who used chemical transport methods. The low resistivity values obtained by them may be due to the incorporation of iodine impurities in the crystals.

In resistivity measurements parallel to c-axis, when the Sn-SnSe₂-Sn structures were heated, the resistance of the samples increased. This may be due to the diffusion of the electrode material (tin) into the crystal.

Table 2

Reported electrical parameters of SnSe₂ crystals (perpendicular to c-axis)

Reference	Method of growth	Conductivity type	ρ Ω cm	μ $\text{cm}^2/\text{V}\cdot\text{sec.}$	n cm^{-3}
Domingo et al /1/	Chemical transport	n	.27	27	10^{18}
Evans and Hazlwood /3/	Chemical transport	n	.1	31	10^{18}
Asanabe /6/	Melting elements	n	1	33	10^{17}
Likhter et al /8/	Chemical transport	n	.13	32	
Lee & Said /7/	Chemical transport	n	-	33	10^{19}
Perluzzo et al /9/	Chemical transport	n	.06	42	10^{18}
Present work	Physical transport	n	17	36	10^{16}

So all the measurements were made after heating the samples for a few hours at the maximum temperature of measurement in vacuum and keeping them in vacuum (10^{-2} Torr) at room temperature for one day. After this treatment, the specimens gave a steady value of resistance. Variation of electrical resistivity parallel to c-axis with inverse temperature is shown in figure 3. It may be seen that the plot gives a good fit to the relation $\rho = \rho_0 \exp(-E_a/k_B T)$ where ρ is the resistivity, ρ_0 is a constant, E_a is the activation energy for electrical conduction, k_B is the Boltzmann constant and T is the absolute temperature. At room temperature, the average resistivity ρ obtained for different crystals is $\approx 35 \Omega \text{ cm}$. From the plot of resistivity versus inverse temperature, the activation energy is found to be within $0.072 \pm 0.002 \text{ eV}$. This activation energy is the same as that reported by Likhter et al /7/ for conduction perpendicular to c-axis in the same temperature range of measurement. It may then be possibly said that the same defect level contributes for both parallel and perpendicular conduction.

Assuming that the number of charge carriers available for conduction along parallel and perpendicular directions to c-axis are equal, it may be inferred from the resistivity values that the mobility perpendicular

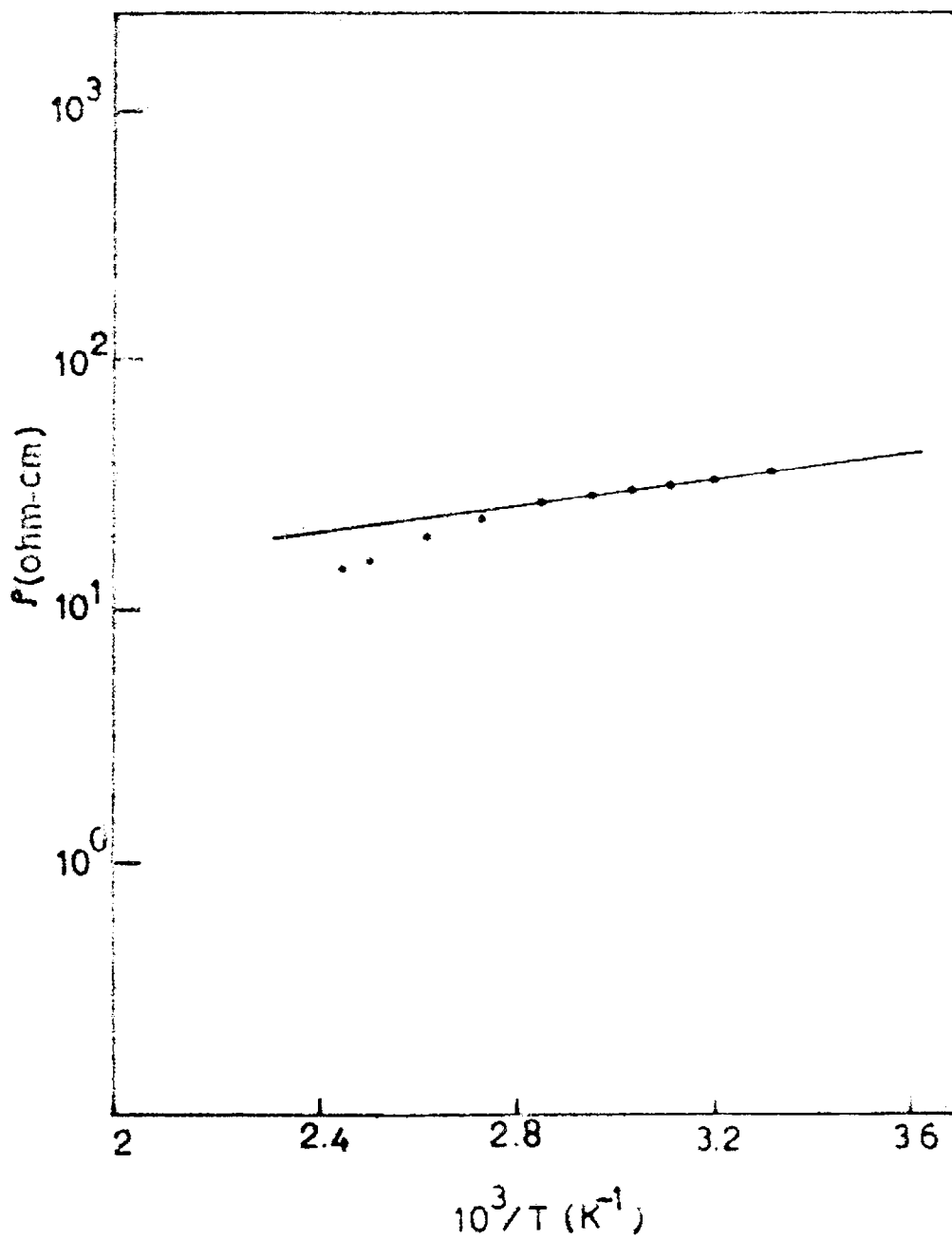


Fig. 3. Resistivity ρ versus inverse temperature.

to c-axis is atleast 2 times greater than that for parallel direction. This type of behaviour was earlier reported in the case of tin disulphide crystals, which is isostructural to tin diselenide, by Gowers and Lee /12/. Their mobility values differed by a factor of 10^5 i.e., $(\mu_{\perp}/\mu_{\parallel} \sim 10^5)$. But from the studies of electrical conduction mechanism in tin disulphide crystals as reported in Chapter VII, mobility parallel to c-axis is $6 \text{ cm}^2/\text{V}\cdot\text{sec.}$ /13/. If we take the mobility value in the perpendicular direction as $18 \text{ cm}^2/\text{V}\cdot\text{sec.}$ /12/, then $\mu_{\perp}/\mu_{\parallel} = 3$, which is quite small compared to 10^5 reported by Gowers and Lee. Tin disulphide crystals used by Gowers and Lee were grown by iodine transport and this growth method may be reducing mobility parallel to c-axis. The large difference between parallel and perpendicular mobility values observed by Gowers and Lee was explained by them as arising due to the existence of inter layer potential barriers and electrons tunneling or hopping between the layers. But from the results given here for tin diselenide and tin disulphide crystals, it may be said that the suggested potential barrier should be of negligible height.

CONCLUSION

Tin diselenide is a semiconductor with an indirect band gap of 1.03 eV. Activation energy for conduction parallel to c-axis is 0.072 eV. Crystals grown by physical vapour transport method have greater purity (carrier concentration $\sim 10^{16}$) than that grown by chemical vapour transport method (carrier concentration $\sim 10^{18} - 10^{19}$).

References

1. G. Domingo, R.S. Itoga and C.R. Kannewurf, Phys. Rev. 143 (1966) 536.
2. P.A. Lee, G. Said, R. Davis and T.H. Lim, J. Phys. Chem. Solids 30 (1969) 2719.
3. B.L. Evans and R.A. Hazelwood, Brit. J. Appl. Phys. 2 (1969) 1507.
4. A.K. Garg, O.P. Agnihotri, A.K. Jain and R.C. Tyagi, J. Appl. Phys. 47 (1975) 997.
5. M.J. Powell and A.J. Grant, IL Nuovo Cimento 38 B (1977) 486.
6. S. Asanabe, J. Phys. Soc. Japan 16 (1961) 1789.
7. P.A. Lee and G. Said, Brit. J. Appl. Phys. 1 (1968) 837.
8. A.I. Likhter, E.G. Pel and S.I. Prysyzhnyuk, Phys. Stat. Sol. (a) 14 (1972) 265.
9. G. Perluzzo, S. Jandl, M. Aubin and P.E. Girard, Solid State Commun. 27 (1978) 1437.

10. L.J. van der Pauw, Philips. Res. Repts. 13 (1958) 1.
11. J. Bardeen, F.J. Blatt and L.H. Hall, Proc. Photoconductivity conf., Atlantic City (New York, Wiley) p-146.
12. J.P. Gowers and P.A. Lee, Solid State Commun. 8 (1970) 1447.
13. J. George and C.K. Valsala Kumari, Solid State Commun. 49 (1984) 103.

ACKNOWLEDGEMENTS

I would like to use this opportunity to express my sincere gratitude to Dr. Joy George, Professor of Industrial Physics, University of Cochin, for his constant encouragement and invaluable guidance all through my work.

I am grateful to Prof. K. Sathianandan, Head of the Department of Physics, for providing the laboratory and library facilities.

I am very much indebted to Dr. R. Rama Varma, Retd. Professor, S.N. College, Quilon who gave me the inspiration to do advanced research work.

I am extremely thankful to all the faculty members and office staff of the department of Physics; staff of University Services and Instrumentation Centre, for the kind help rendered to me during the course of the work.

I am also grateful to Prof. Paul A. Vadakan-cheri, Dr. Sivasankara Pillai, Department of Applied Chemistry; Prof. Joseph Francis, Polymer and Rubber Technology; Dr. Jacob Chacko, Department of Marine Sciences, for providing various research facilities.

I acknowledge the cooperative and very helpful attitude of all my fellow research scholars, especially Dr. K.S. Joseph, Mr. T.I. Palson, Mr. B. Pradeep, Mr. (Fr.) George Peter, Mr. A.V. Alex and Miss Gouri Balakrishnan of our Solid State Physics group.

I wish to thank the Council of Scientific and Industrial Research, New Delhi and the University Grants Commission, New Delhi, for the financial assistance.

Thanks are also due to Mrs. Giriyamma for her excellent typing, Mr. Antony Wilfred for xeroxing the figures and Mr. Peter for cyclostyling.